Numerical investigation with detailed chemistry of CO reduction in biomass combustion

Master Thesis submitted by
Thomas Hartman Meldgaard, TEPE4-1044
Aalborg University, June 2009

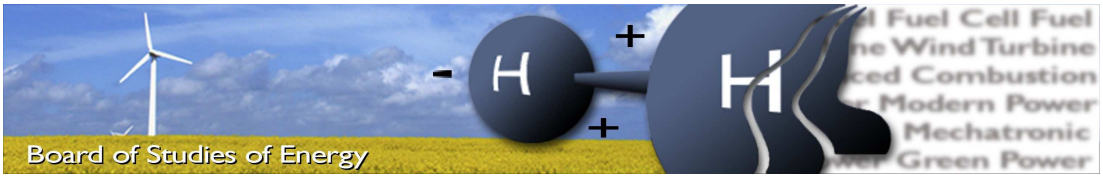

Title:	Numerical investigation with detailed chemistry of CO reduction in biomass combustion
Semester:	TEPE 4. semester
Semester theme:	MASTER THESIS
Project period:	01.02.09 to 03.06.09
ECTS:	30
Supervisor:	Thomas Joseph Roch Condra
Project group:	TEPE4-1044

Thomas Hartman Meldgaard

Copies:	4
Pages, total:	92
Appendix:	77 - 92
Enclosures:	CD-ROM

ABSTRACT:

High CO emissions are often a challenge for biomass boilers combusting moist fuel. The emission limits for CO are restrictive and this presents an incentive to reduce CO emissions. Much research has been directed to improving mixing. This study was concerned with control of temperature and addition of water as possible methods for reducing CO emissions. The chemical kinetics of the combustion were analyzed, showing some potential for CO reduction by temperature control and minor potential with steam injection.

Four CFD simulations implementing detailed chemistry were carried out; A reference case, a case with steam injection and two cases with different parts of the furnace walls insulated. Steam injection resulted in 50 % increased CO emissions. A reduction in CO emissions of 33 % was observed when 19 % of the furnace walls were insulated.

Preface

This master thesis was written by Thomas Hartman Meldgaard on the 4th semester of the Master programme in Thermal Energy and Process Engineering at Aalborg University. The work was carried out in the period between 2nd of February and 3rd of June 2009. The purpose of the thesis was

"...to contribute to students documentation of his/her obtained skills and the level at which he/she is able to exploit these skills in solving a specified task." (N-studyboard Study regulations, 2009)

This was carried out on the subject of analyzing the process of carbon monoxide burnout in biomass boilers.

After an introduction and problem statement, the preconditions for the analysis are described in Chapters 1 and 2. Subsequently, results are presented and discussed in Chapters 3 to 6. References are cited by author and year, and the bibliography is found after the conclusion. A nomenclature is found after the table of contents. In the appendices supporting information is found regarding details on CFD simulation setup in Appendix A, CFD convergence histories in Appendix B and supplementary theory in Appendix C. The standard CFD simulation case and results is included on the enclosed CD-ROM (in a zip-file).

Concerning the software used, Cantera [Cantera, 2008] was used for modelling chemical kinetics through Python programming language [Python, 2008]. Both programs are open source software under the General Public License. CFD simulations were carried out in the commercial software FLUENT under the Aalborg University academic License.

Acknowledgements

Foremost, I would like to acknowledge Aalborg Energie Technik (AET) for proposing this project and for their involvement in defining the objective of the study. Especially thanks to Henrik Widell from AET for his support and inspiration and for many fruitful discussions.

I would like to acknowledge the Department of Energy Technology, for providing computational resources for the CFD simulations and I would like to thank Uwe Schnell and Bjørn Helge Hjertager for their prompt replies to my enquiries.

Project summary

The use of biomass power plants for energy generation is positive in terms of CO_2 emissions, but is often connected with high levels of other pollutants because of for example incomplete combustion. For smaller grate fired boilers combusting high moisture fuel, high emissions of CO are often a challenge. Because of the environmental impact of CO and the additional species associated with the detection of CO, the emission limits are restrictive and are expected to be tightened further in the future. Concerning new plants, the emission limits are often in the range of 150 to 200 mg/Nm^3 at 6% O_2. Much research has been directed to improving the combustion, mostly focussed on mixing and air staging. Appropriate control of the furnace temperature or injection of species could possibly be useful in reducing the CO emissions. This is the concern of this report.

Numerical models of the detailed chemical kinetics in a combustion process was used to study this in a basic manner, through simulations in Cantera. This was based on a representative high moisture fuel. The kinetics were described by a chemical mechanism, GRI-1.2, with 177 reactions. Studying the affect of different temperatures through simulations it was found that an appropriate temperature interval for CO burnout was 1300 K to 1800 K. Through investigation of the effect on the kinetics by adding different species, it was found that injection of steam could possibly increase the burnout rate of CO by increasing the amount of OH radicals in the combustion gas. Also, the effect of injecting steam with secondary air is of practical interest, as moist air, for example from a drying process, is used in some plants.

Both subjects were investigated further through CFD simulations of a simplified biomass furnace. The detailed chemical kinetics were succesfully incorporated into the CFD simulations using the Eddy Dissipation Concept (EDC) model. Turbulence was modelled using the k-ϵ approach, and simulations were carried out in FLUENT. Four different cases were simulated, a reference case, a case with water injection and two cases with different parts of the furnace walls insulated.

In the case where water was injected together with the secondary air, the outlet mass fraction of CO was increased by 50 %. This originated from local spots of low temperatures caused by the presence of water.

The two cases where areas of the furnace wall were insulated, reduced CO emissions were obtained. The reductions was most significant in the case where 60 m^2 (19%) of the wall was insulated, where CO emissions were reduced by 33 %. In practice, the CO reductions obtained by insulating furnace walls are more significant. This was not fully resolved by the model used. Most likely, the phenomenon causing high CO emissions in practice, are cold regions near the walls, why a better resolution of the boundary layer had been needed.

In general, the effects of different temperatures, the creation of radicals etc. was excellent modelled using a detailed kinetic mechanism with the EDC, features that cannot be resolved with simple chemistry models.

Contents

Nomenclature

A	Pre-exponential factor.	(various units)
C_p	Specific heat.	$\left(\frac{\text{J}}{\text{kg-K}}\right)$
C_τ	Fine scale time scale constant.	-
C_ξ	Fine scale volume fraction constant.	-
Da	Damköhler number.	-
E_A	Activation energy.	$\left(\frac{\text{J}}{\text{kmol}}\right)$
G_T^0	Gibbs free energy.	(J)
h	Specific enthalpy.	$\left(\frac{\text{J}}{\text{kg}}\right)$
k	Turbulent kinetic energy.	$\left(\frac{\text{m}^2}{\text{s}^2}\right)$
$k_f(T)$	Arrhenius rate constant.	(various units)
K_p	Equilibrium constant based on partial pressures.	-
k_r	Reverse Arrhenius rate konstant.	(various units)
m	Mass.	(kg)
n	Temperature exponent.	-
p	Pressure.	(Pa)
Q	Heat.	(J)
Q_{EAS}	Equi Angle Skewness.	-
R	Species reaction source term $\left(\frac{\text{kg}}{\text{m}^3\text{-s}}\right)$ or gas constant.	$\left(\frac{\text{J}}{\text{kmol-K}}\right)$
R_u	Universal gas constant = 8314.5	$\left(\frac{\text{J}}{\text{kmol}\cdot\text{K}}\right)$

S	Source term.	(various units)
T	Temperature.	(K)
t	Time.	(s)
t_1	CO reduction time.	(s)
u_τ	Friction velocity.	$\left(\frac{\mathrm{m}}{\mathrm{s}}\right)$
y	Mass fraction.	-
y^*	Mass fraction of a species after reacting over the time τ^*.	-
y^+	Dimensionless wall distance.	-
[A]	Molar concentration of species A. .	$\left(\frac{\mathrm{kmol}}{\mathrm{m}^3}\right)$
U	Mean velocity.	$\left(\frac{\mathrm{m}}{\mathrm{s}}\right)$
u	Velocity vector with x, y, z components u, v, w respectively.	$\left(\frac{\mathrm{m}}{\mathrm{s}}\right)$
u'	Fluctuating velocity.	$\left(\frac{\mathrm{m}}{\mathrm{s}}\right)$
div	Divergence of a vector field, *e.g.*: $\mathrm{div}(\mathbf{u}) = \frac{\partial u}{\partial x} + \frac{\partial v}{\partial y} + \frac{\partial w}{\partial z}$.	-
J	Species diffusion flux.	$\left(\frac{\mathrm{kg}}{\mathrm{m}^2\text{-s}}\right)$
LHV	Lower heating value.	$\left(\frac{\mathrm{MJ}}{\mathrm{kg}}\right)$
M	Arbitrary molecule participating in a third body or termolecular reaction.	
Nm^3	Normal cubic meter *i.e.* at 1 atm pressure and 25^oC.	

Greek letters

ϵ	Surface emissivity (-) or Eddy dissipation rate.	$\left(\frac{\mathrm{m}^2}{\mathrm{s}^3}\right)$
γ_i	Mass fraction of species i in wet fuel (unless denoted 'DAF').	-
μ	Dynamic viscosity.	$\left(\frac{\mathrm{kg}}{\mathrm{m\text{-}s}}\right)$
μ_t	Turbulent viscosity.	$\left(\frac{\mathrm{kg}}{\mathrm{m\text{-}s}}\right)$
∇	The del operator: $\mathbf{i}\frac{\partial}{\partial \mathbf{x}} + \mathbf{j}\frac{\partial}{\partial \mathbf{y}} + \mathbf{k}\frac{\partial}{\partial \mathbf{z}}$.	-
ν	Kinematic viscosity.	$\left(\frac{\mathrm{m}^2}{\mathrm{s}}\right)$

ρ	Density.	$\left(\frac{\text{kg}}{\text{m}^3}\right)$
τ^*	Fine scale time scale.	(s)
τ_w	Wall shear stress.	$\left(\frac{\text{N}}{\text{m}^2}\right)$
τ_{chem}	Chemical timescale.	(s)
τ_t	Turbulence timescale.	(s)
ξ^*	Fine scale length fraction.	-

Subscripts

i	species.
j	Mixture.
vol	Volatile part of fuel

Abbreviations

DAF	Dry ash free.
PA	Primary air.
PAH	Poly Aromatic Hydrocarbons *e.g.* Pyrene.
ppm	Parts per millon by mass.
SA	Secondary air.
TA	Tertiary air.
vppm	Parts per millon by volume.

1 Introduction

Biomass power plants are today widely used on an industrial scale for generating electrical and thermal energy. Politically, these plants have become popular during recent years, due to the fact, that the energy generated is CO_2 neutral. However, the combustion of biomass produces smaller amounts of other pollutants. Some of the major pollutants are NO_X, SO_X, particles (*e.g.* soot), carbon monoxide (CO), unburned hydrocarbons (including PAH) and char, as well as different inorganic species present in the fuel [Yin et al., 2008]. Different well-known methods are used to decrease or capture the various pollutants, *e.g.* particles are removed using cyclones, bag filters and electrostatic filters, whereas NO_X emissions are decreased by injecting urea or ammonia [Zevenhoven & Kilpinen, 2004]. However, no practical post combustion process exists to decrease the amount of CO which is primarily a result of incomplete combustion. This is in particular a challenge for grate combustion compared to for example Fluidized Bed Combustion [Yin et al., 2008].

This study was carried out in cooperation with Aalborg Energie Technik (AET) who is a producer of industrial scale biomass grate boilers. Their interest in proposing the idea of the control of CO is primarily to encourage research in this subject. AET's proposal of this project does not pre-suppose any significant CO emissions in any of the plants they have been involved with.

1.1 Motivation

The CO content in the exiting flue gas varies between different plants and depends primarily on firing conditions, from almost zero to as much as 5000 ppm (for an example, see [Yang et al., 2007]), with normal values around 100-400 ppm mass for grate boilers. Emission limits differ according to fuel type and local authorities, but are also governed by EU directives. The limits are generally quite restrictive. Concerning new plants, the emission limits are often in the range of 150 to 200 mg/Nm^3 at 6% O_2 (approximately 130-180 ppm mass). This is most likely a challenge in smaller plants or in plants combusting wet fuel.

For the industry the emission limits present an economic incentive for reducing CO levels. Emission limits have to be fulfilled as a condition to the granting of a licence

to run the plant. If emission limits are not fulfilled, expensive retrofitting or, as worst case, decommissioning of a plant could be necessary. While retrofitting a plant, the temporary loss of production (and possible contractual violations) is expensive.

The CO level is an indicator of the incompleteness of the combustion and the corresponding loss of efficiency. As an example, the loss due to a CO level of 2000 ppm mass of wet flue gas in plant combusting wet fuel (50% moisture) corresponds to approximately 1 % of fuel heat input. Both the emission limits and the loss of efficiency imply a clear economic incentive for reducing the CO emissions. Therefore, appropriate design of new plants and development of effective retrofitting methods are important.

The global environmental impact of CO emissions is small, and emission limits are mainly due to concerns for local environmental pressure. The hazardous impact of CO results from its ability to occupy blood cells and inhibit oxygen from being absorbed into the blood. High concentrations (> 1000 ppm) of CO are unhealthy for humans, and deadly if exposed through longer periods. However, the CO emissions from a power plant will rarely result in high average concentrations in the local environment (unless you put your head into the stack!).

However, other species resulting from incomplete combustion are hydrocarbons, PAH and tar particles of which many cause human health problems and are undesirable. The CO level is a good indicator of the amount of these species, as both hydrocarbons and CO burnout depend on reactions with OH-radicals. For CO, the reaction with OH given in equation (1.1), is the dominating path for CO oxidation. [Westbrook & Dryer, 1984], [Turns, 2000], [Glassman, 1996], [Zevenhoven & Kilpinen, 2004].

$$CO + OH = CO_2 + H \tag{1.1}$$

Most hydrocarbons consume OH radicals faster than CO, inhibiting the oxidation of CO until hydrocarbon level is highly reduced [Westbrook & Dryer, 1984], [Glassman, 1996]. An example of reactions and their Arrhenius rates at 1000 K is seen in Table 1.1 emphasizing that the rate of the CO reaction is generally one order of magnitude smaller than the hydrocarbon reactions. In this way, even small amounts of hydrocarbons inhibit the oxidation of CO, and furthermore produce CO through their oxidation. Therefore, from an economical as well as environmental point of view, there are good reasons for reducing the CO levels.

Throughout this report the subject of matter is the reduction of CO in grate fired furnaces combusting high moisture fuel.

Reaction	Rate at 1000 K $\left(\frac{\text{cm3}}{\text{mol-s}}\right)$
CO+OH $\rightarrow$ CO_2+H	$1.8 \cdot 10^{11}$
H_2+OH $\rightarrow$ H_2O+H	$1.7 \cdot 10^{12}$
CH_2O+OH $\rightarrow$ HCO+H_2O	$6.9 \cdot 10^{12}$
CH_4+OH $\rightarrow$ CH_3+H_2O	$2.2 \cdot 10^{12}$
CH_3OH+OH $\rightarrow$ CH_2OH+H_2O	$1.5 \cdot 10^{12}$
C_2H_6+OH $\rightarrow$ C_2H_5+H_2O	$3.3 \cdot 10^{12}$
C_2H_4+OH $\rightarrow$ C_2H_3+H_2O	$2.6 \cdot 10^{12}$
C_2H_4+OH $\rightarrow$ CH_3+CH_3O	$1.2 \cdot 10^{12}$

Table 1.1: *Arrhenius rates for reactions between OH radicals and selected species [Westbrook & Dryer, 1984].*

1.2 Efforts in improving combustion

In a combustion problem, the processes going on, are mainly controlled by the three parameters;

- Time - for how much time are the reactants brought together to react. This controls to what extent a reaction will occur.
- Temperature - at what temperature are the reactants brought together. This is important for the rate of most reactions.
- Species composition and their degree of mixing - which species are present in the reactor and how well are they mixed. This determines which reactions are able to occur and the species concentrations influence the reaction rates.

These principles are also seen from the general expression for modelling reaction rates in equation (1.2) [Turns, 2000].

$$\frac{d[\text{A}]}{dt} = AT^n \exp\left(\frac{E_A}{RT}\right)[\text{A}][\text{B}]... \tag{1.2}$$

Some of these principles is also expressed in the above mentioned EU-directive [EU, 2000], by its demand, that all combustion gasses should have a residence time of at least two seconds at temperature of minimum 850°C. The following refer some efforts from the literature in improving the combustion in grate-fired boilers.

1.2.1 Mixing

Improvements could be obtained by optimisation of furnace geometry and the injection of secondary and tertiary air as in a study on a travelling grate boiler, where improved mixing was obtained by changing the direction of secondary air nozzles, forming a stronger swirling flow [Scharler & Obernberger, 2000]. In a study by Dong & Blasiak [2001] the secondary injection was improved by a system called ECO tube, where additional tubes were placed in the radiation pass to inject secondary air, in the middle of the freeboard and not only from the wall. This caused better mixing and resulted in lower CO emissions.

1.2.2 Residence time

Besides mixing, the flow situation resulting from the secondary air jets and the flow in general, it is also important for the residence time of combustion gases. It is of course desirable to achieve sufficient residence time for most of the flue gas, contrary to a situation where some part of the flue gas has a residence time of 10 seconds whilst the rest of the flue gas has only 2 seconds of residence time. This was the focus of an optimisation study by Goddard et al. [2005], where the configuration of secondary air nozzles was optimised to increase the residence time in the boiler radiation pass. Another path to increase residence time is of course to increase boiler volume, but this will increase the capital costs of the boiler.

The examples above mainly focus on the addition of secondary air to improve mixing and residence time. This is also the case with recent efforts in literature on the subject of improving combustion, which reflects the complexity of the mixing problem. The secondary air jets are generally a rather complex problem, which might be more or less specific to boiler geometry and requires extensive modelling for satisfactory results.

1.2.3 Fuel properties and primary air

The fuel moisture level also seems to have a great influence on the CO levels, as found through modelling of straw combustion in a grate furnace by Yang et al. [2007]. It was also found, that the main reason for a rapidly increasing CO level, with increasing fuel moisture, is due to reduced combustion temperature at high moisture levels. Experiments also indicate that CO levels could be reduced by admixing sulphur to the

biomass fuel, but the controlling mechanisms are not yet known and are therefore not possible to model [Strand, 2007].

The part of the combustion air injected as primary air seems, not surprisingly, to affect the CO level, according to Rogaume et al. [2002] and Zhou et al. [2005]. In the laboratory-scale experiment by Rogaume et al. [2002], CO was measured with varying stoichiometry and varying percentage of primary air, showing that keeping the same total stoichiometry but increasing the primary air decreases the CO level. In most grate furnaces, however, it is not desirable to have a too high ratio of primary air because it results in high peak temperatures, which increases the formation of NO_X [Glassman, 1996]. For the same reason, high excess air ratios is not desirable [Zevenhoven & Kilpinen, 2004]. Besides, high amounts of excess air imply lower overall plant efficiency.

1.3 Temperature and species control

Besides improving the mixing through the way of adding secondary and tertiary air, temperature and species are useful parameters to control the combustion. High temperatures are not always desirable, due to the thermal formation of NO, which is why temperatures in the primary combustion zone should not be increased. Instead, temperatures in the secondary combustion zone could be controlled, to favour CO reduction. Details on this area are hard to find in literature. Through correspondence with Prof. Dr.-ing Uwe Schnell, see Appendix D.1, who is chief of department of combustion simulation at the Institute of Process Engineering at Stuttgart University, I found that neither him nor his colleagues had any recommendations in this regard. This is significant, because the emission limits in the new EU-directives is based on the German emission limits, which has been German law for several years.

The focus of this study is on the effect of temperature and species composition on the CO burnout. CO levels could be reduced by controlling the temperature in the secondary combustion zone by maintaining it at a level with high reaction rates of CO reducing reactions, mainly equation (1.1), for sufficient time. The temperature should be at a level where the kinetics in general favour the CO reduction, but still at temperatures low enough that the equilibrium fraction of CO is low. One task in this study was then to investigate the burnout of CO at different temperatures, to decide a suitable temperature to be (almost) maintained. This was investigated through zero-dimensional simulations of the chemical kinetics simulated in Cantera. A second task

was to simulate a furnace and investigate the effect of controlling the temperature by insulating the walls. This was done with the aid of Computational Fluid Dynamics (CFD) using the commercial code FLUENT. The method of insulating the walls has been used in practice by Aalborg Energie Technick (AET). They have achieved good results in cases with CO problems, like cases with high fuel moisture content, where the combustion temperature is low [AET, 2009]. In this study, various part of the furnace wall were insulated, and the effect studied.

Species composition are related to the reaction given in equation (1.1). The question here is if it is possible to increase the amount of OH radicals and thereby increase the burnout rate by changing the combustion gas composition. This could for example be by adding species with the secondary or tertiary air. It required an investigation of the chemical kinetics to identify the species influencing the CO destruction positive by raising the level of OH radicals, which was studied through simulations in Cantera. One possibility could be water, but other species may also influence the reaction positive without reducing the combustion temperature as much as water addition probably will. The addition of water is interesting in practice. The preheated combustion air could be received from for example an industrial drying process, resulting in a high moisture content. The addition of water was analyzed through zero-dimensional simulations of the chemical kinetics and equilibrium conditions of the biomass combustion. The addition of water was further studied through CFD simulations of a furnace. In this study, water was injected together with the secondary air to study the effect.

1.4 Problem statement

Emission limits for CO are restrictive and therefore improved combustion in biomass furnaces is desired. Not only mixing, but also temperature and the present species influences the CO burnout in a furnace.

The objective of this study is to analyze the influence of temperature and addition of species on the burnout of CO in biomass combustion.

The study should include a study of the kinetics of CO burnout in biomass combustion gasses. Taking the kinetic study as starting point CFD simulations should be carried out on a simplified furnace. The CFD simulations should incorporate the complex chemistry to fully model the effects of varying temperature and species composition. Four CFD simulations should be carried out:

- A reference case for comparison.
- Two cases with parts of the furnace walls insulated to maintain an appropriate temperature of the mean flow.
- A case with injection of steam together with secondary air to increase the amount of OH radicals.

1.4.1 Delimitations

The simulations in this study did not model a specific grate boiler, but a furnace of a more simple geometry with a combustion situation comparable to the one found in a grate furnace. Delimitations regarding the simulations are summarized below.

- NO_X chemistry was not considered and other N-species than N_2 was not included in the kinetics, as the subject of NO_X was not within the scope of this report, and the resolution of many reactions can be avoided by ignoring NO_X.
- Heterogeneous chemistry was considered.
- CFD simulations was single phase flow with no particles.

1.5 Method

To study the combustion process under varying conditions, two categories of simulations were carried out;

- Zero-dimensional simulations of the chemical kinetics in a constant pressure Well Stirred Reactor (WSR) were carried out in Cantera. The purpose of these simulations was to study the effect of varying temperature and species addition on the kinetics.
- CFD simulations of a simple furnace with detailed chemical kinetics carried out in FLUENT. The purpose was to study the effect of water addition and insulation of the walls.

The experience from the WSR simulations was used to focus the CFD simulations regarding what species was interesting to study further, and where the furnace walls should be insulated. An overview of the simulations carried out is seen in Figure 1.1.

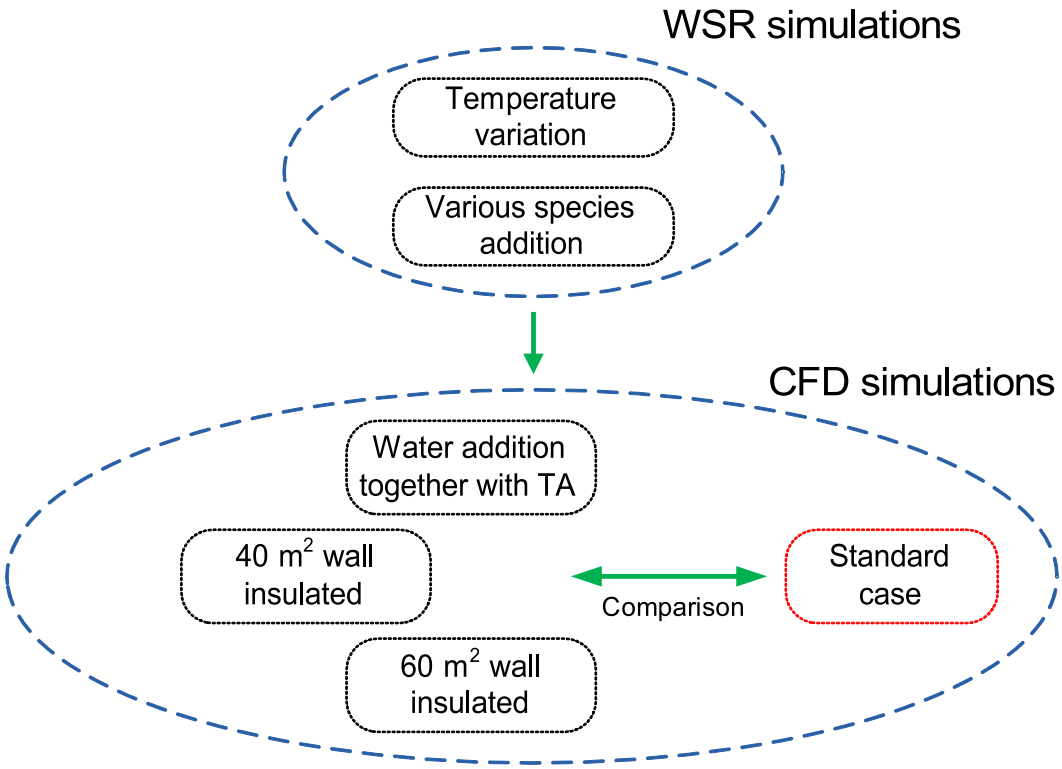

Figure 1.1: *Overview of the simulations carried out.*

The chemical kinetics was modelled in detail using comprehensive mechanisms and zero dimensional reactor simulations. The kinetic mechanism applied in this report,

was the well known GRI mechanism [Frenklach et al., 1994], which is further explained in Section 3.1. Well Stirred Reactor (WSR) simulations, based on the GRI mechanism, was used as a tool to explore the kinetics of CO reduction based on a gas composition representing the species composition in the upper furnace in a wood fired grate boiler. The zero dimensional WSR simulations are less time consuming than CFD simulations, allowing extensive parameter variations in order to identify the parameters that chemically facilitate CO reduction. However, the WSR simulations model only the chemical kinetics and in the idealized situation of perfect mixing on a molecular level. Regarding the parameters of interest, a more complex modelling was also needed to simulate the combustion in a situation where physical aspects like mixing, radiation etc. are included. To obtain results that are more detailed, CFD simulations were carried out on a simplified geometry, representing the conditions in a biomass furnace.

It is important to note that the aim of study was not to model a specific furnace in detail. The focus was on the general methods and tendencies. The CFD models did not model a specific boiler, but a general situation with conditions similar to those found in biomass furnaces. The geometry used in this study is seen in Figure 1.2.

Some important geometric features, like the throat, which is normal in biomass furnace geometries, was not included in this geometry, and therefore the resulting flow pattern will be different from a standard furnace. However, conditions regarding temperature, radiation, level of turbulence and the ratio of fuel input to furnace volume etc. were comparable to a biomass furnace. Therefore, the qualitative results were expected to be comparable to a biomass furnace. The reason for using a more simple geometry is the benefit of a possibly higher grid quality.

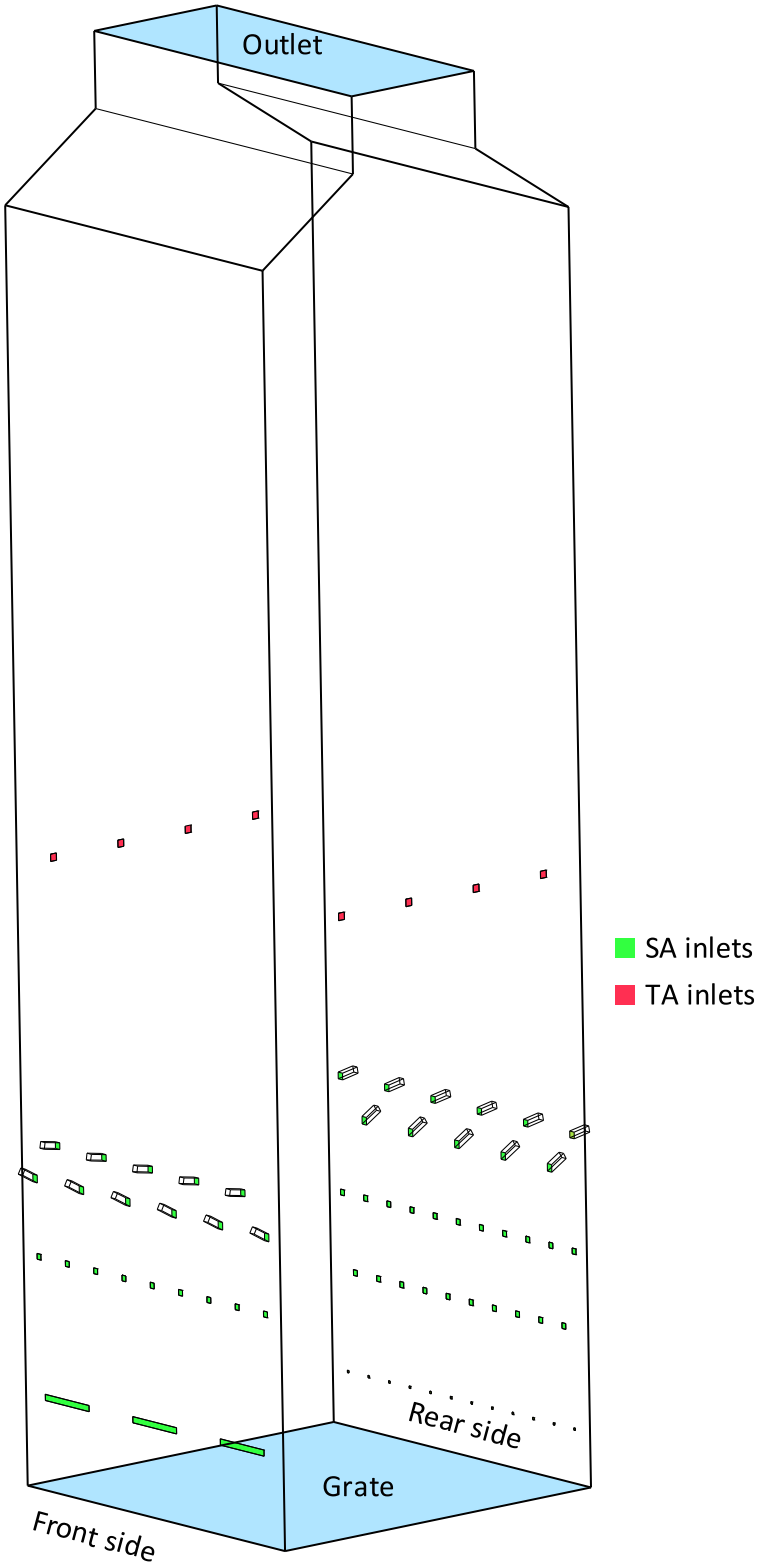

Figure 1.2: *The simplified geometry used in this study to represent conditions in a biomass furnace. (Note that some nozzles are inclined - see Figure 2.2 and Figure 2.6).*

Models setup and physical conditions

2

In this chapter the models and underlying assumptions on which the simulations are based, are explained in more details. This includes the bed model described in Section 2.2), the CFD geometry and meshing presented in Section 2.4 and the simulation settings, which is presented and discussed in Section 2.4.2.

2.1 Operating conditions

The fuel was assumed to be wood with the composition given in Table 2.1 and was unchanged through the study. A fuel with relatively high moisture content was chosen, as this often causes problems with high CO levels.

		Wet	**Dry ash free**
C	(%)	25.10	50.7
H	(%)	2.97	6.0
O	(%)	21.29	43.0
N	(%)	0.15	0.3
Ash	(%)	0.50	0.0
Moisture	(%)	50.00	0.0
Total	(%)	100.0	100.0
Volatiles	(%)	39.6	80.0
LHV	$\left(\frac{\text{MJ}}{\text{kg}}\right)$	8.00	18.65

Table 2.1: *Fuel composition by mass and calorific value.*

This fuel was used as input in the bed model, which specifies the gas composition at the inlet at the bottom of the lower furnace. Generally, the bed model was based on the fuel given in Table 2.1 added the primary air. By assuming a composition of species present in the gaseous product and applying mass and energy conservation, the composition of the gaseous grate combustion products was estimated. The operating conditions considered throughout the study are given in Table 2.2. The conditions presented here served as a constant basis for the simulations throughout the study.

Property		Value
Fuel feed	kg/s	6.24
Total stoichiometric coefficient	λ	1.15
Preheated temperature	°C	270
Primary air	kg/s	8.5
Secondary air	kg/s	11.6
Tertiary air	kg/s	1.15

Table 2.2: *Operating conditions used throughout the study.*

2.2 Bed model and assumed species

The output from the grate consists of primary air, evaporated fuel moisture, volatiles and the gaseous products of char combustion, which takes place on the grate. As presented in Table 2.1 the amount of volatiles for the dry, ash free fuel was 80% (by mass) and 20% was char.

The fuel conversion on the grate is normally assumed to consist of three processes: moisture evaporation, pyrolysis and char burnout. The moisture is first evaporated using heat from the primary air and the incident radiation from the lower furnace. Next, the volatiles are released from the fuel, also as an endothermic process, and finally the remaining char is burned through reaction with oxygen. [Yin et al., 2008], [Tillman, 1987].

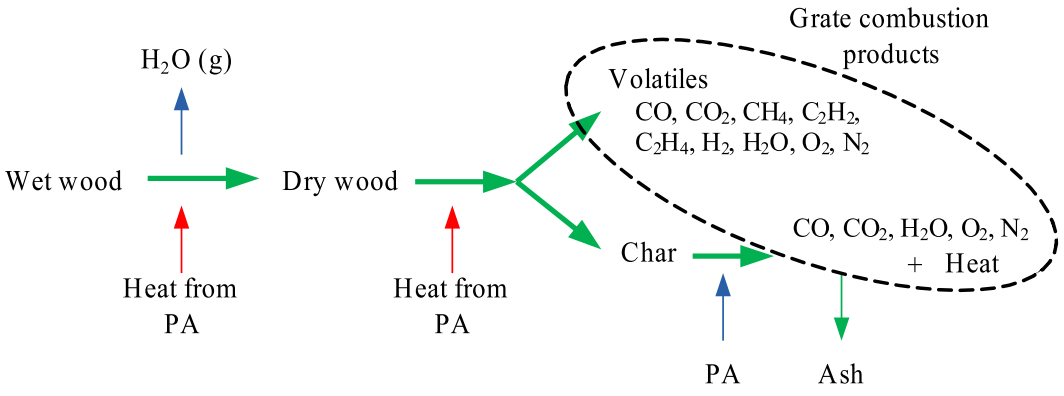

Figure 2.1: *Schematic of the model for fuel conversion on the grate in this study.*

In the following, the bed model used in this study is explained. The bed model was relatively simple as interaction between the grate and the furnace was not considered. This means that the heat of evaporation was only supplied by the primary air. A schematic of the process considered in the bed model is seen in Figure 2.1. Regarding fuel moisture

evaporation, as well as the endothermic release of volatiles, the primary air delivered the necessary heat.

The volatiles released as a product of wood pyrolysis consist, in practice, of a large number of species. The species considered in the volatiles composition in this study is seen in Table 2.3 with their respective lower heating values. These species are normal products of wood pyrolysis as described by [Dupont et al., 2009] and [Zanzi et al., 1996].

Specie	**Formula**	**LHV [MJ/kg]**
Carbon dioxide	CO_2	0.0
Carbon monoxide	CO	10.1
Methane	CH_4	50.0
Acetylene	C_2H_2	48.2
Ethylene	C_2H_4	47.2
Hydrogen	H_2	120.0
Water	H_2O	0.0
Nitrogen	N_2	0.0
Oxygen	O_2	0.0

Table 2.3: *Volatile products of wood pyrolysis and their lower heating values.*

The char reacted to some extent with oxygen, to release products and heat. The char composition was assumed to be 80.7% C, 3.3% H, and 16% O by mass, based on Tillman [1987]. From the char combustion on the grate, equal mass fractions of CO to CO_2 were assumed to be produced, *i.e.* $y_{\mathrm{CO}} = y_{\mathrm{CO_2}}$.

The bed model was based on the above considerations, applied conservation of mass and energy. The continuity equation applied is seen in equation (2.1), where m denotes relative mass (kg/kg fuel (wet)).

$$m_{gas} \;=\; 1 - y_{ash_{fuel}} + m_{PA} = \sum_{i^{th},product} m_i \tag{2.1}$$

Elemental mass balance was applied for the four elements; C, H, O and N, as seen in equation (2.2) to equation (2.5). γ_i denotes the mass fraction of species i in wet fuel, and of Dry Ash Free (DAF) fuel if specified. y_{i_j} is mass fraction of species i in mixture j.

$$\gamma_{C,DAF} = \frac{\gamma_C}{1-\gamma_{H_2O}-\gamma_{ash}} = \gamma_{vol,DAF} \cdot y_{C_{vol}} + (1-\gamma_{vol})\, y_{C_{char}} \quad (2.2)$$

$$\gamma_{H,DAF} = \frac{\gamma_H}{1-\gamma_{H_2O}-\gamma_{ash}} = \gamma_{vol,DAF} \cdot y_{H_{vol}} + (1-\gamma_{vol})\, y_{H_{char}} \quad (2.3)$$

$$\gamma_{O,DAF} = \frac{\gamma_O}{1-\gamma_{H_2O}-\gamma_{ash}} = \gamma_{vol,DAF} \cdot y_{O_{vol}} + (1-\gamma_{vol})\, y_{O_{char}} \quad (2.4)$$

$$\gamma_{N,DAF} = \frac{\gamma_N}{1-\gamma_{H_2O}-\gamma_{ash}} = \gamma_{vol,DAF} \cdot y_{N_{vol}} \quad (2.5)$$

The overall energy conservation is seen in equation (2.6) on a unit mass fuel basis.

$$\begin{aligned} & m_{gas}h_{gas} + \gamma_{ash}h_{ash} \\ = \;& h_{fuel} - \gamma_{H_2O}\Delta h_{evap,H_2O} - \gamma_{vol}\Delta h_{pyrolysis} + (1-\gamma_{vol})\,\Delta h_{charcombustion} \end{aligned} \quad (2.6)$$

To determine the nine species unknown mass fractions mass and energy conservation equations were applied. However, the conservation equations only provide five equations of the nine required. The remaining four equations was provided by assuming mass fraction of C_2H_2, C_2H_4 and O_2 in pyrolysis products as given in Table 2.4. In the pyrolysis process, the only oxygen present is from the fuel, which is why the product mass fraction of O_2 was assumed zero. The assumed pyrolysis mass fraction of ethylene, acetylene and water was based on pyrolysis experiments and models in [Dupont et al., 2009]. The resulting species composition is seen in Table 2.5.

- Volatiles, which is the product of wood pyrolysis.
- Grate combustion products, which consist of the volatiles, the char combustion products and the primary air.
- Basis mixture, which consist of the grate combustion products and the secondary and tertiary air. (A convenient definition for later use).

These compositions are referred to throughout the report by the corresponding names.

In practice, the released combustion products from are not uniformly distributed over the grate. The fuel is combusted as it is moved along the grate, resulting in changing product compositions along the line of movement [Yin et al., 2008]. This could be modelled using empirical models or by developing numerical models for the fuel

Species	Mass fraction (%)
C_2H_2	4.2
C_2H_4	5.0
H_2O	10.0
O_2	0.0

Table 2.4: *Assumed mass fraction of selected species in wood pyrolysis products.*

Specie	Volatiles	Grate combustion products	Basis mixture
Carbon dioxide	21.8	9.8	3.21
Carbon monoxide	43.8	11.3	3.68
Methane	13.8	2.3	0.76
Acetylene	4.2	0.7	0.23
Ethylene	5.0	0.8	0.27
Hydrogen	1.0	0.2	0.06
Water	10.0	24.1	7.86
Nitrogen	0.4	44.6	66.31
Oxygen	0.0	6.2	17.62
Total	100.0	100.0	100.0

Table 2.5: *Products %-mass fraction in the mixtures.*

conversion based on mass and energy conservation as for example done by Kær [2004, 2005]. In these models, the fuel bed is discretized and solved together with the CFD analysis. Numerical bed models could also be implemented using the commercial software FLIC as done by Ryu et al. [2004]. In this study, however, the distribution was simplified, by assuming the grate combustion product to enter uniformly distributed over the grate surface.

2.3 Chemical kinetics modelling

As mentioned in Section 1.1, the primary path of CO oxidation is through the reaction with OH radicals equation (1.1), as the reaction with oxygen in equation (2.7) is slow. If water is the primary hydrogen containing specie, as is the case when the fuel moisture content is 50%, OH is formed through the reaction equation (2.8) [Turns, 2000]. Besides the reaction with hydroxyl radicals, another path for CO oxidation could be through reaction with HO_2 equation (2.9), which is however not as important as the

hydroxyl reaction [Glassman, 1996].

$$O_2 + CO = O + CO_2 \tag{2.7}$$

$$O + H_2O = OH + OH \tag{2.8}$$

$$CO + HO_2 = CO_2 + OH \tag{2.9}$$

These reactions, and several others, are a part of the GRI-1.2 kinetic mechanism, which was used for modelling the chemical kinetics in this study [Frenklach et al., 1994]. The newer GRI mechanism, GRI-3.0 was not used, as it also contains nitrogen reactions (about 150 reactions). According to experiments, [Dagaut et al., 2003], the presence of NO has a minor inhibiting effect on CO oxidation under stoichiometric conditions above 1000 K, and a small promoting effect in fuel lean mixtures below 1000 K. The effect however, is not significant and was not considered to impact the results. All GRI mechanisms is free for downloading, together with validation data [Frenklach et al., 2000]. The GRI-1.2 mechanism contains 177 reactions and 32 species, with ethane as the highest order hydrocarbon. The species are listed in Table 2.6

Species considered				
H_2	H	O	O_2	H_2O
HO_2	H_2O_2	C	CH	CH_2
CH_2(s)	CH_3	CH_4	CO	CO_2
HCO	CH_2O	CH_2OH	CH_3O	CH_3OH
C_2H	C_2H_2	C_2H_3	C_2H_4	C_2H_5
C_2H_6	HCCO	CH_2CO	HCCOH	N_2
Ar				

Table 2.6: *Species considered in the GRI-1.2 mechanism.*

In Chapter 3 results are presented from zero-dimensional simulations of the chemical kinetics of the reacting basis mixture (Table 2.5) which was modelled using the GRI mechanism. In these simulations, a mixture was assumed to react for a given time in a Well Stirred Reactor (WSR). In a WSR, perfectly mixing is assumed. Consequently, temperature, reaction rates and concentrations has no positional dependence, meaning that the simulations are zero dimensional. The simulations were carried out in Cantera, which is an open source tool for modelling chemical kinetics. Cantera and similar tools, *e.g.* CHEMKIN, simulate the kinetics by solving the stiff system of ODE's formulated by the reaction rates, as seen in general in equation (2.10).

$$\frac{\mathrm{d[A]}}{\mathrm{d}t} = -k_f(T)[\mathrm{A}]^a[\mathrm{B}]^b[\mathrm{C}]^c... \tag{2.10}$$

Where a, b, c... are rate exponents. In bimolecular and termolecular reactions, as mostly present in combustion, the rate exponents are normally one, but could be adjusted for some reactions in a mechanism to fit experimental data, or to model third body influence.

In case of reversible reactions, both Cantera and FLUENT calculate the reverse reaction k_r from the expression equation (2.11) using the equilibrium constant K_p and the forward rate k_f.

$$K_p(T) = \exp\left(\frac{-\Delta G_T^0}{R_u T}\right) = \frac{k_f}{k_r} \tag{2.11}$$

2.3.1 Modelling of chemical kinetics in FLUENT

FLUENT enables modelling of volumetric reactions mainly by two concepts; "species transport and reaction" or the "Probability Density Function". Focus is here on the species transport and reaction, as the PDF concept is mostly used to generate initial solutions, and is generally less accurate than the species transport concept [FLUENT, 2006]. When the species transport and reaction model are enabled, FLUENT calculates the mass fraction of each species by the species transport equation (2.12) where J_i is the diffusion flux, R_i is the mass production rate of species i by chemical reactions and S_i is the production rate from other sources, *e.g.* condensation in multiphase flow. The simulations in this study were with heterogeneous reactions, but single phase flow, implying that the S_i term is zero. The R_i term was predicted by the chemistry model.

$$\frac{\partial}{\partial t}(\rho y_i) + \text{div}\,(\rho \mathbf{u} y_i) = \text{div}\,(\mathbf{J_i}) + R_i + S_i \tag{2.12}$$

The effects of varying temperature and species concentration are not well captured by the Eddy Dissipation model, which is only suited for one or two step global mechanisms and where the reaction rate is proportional to the large eddy mixing time scale $\frac{k}{\epsilon}$ (Similar to the eddy-breakup model [Spalding, 1970]). Because of this, the GRI mechanism was implemented in the simulations using the Eddy Dissipation Concept (EDC), developed by Magnussen [1981]

The EDC model is built to include detailed chemistry. It assumes the reactions to occur in small structures, called fine scales, that are treated as constant pressure WSR (like Cantera simulations) and solves the finite rate chemistry for these structures. The source term R_i is then calculated as seen in equation (2.13) where τ^* is the timescale

and y_i^* is the mass fraction of species i after reacting over the time τ^*.

$$R_i = \frac{\rho \left(\xi^*\right)^2}{\tau^* \left[1 - \left(\xi^*\right)^3\right]} \left(y_i^* - y_i\right) \tag{2.13}$$

The fine scale time scale τ^* and length fraction ξ^* is given by equation (2.14) and equation (2.15) respectively. The constants C_ξ and C_τ are adjustable in FLUENT.

$$\tau^* = C_\tau \left(\frac{\nu}{\epsilon}\right)^{1/2} \tag{2.14}$$

$$\xi^* = C_\xi \left(\frac{\nu\epsilon}{k^2}\right) \tag{2.15}$$

As seen from equation (2.14) and equation (2.15) both τ^* and ξ^* depend on the turbulent kinetic energy k, and its rate of dissipation ϵ. In this way equation (2.13) models the interaction between the turbulence and the detailed chemistry to calculate the source term R_i [Magnussen, 1981].

The EDC model is computationally expensive due to the numerical integration of the 177 ODEs from the chemistry. In order to speed up the calculations, the chemistry was integrated using the ISAT algorithm, which generates a table of frequently used solutions to speed up later iterations. See Appendix A.3 for details on the use of the ISAT algorithm and FLUENT [2006] for further information.

2.4 CFD setup

The following section describes the setup of the CFD simulations. Firstly, the geometry used for the simulations is explained and an overview of the mesh is given. Secondly, the most important considerations and setting regarding turbulence and radiation models are discussed. Lastly the boundary conditions used in the standard case CFD simulation is described. These boundary conditions were used in all simulations, unless other conditions are stated.

2.4.1 CFD geometry

The furnace geometry presented in Figure 1.2 was used for CFD simulations with parameter variation. It is seen in two dimensions in Figure 2.2. Two significant modifications make this geometry differ from a normal biomass boiler. Firstly, the throat was removed to simplify the geometry. Most likely, the removal of the throat causes an inferior mixing of the products from the lower furnace, and perhaps bad mixing of

the flow adjacent to the walls. Secondly, the furnace outlet was at the top instead of at the top of the rear wall to avoid a skewed flow, and a constriction was added to prevent recirculation at the outlet. Originally the constriction was not added, but was added after about 3000 iterations as backflow was encountered.

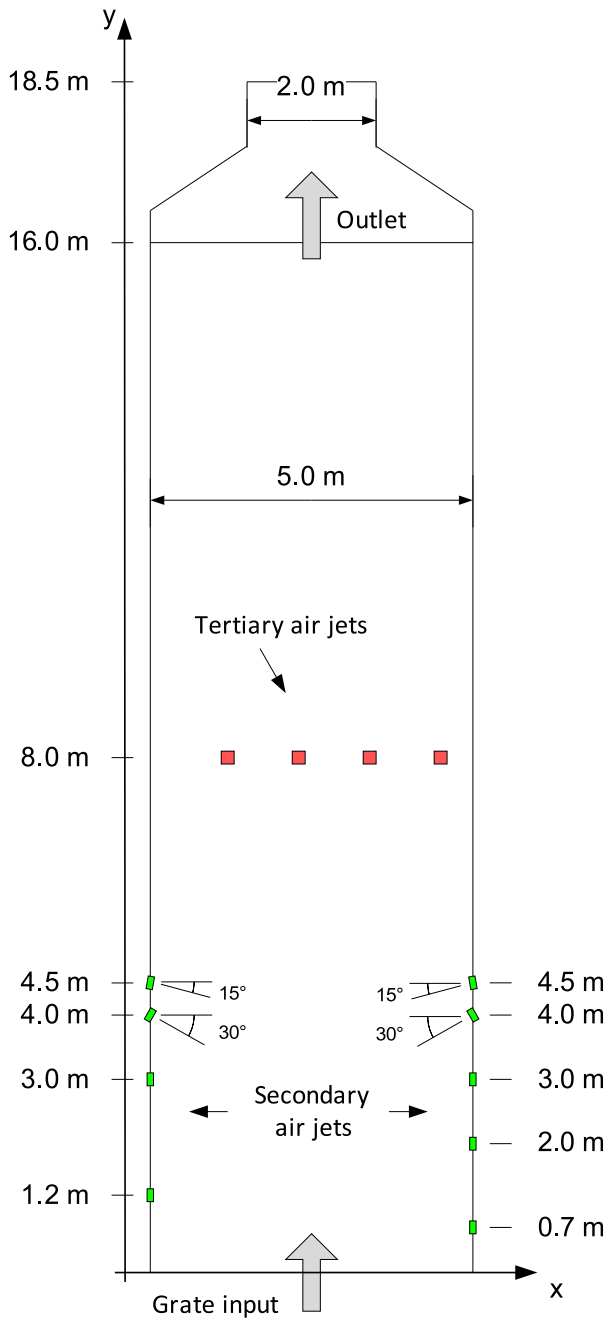

Figure 2.2: *Geometry of furnace in 2D seen from right side (y-x plane). Air jets are enlarged.*

In Figure 2.2 the secondary and tertiary air inlets are seen with their positions given. The inlets are slightly enlarged for the sake of readability. As seen from the figure, the furnace had several rows of air jets, as is the case in most industrial furnaces. Secondary air jets were placed on the front and rear walls of the furnace, while tertiary air jets were placed on left and right walls of the furnace as indicated in Figure 2.2

The secondary air inlets are also seen in figures 2.3, 2.4, where the number of inlets in each row is seen. The upper two rows were inclined as indicated in Figure 2.2. This geometry was selected to create a combustion situation comparable to the one in a industrial biomass furnace with regard to overall turbulence level and mixing.

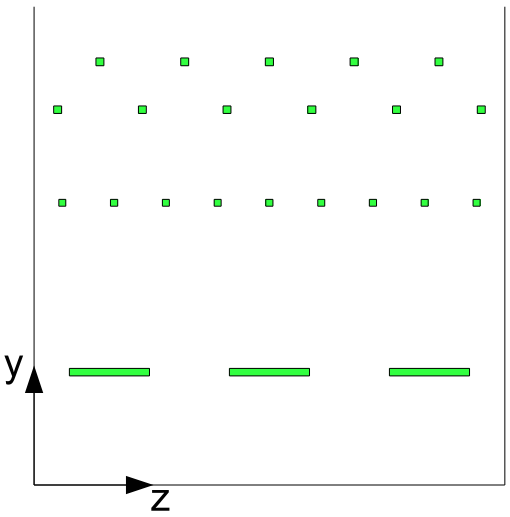

Figure 2.3: *Furnace front wall with secondary air inlets.*

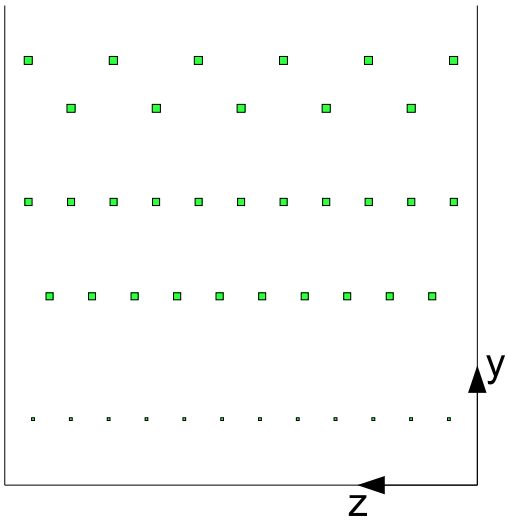

Figure 2.4: *Furnace rear wall with secondary air inlets.*

The furnace geometry was meshed using 1,377,452 hexahedronal cells. Brief mesh statistics is given in Table 2.7, showing the amount of cells and the amount of cells in intervals of equi angle skewness, Q_{EAS}. The cell skewness was quite low, which indicate a high mesh quality. This was possible because of the simple furnace geometry. A part of the mesh is seen in Figure 2.5.

Standard wall treatment was used in the simulations as a detailed resolution of the viscous boundary layer was not supposed to be very important for the solution of the mean flow. The thermal boundary layer has some importance, regarding the near wall temperature, but the standard wall treatment was supposed to be appropriate. The resolution of the boundary layer is well analysed studying the y^+ value, defined in

Equi Angle skew range	**Percentage (%)**
$0 \leq Q_{EAS} < 0.1$	74.97
$0.1 \leq Q_{EAS} < 0.25$	18.19
$0.25 \leq Q_{EAS} < 0.56$	6.84
$0.56 \leq Q_{EAS}$	0.0
	100.0

Table 2.7: *Mesh statistics.*

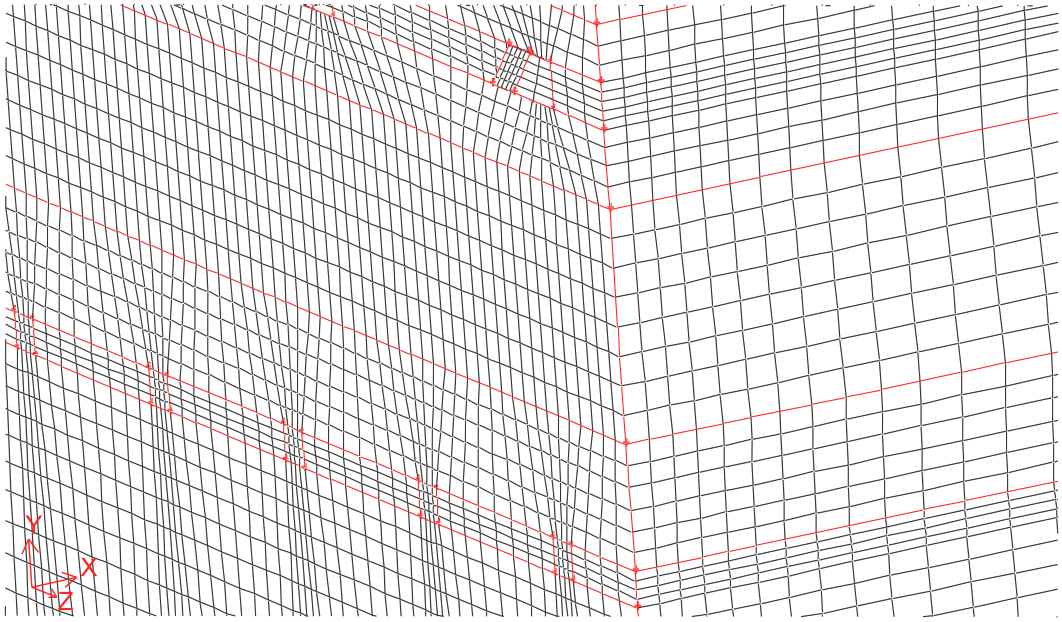

Figure 2.5: *The mesh on a corner of the furnace with some secondary air inlets.*

equation (2.16).

$$y^+ = \frac{y\rho u_\tau}{\mu} \tag{2.16}$$

$$u_\tau = \left(\frac{\tau_w}{\rho}\right)^{\frac{1}{2}} \tag{2.17}$$

Using standard wall treatment, y^+ values should be in the range 30-300 [FLUENT, 2006]. The average y^+ value was around 200. However, the value exceeded the appropriate range near inlets and in some areas near the grate. Despite this, the mesh was generally considered of acceptable quality for this study. Further figures illustrating the mesh are found in Appendix A.1.

A mesh independency study was not carried out. A mesh where cell sizes was doubled was tried, but this resulted in a too crude mesh. A smaller cell size, which results in a greater number of cells, was not possible due to the available computational resources.

However, the quantitative results depend most likely on the mesh used. In a study by Yin et al. [2008], a grate fired biomass furnace was modelled using two different mesh, a structured and an unstructured, each with $3.8 \cdot 10^6$ cells. They found that the mesh had even greater influence than the bed model on the results in terms of the overall mixing and combustion patterns. All simulation in this study was based on the same geometry and mesh, and should therefore be comparable to each other.

2.4.2 CFD model setup

The CFD simulations were based on the commercial code FLUENT. All simulations were steady state and the chemistry was modelled using the EDC model as described in Section 2.3.1. The following describes the simulation setup regarding turbulence and radiation models and boundary conditions for the standard case, as well as considerations on the choice of settings.

Essentially, the purpose of CFD is to model the motion of the fluid, with aspects of radiation, chemistry etc. added to the problem. The fluid motion is described by the Navier-Stokes equations. They are derived from Newton's second law, using considerations on stress and strain in fluids and applying Stokes hypothesis to yield the three partial differential equations for x-, y- and z-momentum, as seen for the x-momentum in equation (2.18), here for the case of incompressible flow of a Newtonian fluid [Schlichting, 1979].

$$\frac{\partial(\rho \mathbf{u})}{\partial t} + \text{div}(\rho u \mathbf{u}) = -\frac{\partial p}{\partial x} + \left(\frac{\partial^2 u}{\partial x^2} + \frac{\partial^2 u}{\partial y^2} + \frac{\partial^2 u}{\partial z^2} \right) \tag{2.18}$$

However, the Navier-Stokes equations are only analytically solvable for a limited type of problems and numerical solution are expensive in terms of computational time. Therefore, different approaches on the Navier-Stokes equations are used in CFD simulations. For turbulent flow, one commonly used approach is the Reynolds average Navier-Stokes (RANS), where the instantaneous velocity fluctuations are time averaged, making the problem less computationally expensive to solve. In this study, the turbulence was modelled using the Realizable k-ϵ (rke) model, which is a modification of the standard k-ϵ model.

The advantage of the k-ϵ model is that it is a simple model applicable to a wide range of different flows. The k-ϵ approach avoid directly simulation of the turbulent scale fluctuations by time averaging the instantaneous velocity in the Navier-Stokes equations. This is done by introducing the turbulent kinetic energy, k, and the eddy dissipation rate, ϵ. [Versteeg & Malalasekera, 2007]. In this way, the k-ϵ model, approaches

the turbulence relatively cheaply, compared to more detailed models, *i.e.* the Reynolds Stress Model (RSM) or Large Eddy Simulation (LES).

The standard k-ϵ has some drawbacks, why different improvements has been proposed. Shih et al. [1995] introduced a k-ϵ model with new equations for the dissipation rate and the eddy viscosity called the "Realizable" k-ϵ model exhibiting a better prediction of the spreading rate of jet flows, rotation and recirculation. Therefore the Realizable k-ϵ model was appropriate for modelling combustion in case in this study, and is used in several studies modelling combustion in a biomass furnace, *e.g.* [Yin et al., 2008]. Theory on turbulence and turbulence models is summarized in Appendix C.1 and details are available in the literature.

Radiation is an important aspect in modelling combustion, as most heat transfer from the hot combustion gas to the furnace walls is radiant. The heating and cooling of the combustion gas is also important for prediction of the chemistry. The radiation was modelled using the Discrete Ordinates model (DO) implemented for gray radiation. Some gasses, mostly H_2O and CO_2 exhibit actually non-gray behaviour (with absorption coefficient varying in spectral bands), but the assumption of gray radiation was considered sufficient. To approach the gas absorption coefficient, the cell based Weighted Sum of Grey Gasses Model (wsggm) was used, as a reasonable approach. Further theory on radiation and the DO model can be found in Versteeg & Malalasekera [2007] or FLUENT [2006].

2.4.3 Boundary conditions

An overview of the boundary conditions is seen at Figure 2.6, where the different boundaries and their type is indicated. Essentially only three types of boundaries were used. Inlets, for the grate, secondary air and tertiary air, outflow, in the top of the furnace, and wall boundaries. All inlets were set to mass flow inlet, to easily control the amount of air and grate combustion products entering the furnace. At the mass flow inlet at the bottom of the furnace, the grate combustion products from the bed model entered. From the secondary and tertiary air inlets, air entered, distributed between the inlets as given in Table 2.8. At the outlet, the flue gas left the furnace.

The walls were supposed to be water tube membrane walls evaporating water at a temperature of 270^{o}C (corresponding saturation pressure of 55 bar). The temperature difference between water temperature and surface temperature of the tubes at the face inside the furnace, was approached by 60 K constant difference, resulting in a inner surface temperature of the walls of 330^{o}C. The surface emissivity was set to 0.6 as an

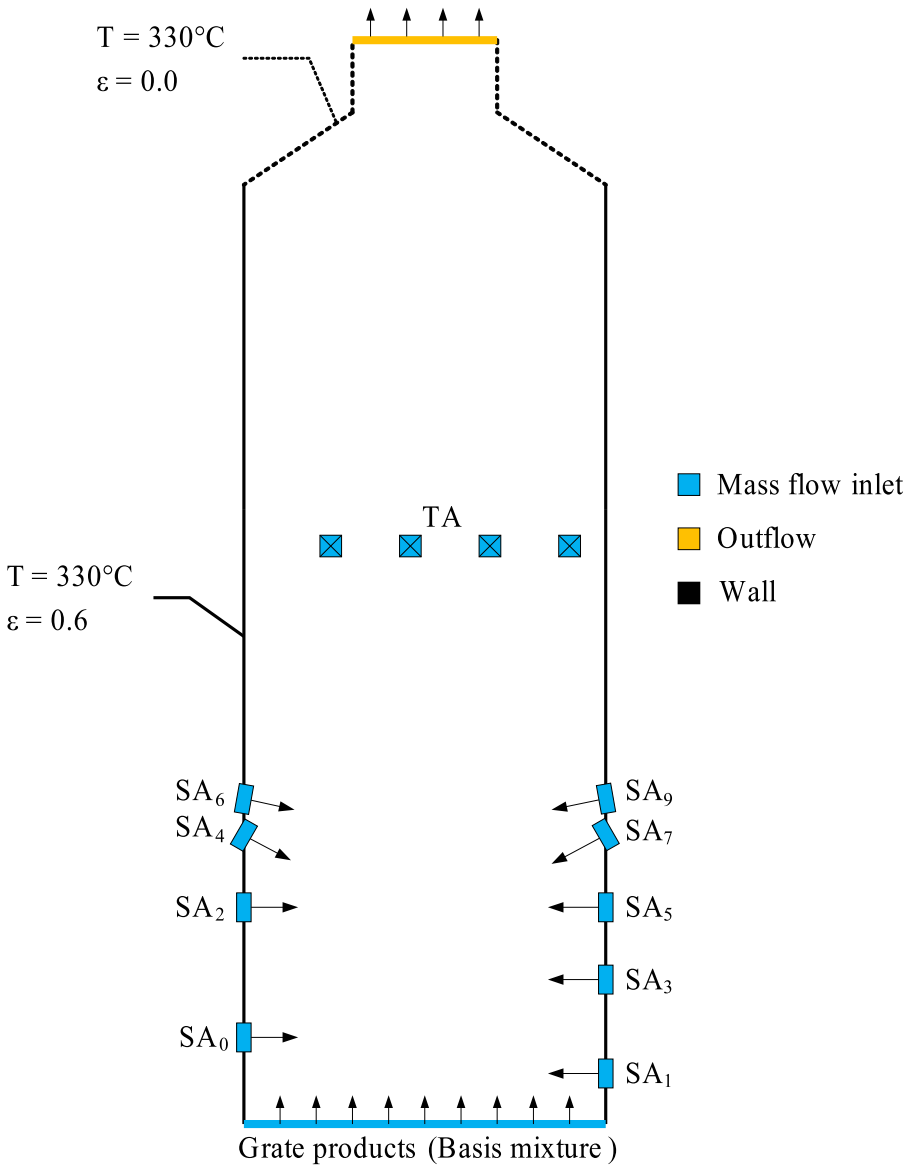

Figure 2.6: *Boundaries of the furnace. View in 2D seen from right side (y-x plane). Not to scale.*

approach for a metal surface with a thin layer of fouling or deposits, based on values from Cengel [2006]

At the bottom of the furnace, the grate combustion products from the bed model entered, which had the composition given in Table 2.5. Both physical properties as well as species composition were uniformly distributed over the inlet surface. This was rather simplified compared to the actual distribution in grate-fired furnaces. Because the bed model and the furnace were not coupled regarding heat exchange, the grate products entered at a temperature of 523 K. This implied that the temperature in the bottom section was rather low until the gas was heated and ignited.

Front wall	(%)	Rear wall	(%)	Tertiary	(%)
SA_0	15.0	SA_1	3.0	TA_{left}	4.5
SA_2	3.5	SA_3	12.5	TA_{right}	4.5
SA_4	11.0	SA_5	12.5		
SA_6	11.0	SA_7	9.0		
		SA_9	13.5		
Total	40.5	Total	50.5	Total	9.0

Table 2.8: *Distribution of secondary and tertiary air in percentage of secondary + tertiary air* $(12.8\ (\frac{kg}{s}))$.

Details on the settings used in the simulations are found in Appendix A and further theory on turbulence is found in Appendix C.

CO chemistry and WSR simulations

3

The following chapter first describes the general characteristics of CO oxidation and the chemical behaviour of the basis mixture is analyzed. This includes details on the equilibrium level of CO at varying temperature, and analysis of the kinetic behaviour of the mixture with focus on the CO burnout. Throughout this chapter, the "grate combustion products" refer to the composition in Table 2.5 of gaseous species calculated using the bed model described in Section 2.2. The "basis mixture" refers to the grate combustion products added secondary and tertiary air. The figures presented in this chapter are based on a large number of data point, and therefore the data points are not shown, but only the curve through them.

3.1 CO equilibrium level

Before analyzing the kinetics of the reactions between the combustion products from the grate, it is convenient to present a brief description of the equilibrium conditions of the basis mixture. The equilibrium level of CO will, most likely, never be reached in a boiler, due to limitations on mixing and residence time. In a Well Stirred Reactor (WSR), however, equilibrium is almost reached in a few milliseconds. Due to dissociation, the equilibrium level of CO increases with increasing temperature, as seen in Figure 3.1. The figure shows the equilibrium CO mass fraction (in ppm) of the basis mixture. Even though the CO consuming reactions occur more rapidly at higher temperatures, the minimum mass fraction that can be achieved increases with temperature.

Equilibrium conditions of the basis mixture with minor variations in the species composition is seen in Figure 3.2 for a constant temperature of 1600 K. The mixture in Figure 3.2 was based on the basis mixture, but the mass fractions of selected species were varied separately, relative to its mass fraction in the basis mixture. Each graph indicates the equilibrium dry mass fraction of CO (ppm) at varying mass fraction of the specie given by the legend. As seen from the figure, the variation of the initial fraction of the selected species in the given range did not affect the equilibrium level of CO significantly. Lower amounts of oxygen would, of course, make the mixture sub-stoichiometric, resulting in much higher CO levels.

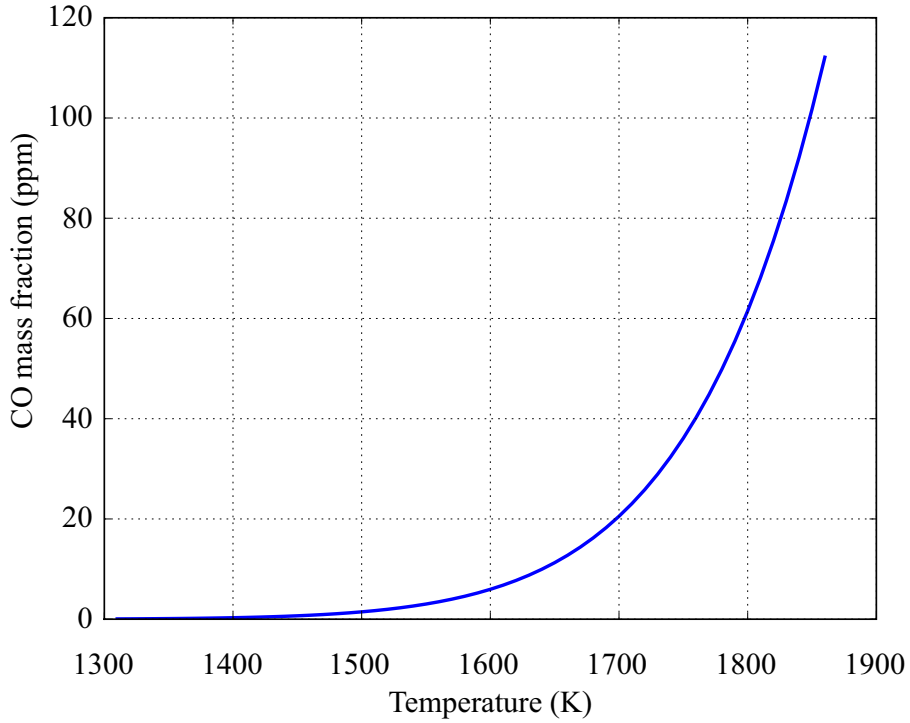

Figure 3.1: *Equilibrium dry mass fraction of CO in ppm, as a function of temperature.*

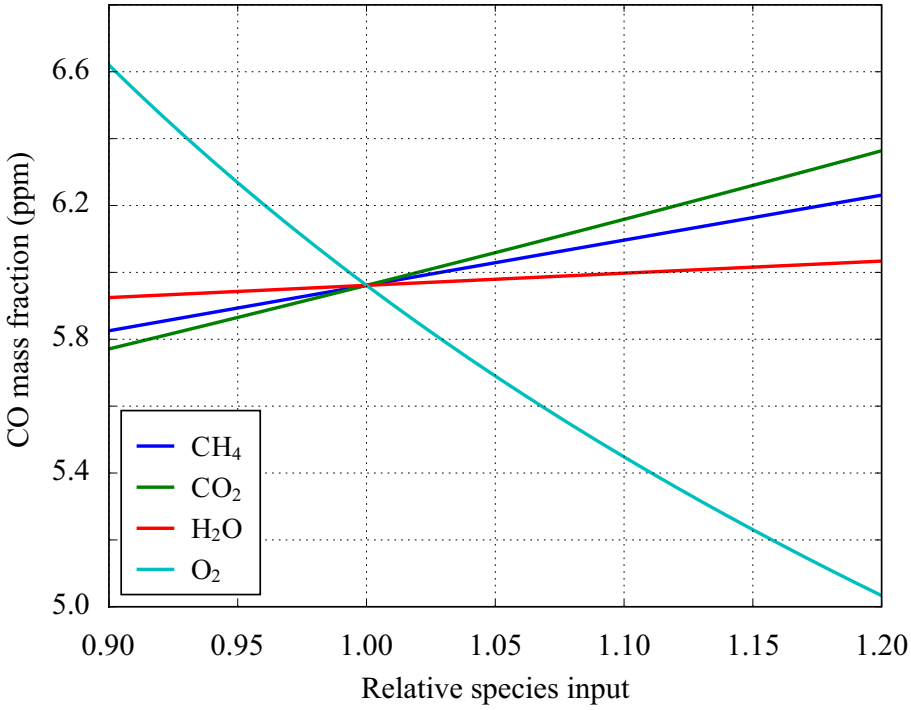

Figure 3.2: *Equilibrium dry mass fraction of CO at 1600 K as a function of species inlet amount relative to basis mixture. A curve values show the CO mass fraction values (y-axis) when the initial amount of the specie specified, by the curve label, is varied in the interval on the x-axis.*

3.2 CO kinetics

To study the kinetics of the mixture in a basic manner, a constant temperature WSR simulation was made on the basis mixture. In a furnace, the products are not perfectly mixed as in the WSR simulations, but the simulations are useful in studying the kinetics. Studying an arbitrary small volume of gas in a boiler, the composition of gasses is approximately constant throughout the volume, why it acts almost like a WSR if the effective diffusion is sufficient. This is also the principle used in the Eddy Dissipation Concept (EDC) as described in Section 2.3. Although it is an ideal situation, WSR simulations should still indicate relevant tendencies when varying parameters.

Some results are seen in Figure 3.3, where the constant temperature is 1523 K. It is seen that the CO was initially steady for a short time, although the oxygen level peaked at initiation. The CO fraction increased shortly and started to decrease after a time of about 0.12 ms. This is also the time where OH radicals mass fraction was just about to peak, which supports the statement, that OH radicals are of importance for CO reduction. The importance of reaction 1.1 is also indicated by comparing the timescales of selected reactions as seen in Figure 3.4.

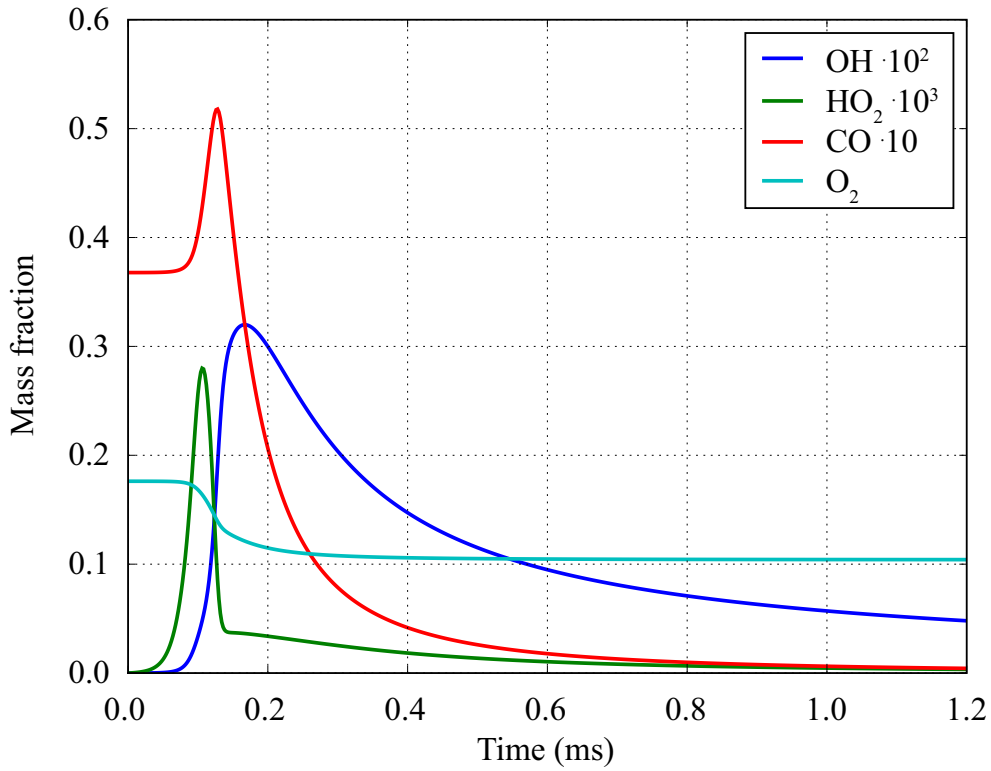

Figure 3.3: *Scaled mass fraction of selected species as a function of time when the basis mixture reacts in a WSR at a constant temperature of 1523 K.*

As seen in Figure 3.3 the basis mixture reacted quite fast and reached almost equilibrium in a few milliseconds, when reacting in a WSR. This makes it clear that the gas in a boiler is far from being well mixed, as the residence time of say 3 seconds is not enough to reach equilibrium in a boiler.

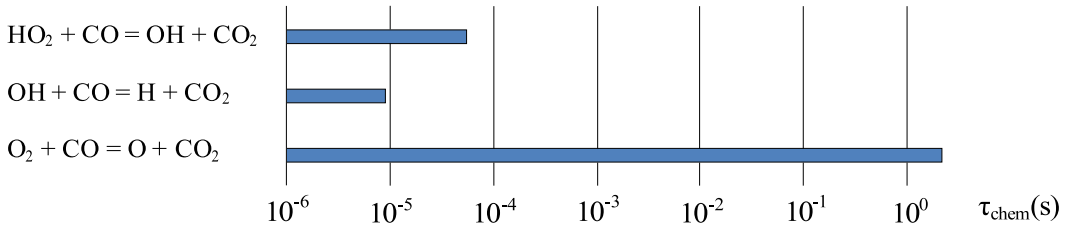

Figure 3.4: *Chemical timescale of selected CO consuming reactions at T = 1523 K.*

3.3 Parameter study of kinetics

The primary combustion occurs at relatively high temperatures, say 1900 K, and high CO mass fractions (4 %) and therefore most CO is easily combusted in the primary zone. Assuming that the CO level is easily reduced to 1.0 % this was the starting point for the following parameter study through WSR simulations. In other words; the initial species composition in these simulations, denoted Mix_{var}, was the resulting composition from letting the basis mixture react at 1900 K, until the CO mass fraction was y_{CO} = 1.0 %. In the simulations, the mixture, Mix_{var} continued to react, with different parameters varied as listed below.

- Temperature variation: The temperature of Mix_{var} was varied, and the mixture reacted at these constant temperatures. (Figure 3.6)
- Species variation: The mass fractions of selected species is increased at different constant temperatures: 1300 K (Figure 3.7), 1400K (Figure 3.8) and 1500K (Figure 3.9).

The effect on CO reduction of varying a parameter is here compared through the reduction time t_1, which is the time necessary for the CO mass fraction to be reduced to 1.0 % of the initial CO mass fraction.

The mixture reacted at constant temperature, both when adding species and when varying the constant temperature, because the purpose was to compare the CO reduction in different temperature regimes of the furnace. Basically, the cross sectional average

temperature of a furnace was expected to behave like in Figure 3.5. Through the primary combustion zone, most heat from the combustion is released, and the temperature rises. Although the gas reacts further in the secondary combustion zone, less heat is released and the cross sectional average temperature decreases as heat is absorbed by the walls. In the parameter variations described below the objective was to simulate the kinetics in different regimes in the secondary zone, where temperature is slowly decreasing, and for this reason the temperature in the simulations was kept constant.

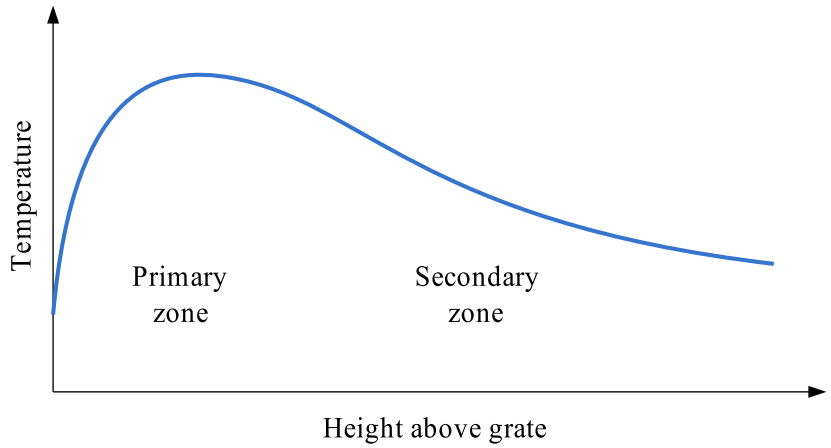

Figure 3.5: *Schematic of expected progress of cross sectional average temperature as a function of height above the grate in a furnace.*

3.3.1 Temperature variation

At various temperatures, a number of WSR simulations were performed at constant pressure and different constant temperatures with Mix_{var} as the initial composition, and the reduction time t_1 was recorded. The reduction time as a function of the reaction temperature is seen in Figure 3.6. Studying the figure, it is seen that relatively low values of t_1 were obtained at temperatures between 1300 and 1800 K, which indicates that CO reduction occurs relatively faster in this interval compared to lower or higher temperature regimes. At lower temperatures, t_1 increases probably because the reaction rate of the involved reactions has decreased, as seen by the rate constants temperature dependence in the improved Arrhenius expression, equation (3.1), [Turns, 2000].

$$k_f(T) = AT^n exp\left(\frac{E_A}{R_u T}\right) \tag{3.1}$$

At higher temperatures, t_1 also increases, even though the Arrhenius rate is increased. This is because the reverse reaction rate increases as the equilibrium level of CO increases with temperatures *i.e.* the equilibrium constant K_p, changes with temperature, as expressed in equation (2.11).

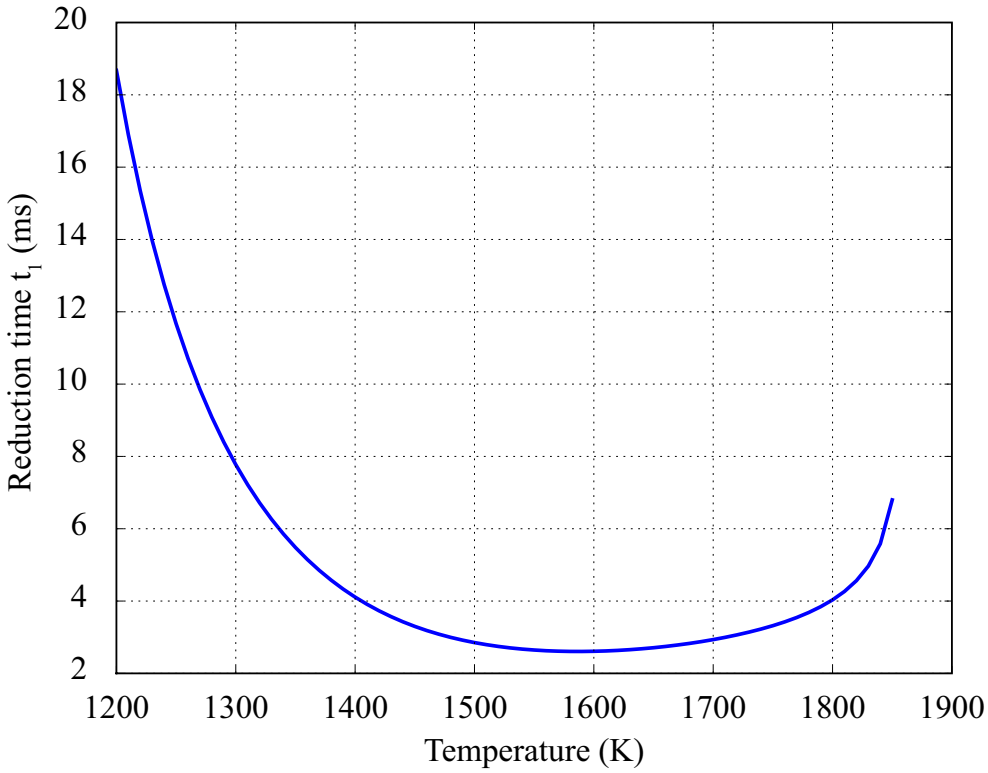

Figure 3.6: *Reduction time, t_1, at varying temperatures.*

3.3.2 Species variation

For a series of simulations, the temperature was kept unchanged whilst the mass fractions of selected species were separately increased. The objective was to model that an amount of a species is added, for example with the secondary or tertiary air, to increase its mass fraction. The selected species whose mass fraction was varied was CH_4, H_2O, H_2, O_2, CO_2, HO_2 and OH. The addition of OH and HO_2 is not possible in practice, but was simulated for comparison. The fraction of H_2O was expected to have some influence on the CO reduction, although the water fraction is already high, due to the high moisture content of the fuel. The influence of water additions was expected to increase with temperature due to increasing dissociation into OH radicals.

The t_1 reduction time is seen as a function of species addition in figures 3.7, 3.8 and 3.9, modelling the species variation in the temperature regimes 1300 K, 1400 K and 1500 K respectively. At 1600 K the picture is almost similar to the one at 1500 K. In the figures, the addition of a specie is varied in the range of 0 to 0.026 kg/kg fuel. This correspond in absolute values from 0 to 0.16 $\left(\frac{\text{kg}}{\text{s}}\right)$ for a fuel feeding of 6.24 $\left(\frac{\text{kg}}{\text{s}}\right)$

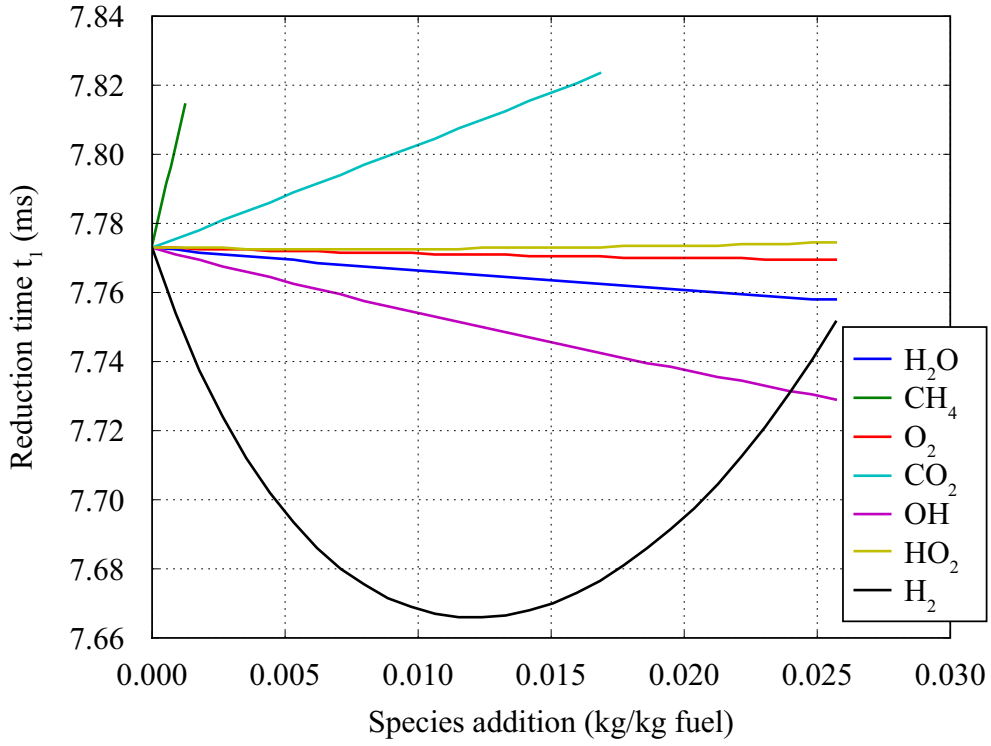

Figure 3.7: *Reduction time, t_1, at varying addition of species at 1300 K. A curve values show the CO mass fraction values (y-axis) when the added amount of the specie, specified by curve label, is varied in the interval on the x-axis.*

Studying the simulations results in Figure 3.7, it is seen that the addition of H_2O had a minor influence on the reduction time, while the (academic) addition of OH radicals had a slightly higher influence. It appears that the addition of H_2 in smaller amounts has a positive influence on CO reduction, until approximately 0.012 kg/kg fuel, after which the positive influence disappeared. The positive effect of H_2 addition also disappears at higher temperatures, as seen in figures 3.8 and 3.9. Apparently, the (academic) addition of HO_2 had no positive influence at a temperature of 1300 K. At temperatures of 1400 K and 1500 K, the addition of HO_2 had almost the same influence as adding oxygen. This is different from the expectation discussed in Section 3.2 on basis of the time scales in Figure 3.4.

At temperatures of 1400 K and 1500 K, it is seen that the largest reduction in t_1 was obtained by adding OH, which is in line with the expectations in Section 3.2. The positive influence of adding water increased slightly with temperature, as did the influence of oxygen, hydroxide and hydroperoxyl. Performing similar simulations in an adiabatic reactor resulted in an improved reduction in t_1 by water addition. The negative influence of adding methane and hydrogen were further pronounced however; probably because they caused the temperature to rise too much in the adiabatic reactor.

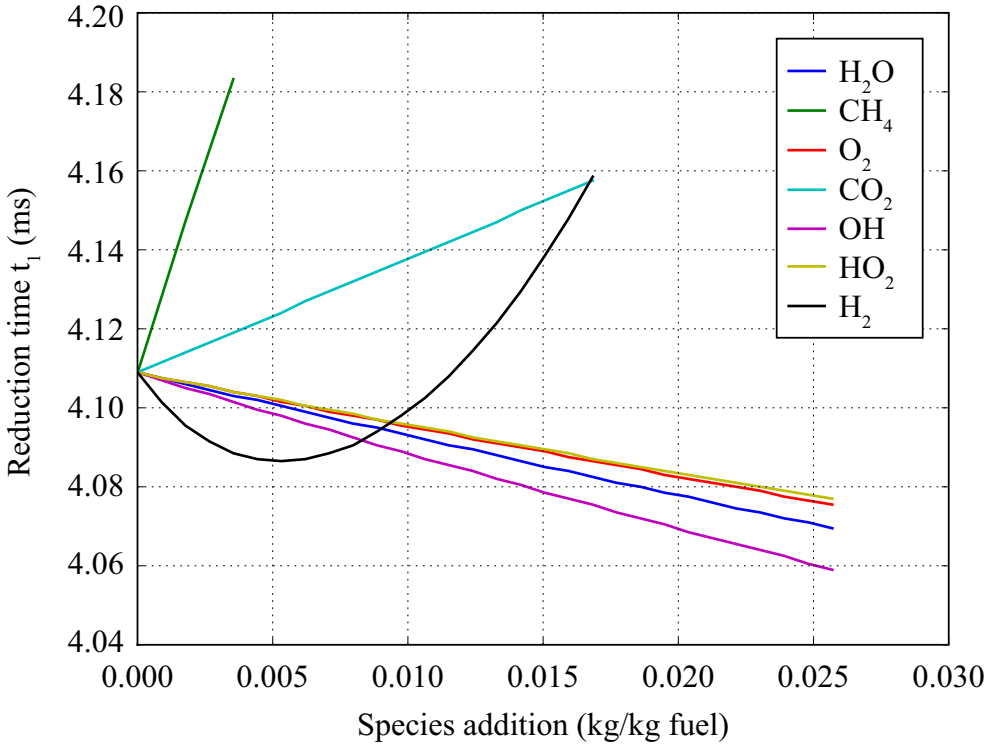

Figure 3.8: *Reduction time, t_1, at varying addition of species at 1400 K. A curve values show the CO mass fraction values (y-axis) when the added amount of the specie, specified by curve label, is varied in the interval on the x-axis.*

Among the investigated species, only H_2O, CO_2, CH_4 and H_2 are possible in practice and could be injected for example together with secondary or tertiary air.

- H_2 is rather unpractical in a biomass furnace because of its high flammability, high cost and the difficult storage.
- CH_4 has a negative influence on the reduction time, even when considering the temperature rise. If using methane to maintain a flue gas temperature of 1500 K - 1700 K in the furnace, the influence on reduction time could possibly be positive.
- O_2 has of course a positive influence on the reduction time, but adding more air is not wanted due to the formation of NO_X
- CO_2 has, not surprisingly, a negative influence.
- H_2O is easy to add and is wonderfully cheap. H_2O had kinetically a positive influence on the reduction time, which increased with temperature. This was expected, because the increasing fraction of H_2O increases the fraction of OH

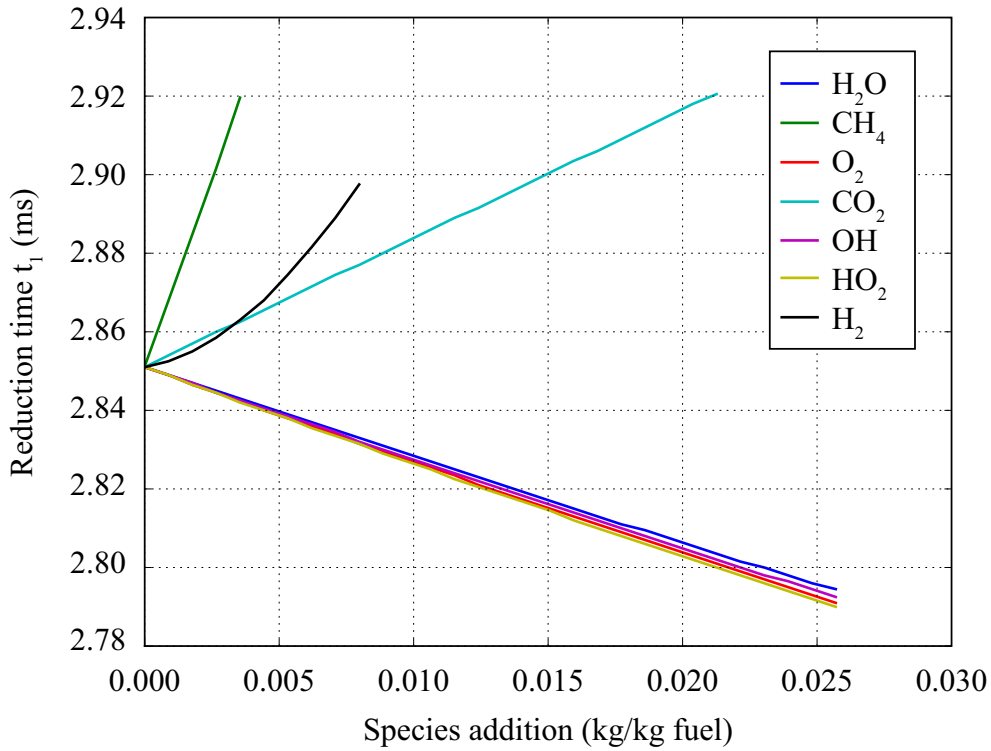

Figure 3.9: *Reduction time, t_1, at varying addition of species at 1500 K. A curve values show the CO mass fraction values (y-axis) when the added amount of the specie, specified by curve label, is varied in the interval on the x-axis.*

radicals due to dissociation for example through the reverse of termolecular reactions like equation (3.2). As the equilibrium constant changes with temperature, the level of OH radicals increases with temperature.

$$H + OH + M \Leftrightarrow H_2O + M \tag{3.2}$$

A practical way of adding water is to inject it as steam together with the secondary air.

3.4 Summary

In this chapter different aspects of the combustion chemistry of the basis mixture defined in Table 2.5 was analysed and described. It was expected that OH and perhaps HO_2 would prove important in the oxidation of CO as well as the temperature.

To study the CO burnout, simulations were carried out with variation of temperature and selected species. The basis mixture was assumed to react until a mass fraction of

1% CO was reached after the primary combustion zone. The following combustion was simulated with separate variation of temperature and addition of the species H_2O, CO_2, CH_4, O_2, OH, HO_2 and H_2 and results was compared through their resulting reduction time t_1, which is the necessary time to reduce CO level to 100 ppm.

It was found, that the temperature has a major influence on the CO burnout, and that the appropriate temperature regime for CO burnout is from 1400 K to 1800 K. The highest temperatures are not likely to occur in the upper part of the furnace whilst combusting high moisture fuel. The challenge is more likely to maintain a appropriate gas temperature for a increased part of the gas residence.

Studying the influence of the selected species, it was found that addition of H_2O has a positive influence on the speed of burnout. OH has also a positive influence and HO_2 has some positive influence at higher temperatures. However, OH and HO_2 are not realistic additives. Relative to the influence of varying the temperature the influence from water addition was smaller, but quite cheap and easy in practice. However, water addition will cause the temperature to decrease. Although the addition of water kinetically favours CO burnout, the temperature loss might have an adverse influence. The combined effect was not possible to predict from the above analysis but was studied in the CFD simulations.

CFD Simulation overview

4

This chapter gives an overview of the different CFD simulations, the differences between the cases and the expectations to the results. Subsequently, the simulation procedure, which is important in simulations with detailed chemistry, is presented. Thereafter, the convergence history of the cases is discussed.

4.1 Cases overview

An overview of the four simulation cases is given in Table 4.1. The standard case served as a basis of comparison of results for the other cases, and the boundary conditions in the standard case were as described in Section 2.4.2.

Case name	Case characteristics	Expectation to results
Standard	Settings were as described in Section 2.4.2	Conditions comparable to a biomass furnace.
Ins40	40 m^2 of the furnace wall was insulated	CO emissions was expected to decrease because of increased gas temperature in
Ins60	60 m^2 of the furnace wall was insulated	the mean flow.
Water injection	$0.3 \frac{kg \text{ water}}{kg \text{ air}}$ was injected together with the secondary air in the rows SA_6 and SA_9.	CO emissions was expected either to decrease, due to an increased amount of OH, or to increase because of reduced temperature.

Table 4.1: *CFD simulation cases and expectations to case results*

In the cases Ins40 and Ins60 were 40 m^2 and 60 m^2 of the furnace wall insulated respectively. The areas insulated is indicated in Figure 4.1. These areas were insulated to maintain an average temperature above 1300 K, as was found appropriate in the WSR analysis in Chapter 3. Studying the average temperature in the standard case, it was found that insulation should be placed in the shown areas for the gas to maintain an appropriate average temperature for a longer time compared to the standard case. As discussed in Chapter 3 the CO reduction is sensitive to the temperature, and there-

fore, CO emissions were expected to be decreased. At the insulated areas, the wall temperature was assumed to be 903 K and the emissivity was set to 0.3.

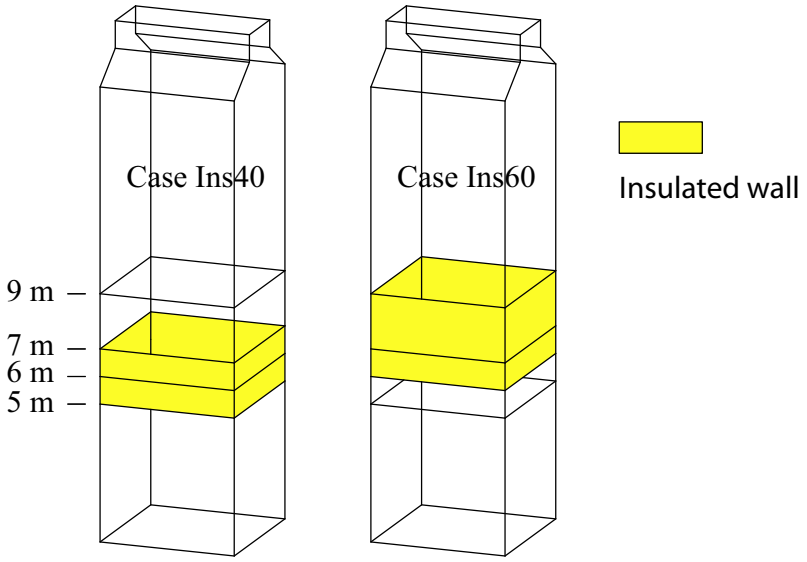

Figure 4.1: *Indication of the furnace wall areas that was insulated in the cases Ins40 and Ins60.*

In the case of water injection, $0.3 \frac{kg \text{ water}}{kg \text{ air}}$ was injected together with the air in the two upper rows of secondary air jets, SA_6 and SA_9 (see Figure 2.6). From the analysis in Chapter 3 it is seen that a temperature of about 1400 K was appropriate for water injection. The injection point was decided upon the basis of the average temperatures in the standard case, and a height of 4.5 meter was found appropriate. The injection of water was expected to increase the amount of OH radicals in the region of tertiary air injection, which favours CO reduction. However, the water was also expected to decrease the temperature, giving the opposite effect.

The average temperature decreases because the water is heated by the combustion gas from its injection temperature $(T_w = 543K)$ to the gas temperature $(T_{gas} \approx 1400K)$. With a mass flow rate of water $\dot{m}_w$, the rate of heat energy $\dot{Q}_w$ to the water is estimated in equation (4.1). The amount of water injected was the same as in the standard case, to maintain the same stoichiometry. As a rough estimate calculated in equation (4.2), this was only expected to decrease the average gas temperature by about 19 K compared to the standard case.

$$\begin{aligned} \dot{Q}_w &= [h(T_{gas}) - h(T_w)] \cdot \dot{m}_w \\ &= \left[4961 \left(\frac{\text{kJ}}{\text{kg}}\right) - 3013 \left(\frac{\text{kJ}}{\text{kg}}\right)\right] \cdot 0.3 \cdot 1.15 \left(\frac{\text{kg}}{\text{s}}\right) \\ &= 670 \text{ (kW)} \end{aligned} \tag{4.1}$$

$$\Delta T_{gas} \approx \frac{\dot{Q}_w}{\dot{m}_{gas} C_p} = \frac{670 \ \left(\frac{\text{kJ}}{\text{s}}\right)}{27.5 \ \left(\frac{\text{kg}}{\text{s}}\right) \cdot 1.3 \ \left(\frac{\text{kJ}}{\text{kg-K}}\right)} = 19 \ (\text{K}) \tag{4.2}$$

However, the local temperature decreases were expected to be larger. A local temperature decrease in the order of 100 K could have a more significant impact on the CO burnout.

4.2 Solution procedure

When simulating combustion with detailed chemistry, obtaining a solution needed some care, especially on decreasing the computational time, as the chemistry integration has excessive computational costs. The procedure used to obtain a solution is summarized below.

- Setup case and initialize all values.
- Solve flow field without chemical reactions
- Enable chemical reactions, patch the domain temperature properly and solve flow with chemical reactions.
- Increase quality of the solution of the chemistry and continue iterations.

When the case setup was complete and all values were initialized, cold flow iterations (without reactions) were computed. If reactions were enabled from the beginning, the solution would diverge. Later on, chemical reactions were enabled, and temperature distribution in the furnace was properly set in order to ignite the combustion. The EDC time scale constant, see equation (2.14), was initially set to 0.04, as the default value of 0.4082 could result in divergence in the initial chemistry iterations.

As simulation proceeded, the quality of the kinetics integration was increased, first by setting the time scale constant to a value of 0.3082, to achieve an appropriate integration time. At the early stages, chemistry was only solved for every 15th flow iteration. Later, chemistry was solved at every flow iteration. Due to the complex chemistry, iteration time was about 1.5 to 3 minutes per iteration, when a good ISAT table had been build up. Building a good ISAT table took about one day of iterations. A new table

had to be built occasionally, as the simulation progressed, or when the time scale constant was changed in order to clear out old values. Details of the procedure to obtain a solution is given in Appendix A.3.

The convergence of a solution was evaluated based on temperature, CO mass fraction and residuals. For a solution to be converged the residuals should be converged, *i.e.* not decrease further. Temperature and CO mass fraction was monitored in horizontal planes as seen in Figure 4.2. In this and following chapters, results are often given for horizontal planes in a given height above the grate or in the vertical cross section in the middle of the furnace as seen in Figure 4.2.

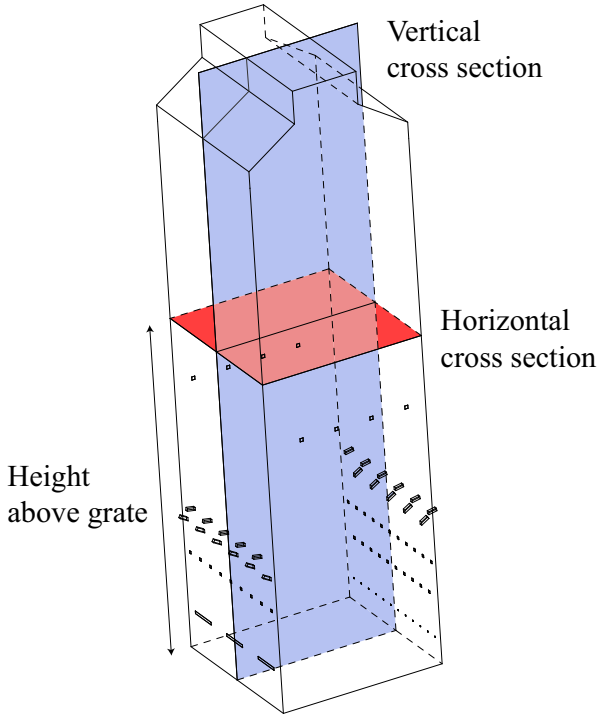

Figure 4.2: *Horizontal and vertical planes.*

Average values from a cross section can be calculated in several ways in FLUENT. Here, the average temperature is calculated as the area weighted average, whilst average mass fraction of CO is calculated as the mass weighted average, see FLUENT [2006] for definitions.

4.3 Simulation convergence I

The average temperature was monitored for each iteration in a horizontal cross section at heights of 7 or 10 meters. The monitored temperature should be converged for a solution to be converged. Similarly, the CO mass fraction was monitored in a horizontal cross section at 16 meters height and at the outlet, and should be converged for a simulation to be converged.

The flow was, in general, able to converge acceptably. Regarding residuals, seen in Figure 4.3, flow values (*e.g.* velocities, k etc.) was not decreasing further. This was similar for the residuals in the cases with insulated walls and the case with water injection, of which figures can be found in Appendix B.

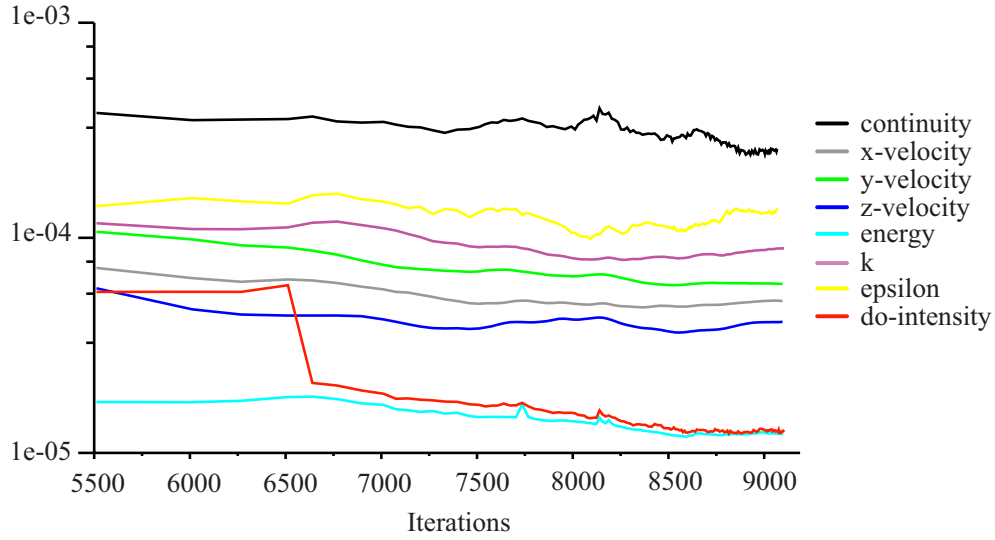

Figure 4.3: *Residuals history for flow variables for the standard case.*

The iteration history of average temperature in horizontal cross sections in 7 or 10 meters height is seen in Figure 4.4 for all cases. These show that the average temperature in the planes has converged acceptably. Together with the residuals, this indicates that the flow has converged acceptably.

However, the simulation encountered problems with fully convergence of the mass fraction of CO. This is seen from Figure 4.5, showing the iteration history of average CO mass fraction in the 16 meter cross section. As seen from the figure, the fluctuations of the CO mass fraction are in the order of 200 ppm. This was a problem as the CO values were supposed to be compared the cases in between.

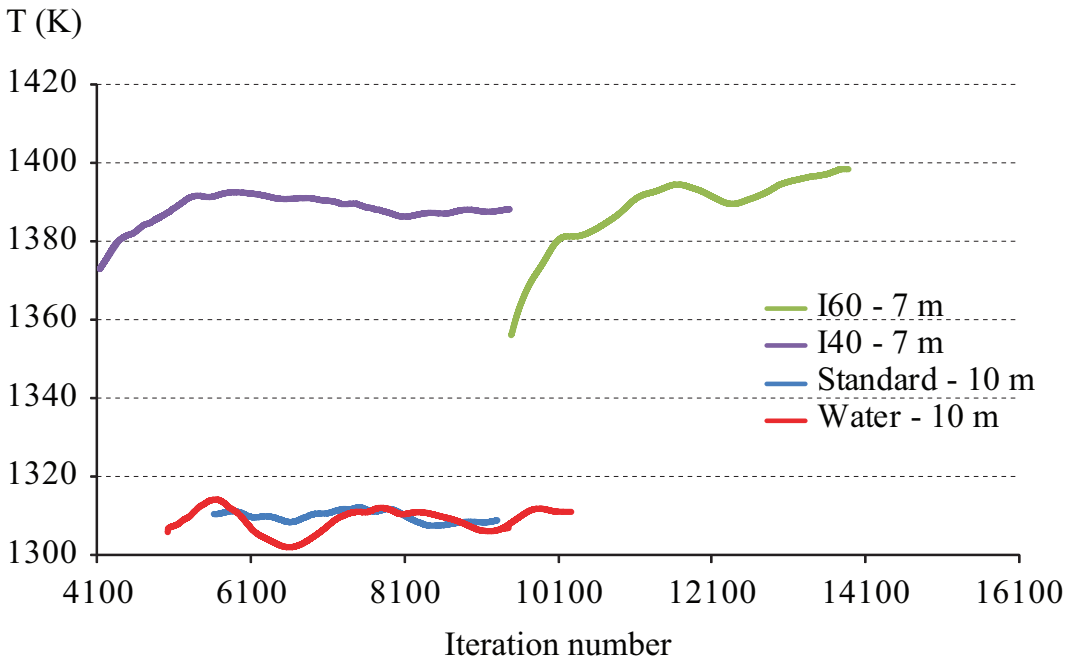

Figure 4.4: *Iteration history of average temperature in horizontal cross sections at 7 or 10 meters height.*

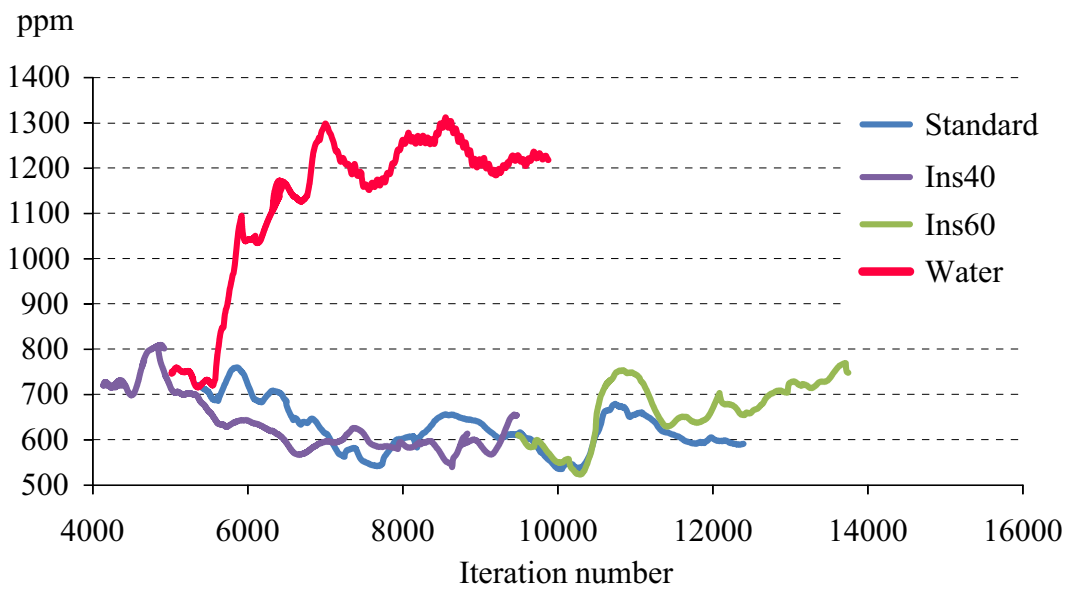

Figure 4.5: *Iteration history of average CO mass fraction in a horizontal cross section at 16 meters height.*

In the attempt to obtain convergence, different options were tried regarding:

- Under relaxation factors for species and energy.
- EDC time constant.
- Discretization schemes.
- Decreasing error tolerance on the ISAT table and chemistry integration.
- Varying the "'acceleration factor"' (Feature in FLUENT) for flow-chemistry interaction.

Bjørn Hjertager, who worked together with Bjørn Magnussen on developing the EDC model, was also contacted for advice, see Appendix D.2. The advice from Hjertager was to use an upwind scheme on all species equations. There were no convergence problems in the numerical solution of the kinetics. The flow was also converged acceptably, so it is most liable that the chemistry convergence problems was caused by small variations in the flow.

4.3.1 System stiffness

Therefore, the convergence problem of the chemistry was probably due to the model combination of flow and chemistry and the nature of that situation. The system of flow and chemistry is a highly stiff system of differential equations. A stiff system is a system of differential equations whose matrix has eigenvalues of very different magnitude [Kreyszig, 2006]. For the chemistry as well as the combination of chemistry and flow, this happens when the different time scales are of very different magnitude. The chemical timescales vary by several orders of magnitude. The smallest time scales are typically found in reactions with radicals, for example the OH reaction in Figure 3.4 with a timescale in the order of $\tau_{chem} = 10^{-5}$. Some time scales of the turbulence τ_t are much larger. For example, a large recirculation could have a timescale of say 1 s. The condition of the system is well expressed by the ratio between these timescales, named the Damköhler number, as seen in equation (4.3) [Fogler, 2006].

$$Da \equiv \frac{\tau_t}{\tau_{chem}} \approx \frac{1\text{s}}{10^{-5}\text{s}} = 10^5 \tag{4.3}$$

The very high Damköhler number $(Da >> 1)$ indicate that the chemistry is much faster than the flow, and that the system is very stiff. When solving a stiff system

numerically, an implicit method, for example the backward Euler method, is to be preferred [Kreyszig, 2006]. Using a pressure-based solver in FLUENT it is possible to solve the flow implicitly, but the species and energy equations have to be solved segregated from the flow. In this case, this implied convergence difficulties, for the combined solution of flow and chemistry. Perhaps better convergence could have been achieved using the implicit density based solver, where energy and species is solved implicitly simultaneously with the flow [FLUENT, 2006]. The density-based solver requires more available memory than the pressure based, as more values have to be stored in the memory while solving the implicit equations. For the models described in this study, about 13 GB of memory was required for the density-based solver, which exceeded the available memory on the system used.

4.3.2 Further efforts to obtain convergence

The fluctuations in the CO mass fraction did not have major implications on the flow. The fluctuations in the CO were in the order of 200 ppm. Considering the heat energy in 200 ppm, it would not affect the flow significantly whether it was combusted or not. This can be seen from the estimate in equation (4.4), of the ratio of the heat energy in 200 ppm CO to the heat release from the fuel in total.

$$\frac{y_{CO} m_{gas} LHV_{CO}}{Q_{fuel}} = \frac{200 \cdot 10^{-6} \cdot 27.5 \left(\frac{\text{kg}}{\text{s}}\right) \cdot 10.1 \left(\frac{\text{MJ}}{\text{kg}}\right)}{50 \ (\text{MW})} = 0.00011 \tag{4.4}$$

As seen from equation (4.4), the heat energy in 200 ppm CO corresponds to only 0.1% of the fuel heat release. Therefore, the impact of the fluctuations in CO mass fraction on the flow was most likely not at all significant.

To obtain a better convergence of the chemistry, when the flow was converged, the flow equations were disabled for the solution (*i.e.* the flow field was held constant) and the chemistry and energy were solved until convergence. This was done for all the simulations. This method is also proposed in the FLUENT manual [FLUENT, 2006]. After chemistry and energy convergence, the flow equations should be enabled again, to let the flow finally settle down. This was not done because it would have required one to two additional weeks of iterations.

4.4 Simulation convergence II

Keeping the flow field constant for the last 3-4000 iterations, the chemistry was able to converge. Residuals history for the standard case is seen in Figure 4.6, where the residuals for selected species are seen. Residuals history for the three other cases are found in Appendix B. The convergence of species residuals are acceptably. The

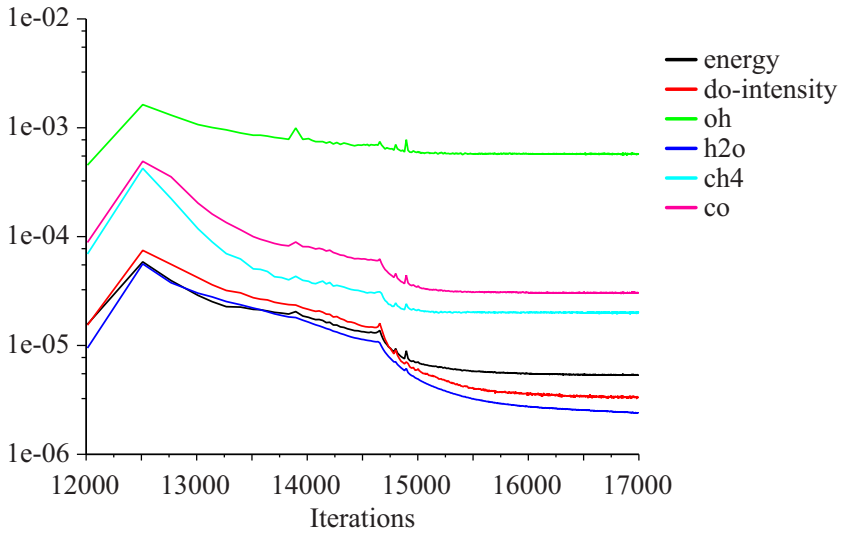

Figure 4.6: *Iteration history of average temperature in horizontal cross sections at 7 or 10 meters height.*

iteration history of average temperatures is seen in Figure 4.7 for all four cases. For all simulations the average temperature was almost constant for the last 2000 iterations, and was considered to be converged. Note that the temperature history of Ins60 has some fluctuations at about 14000 iterations. All other cases were continued from the standard case. In case Ins60 the flame position is slightly different from the other case (as will be shown in Section 7). This possibly explains the fluctuations, as this were the iterations where the flame position changed.

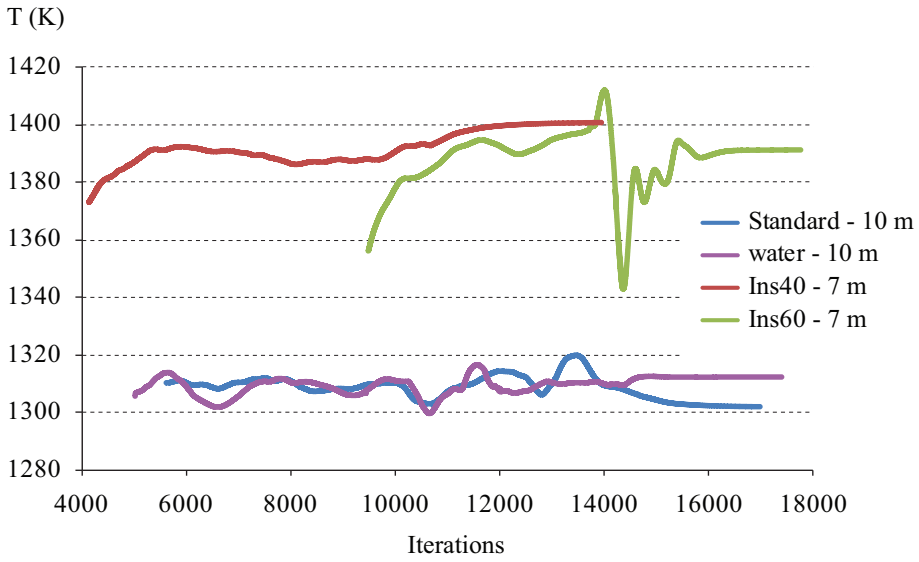

Figure 4.7: *Iteration history of cross sectional average temperature.*

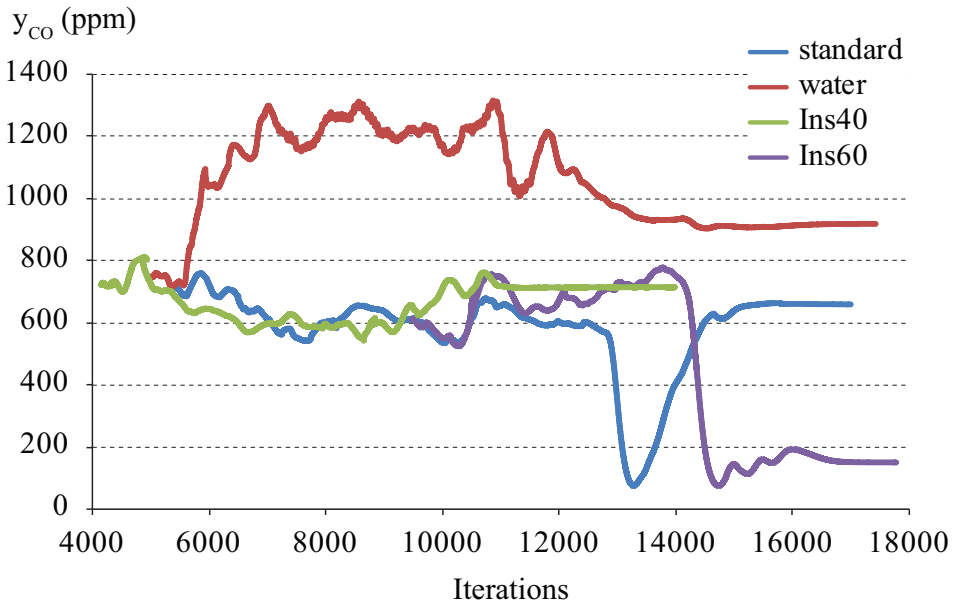

Figure 4.8: *Iteration history of average CO mass fraction in a horizontal cross section at 16 meters height.*

The average mass fraction of CO was also constant for the latter 2000 iteration in all cases, and were considered to be converged. This is seen for a 16 m horizontal cross section in Figure 4.8 and for the outlet in Figure 4.9.

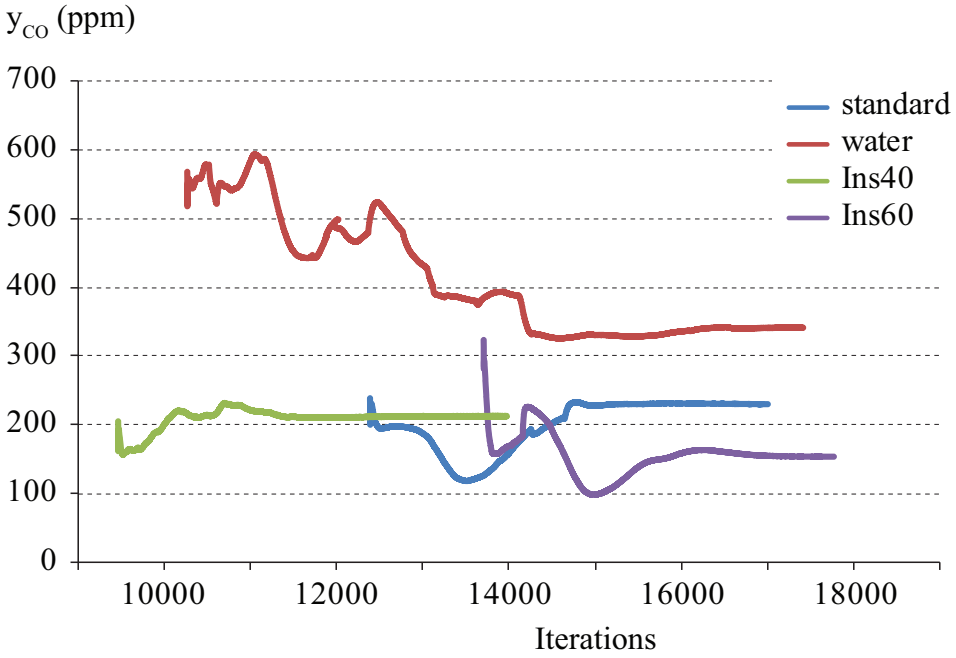

Figure 4.9: *Iteration history of average CO mass fraction at the outlet.*

4.5 Summary

Despite convergence difficulties, all simulations were acceptably converged, with the average CO mass fraction at the outlet being constant for about 2000 iterations. In cross sections inside the furnace, average temperatures and CO mass fractions were monitored, and these were constant for the last 2000 iterations.

To obtain convergence of the chemistry and energy, the flow and turbulence equations were disabled for the latter iterations. If further time had been available for the study, these should have been enabled again after chemistry convergence to get a final solution. However, the present results are considered as reliable in showing the right tendencies. The quantitative results could however be slightly different in a final solution.

Chapters 5, 7 and 6 are concerned with the CFD simulation results. Foremost, results from the standard case are presented. The results in a general picture are discussed and compared to the expectations. The general results *e.g.* flame position, ignition front and flow pattern, do not differ much between the different cases. Therefore, these are mostly presented for the standard case, unless significant differences exist. Subsequently, the results from the cases with insulated walls are presented and discussed in comparison with the standard case. Lastly, the results from the case with water injection is presented and discussed.

5 Standard case results

In the standard case, all boundary conditions were set as described in Section 2.4. In this section the results are discussed in general with regard to how they differ from, or are similar to what was expected.

5.1 General results

As mentioned in Section 2.4 the temperature right above the grate was expected to be rather low, but the condition in the upper furnace, which is of our primary concern, was expected to be comparable to a general biomass furnace. The cross sectional average temperature as a function of height above the grate is seen in Figure 5.1. As expected, the bottom region was rather cold until the gas was ignited about two meters above the grate.

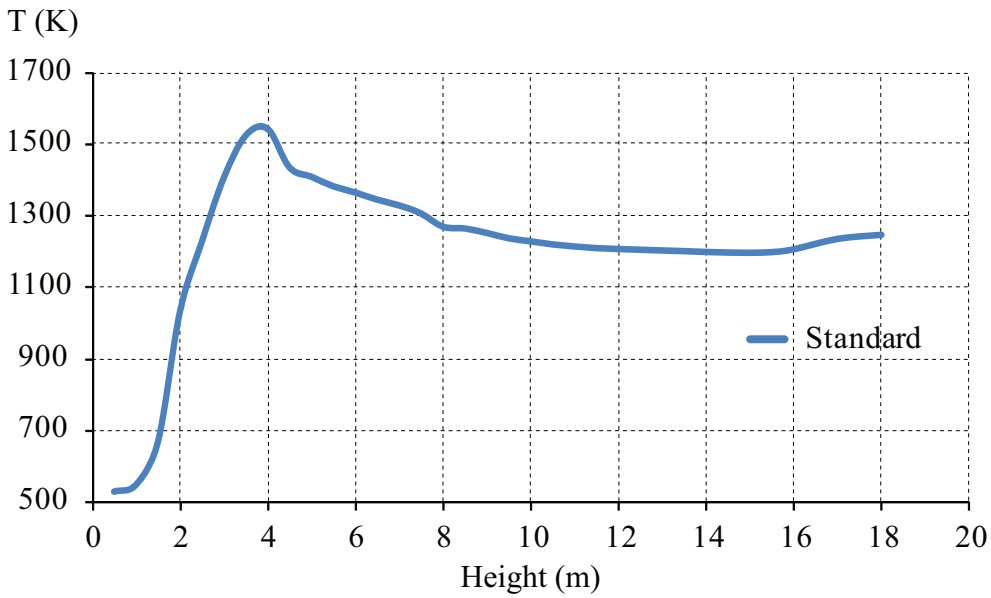

Figure 5.1: *Cross sectional average temperature in the furnace.*

Contours plot of temperature and logarithmic O_2 mass fraction in a vertical cross section is seen in Figures 5.2 and 5.3 respectively. As seen in 5.2 the temperature was generally higher in the front part of the furnace.

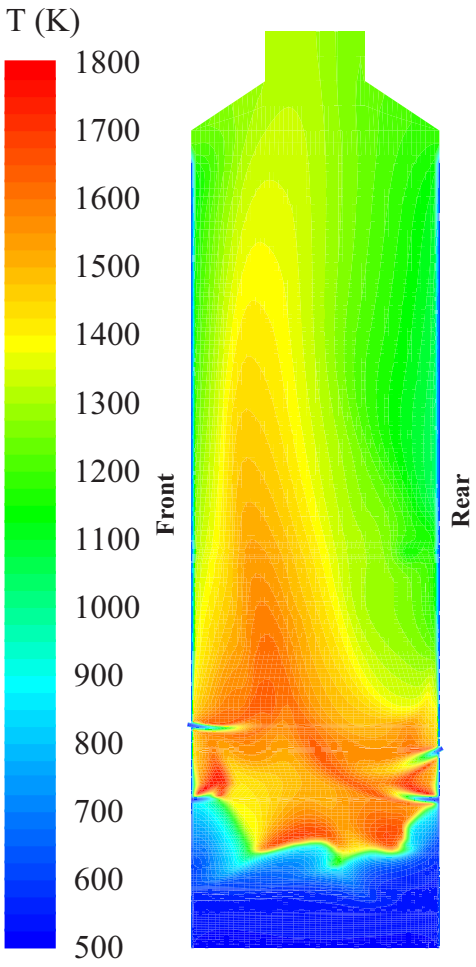

Figure 5.2: *Temperature in vertical cross section.*

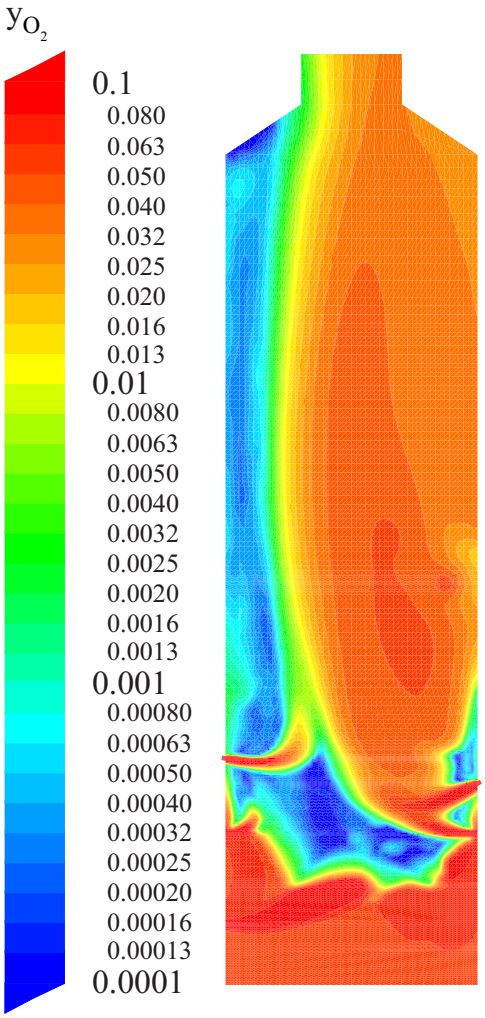

Figure 5.3: *Mass fraction of O_2 in vertical cross section. Logarithmic scale.*

As described in Section 2.4.2, 40% of the secondary air was injected from the front wall, while 60% was injected from the rear wall. The combustion products from the grate entered uniformly distributed over the grate area. Therefore, the rear part of the furnace was generally more oxygen rich than the front part, as seen in Figure 5.3. Because of this, the volatiles were combusted relatively rapidly in the rear part, but more slowly in the front part. Also, combustion products from the grate was pushed to the front part of the furnace as seen in Figure 5.4, by the greater volume of secondary air injected from the rear wall. As more volatiles are combusted in the front part, the temperature is also higher in this region. In contrast, more cold air was injected into the rear part, and consequently the temperature in this region is relatively lower.

This results also in an oxygen deficit zone along the front wall in the upper part of the furnace, as indicated in Figure 5.3.

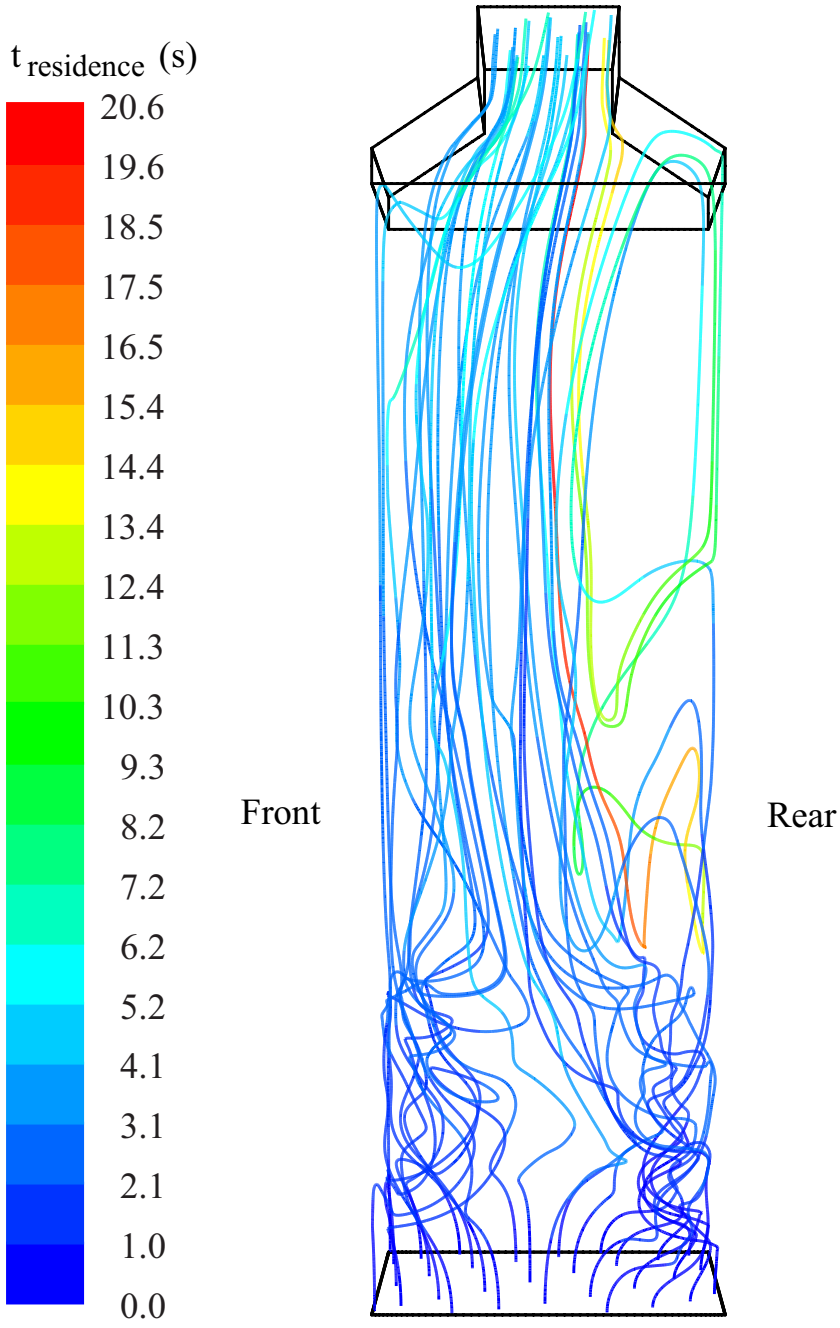

Figure 5.4: *Path lines of gas released from the grate, coloured by residence time.*

As seen in Figure 5.4, a large vertical recirculation zone was formed in the rear part of the furnace, resulting in a larger residence time for the gas in this region. Gas from the front part of the furnace had residence times of approximately 3 to 6 seconds,

whilst gas from the recirculation zone had a residence time of approximately 12 to 20 seconds.

The low mass fraction of oxygen, and the short residence time in the front part of the furnace, resulted in high CO mass fractions in this region, even though the temperature was quite high. Conversely, the high fraction of oxygen and the relatively long residence time resulted in low CO mass fractions in the rear part of the furnace. As seen in Figure 5.5, a band of high CO mass fraction was formed in the front part of the furnace.

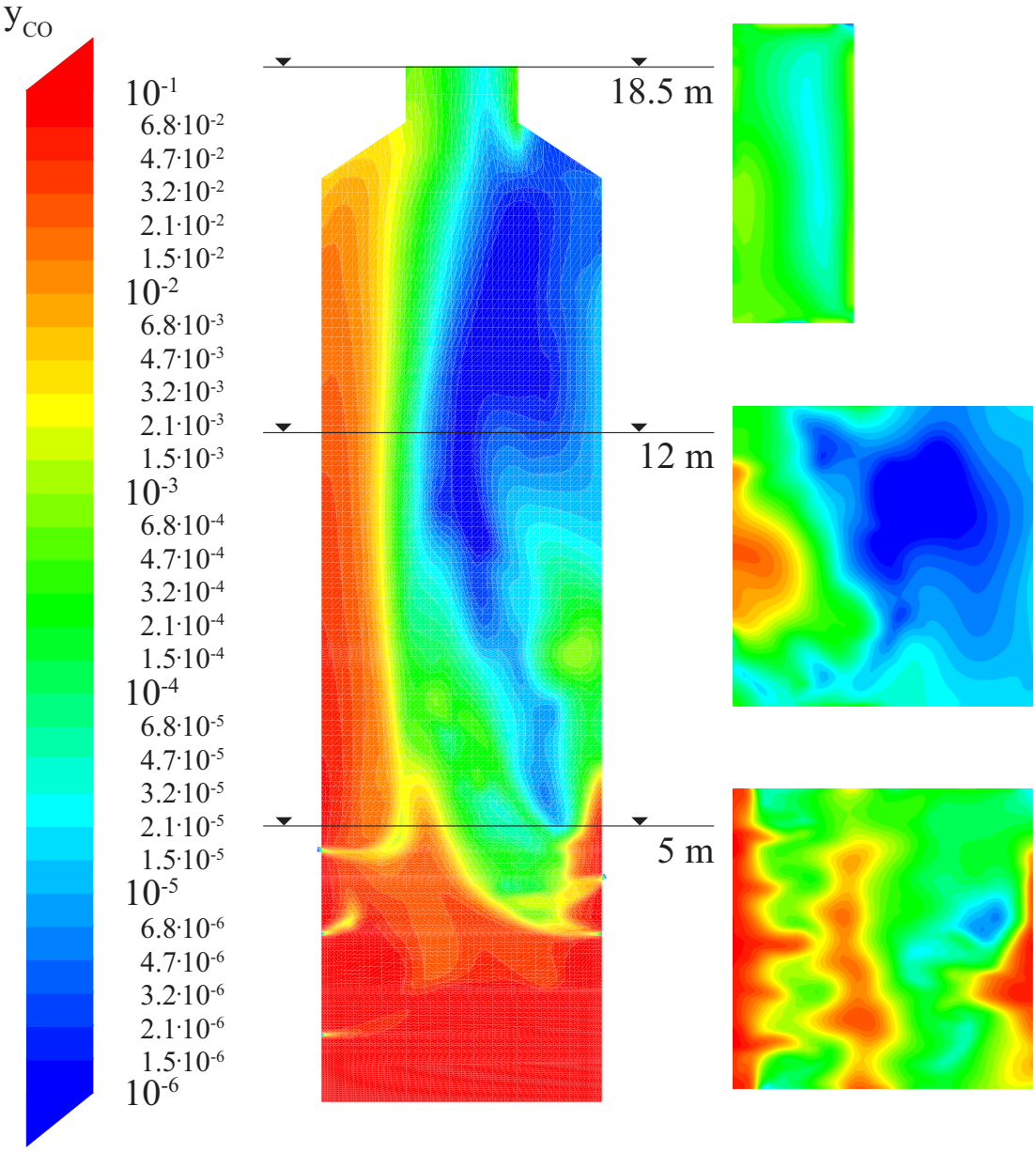

Figure 5.5: *Mass fraction of CO in vertical cross section and three horizontal cross sections. Logarithmic scale.*

In the upper part of the furnace, the band of CO was most significant in the middle of the front part, as seen from the 12 m horizontal cross section. The traces from the band of CO are also seen in the outlet, in 18.5 meters height, where the CO mass fractions in the front side of the outlet are slightly higher than in the rear side and the middle. Right above the primary combustion zone, at a height of 5 meters, the mass fractions of CO are relatively high in both the front part and the rear part of the furnace as seen from the 5 m horizontal cross section.

The conditions in the upper furnace were generally comparable to the conditions found in many biomass furnaces. The temperatures were relatively low, which of course was due to the high moisture content in the fuel. Bands of CO with mass fractions of this order, are often found in biomass furnaces, see for example [Scharler & Obernberger, 2000], [Dong & Blasiak, 2001] and [Yang et al., 2007]. These studies also show a band of high CO fraction in a band of high temperature. In this way, the results in a general picture were as expected and the conditions in the upper furnace comparable to a biomass furnace. The first two meters are not comparable to a grate fired furnace, because the temperatures are lower than normally observed. Temperatures right above the grate are often in the range of 800 K to 1000 K, for example in measurements by Lans [1998].

5.2 Jet resolution

An adequate resolution of the secondary and tertiary air jets are important in order to model the overall turbulence and flow field as well as the gradients in species composition and temperature. The entrance surface of the air jets were modelled relatively simple, as they did not extend much outside the furnace, and were only meshed by 16 faces. However, the effect of the jets in the freeboard of the furnace seemed to be reasonably modelled. In figures 5.6 and 5.7, contours of velocity magnitude and temperature respectively, are seen in a 3 m horizontal cross section near a secondary jet entrance. Note that the effects of nearby jets are seen near the boundaries of the figures. The jet seen in the figures is from row SA_3. As seen from the figure both velocity and temperature are reasonably resolved around the jet entrance. The velocity profile is as expected for a free jet, and the gradients in velocity were reasonable resolved. Similarly, the temperature gradients are reasonable resolved.

In the region around the air jet, high mass fractions of OH radicals were found, as seen in Figure 5.9. OH radicals are formed because oxygen from the air are mixed with the

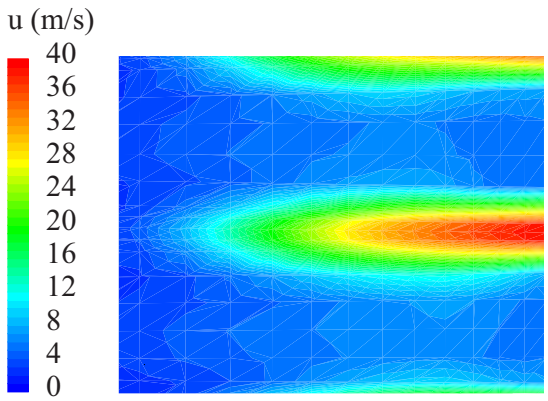

Figure 5.6: *Velocity magnitude in 3 m horizontal cross section.*

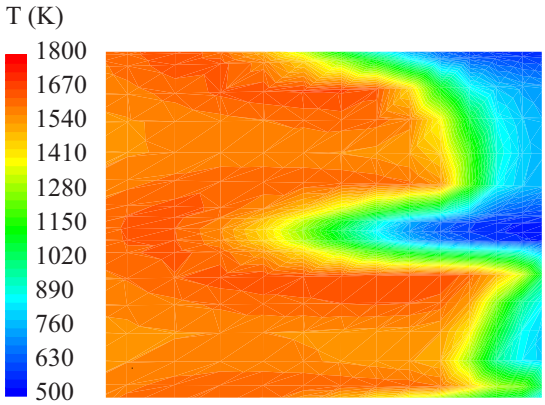

Figure 5.7: *Temperature in 3 m horizontal cross section.*

hot combustion gas. Moreover, it is seen from Figure 5.8 that high rates of reduction of CO are found in this same area (the reduction rate are the negative of the creation rate). This supports the expectation of OH radicals being important for the combustion of CO also under the combustion conditions in the primary combustion zone in a furnace. The resolution of the phenomenon of the chemistry around jet entrance which is seen in Figures 5.8 and 5.9 are well captured by the model.

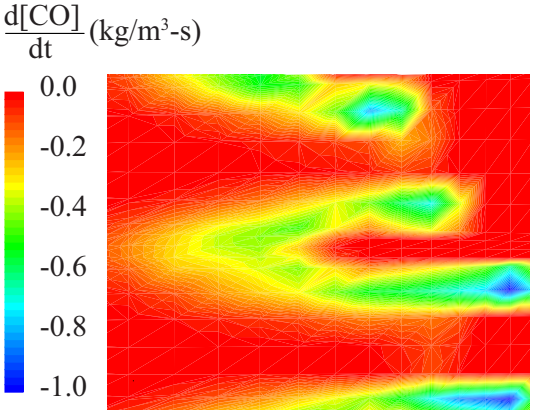

Figure 5.8: *Net creation rate of CO in 3 m horizontal cross section.*

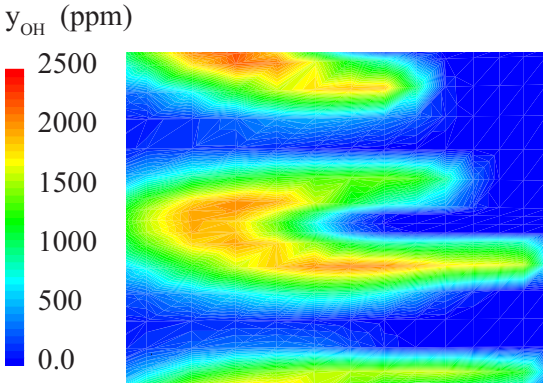

Figure 5.9: *Mass fraction of OH in 3 m horizontal cross section.*

Due to the jets, local circulation were also formed, as seen in Figure 5.10, which shows velocity vectors in a 5 m horizontal cross section (projected onto the cross section plane).

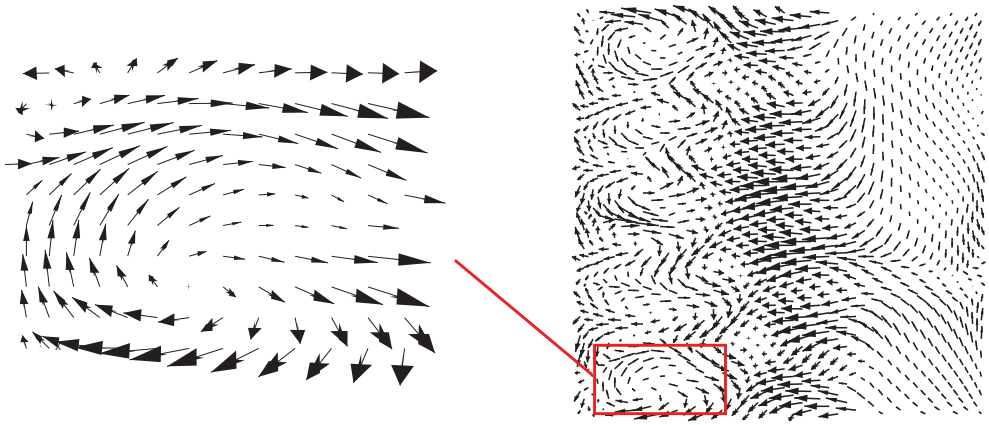

Figure 5.10: *Velocity vectors in a 5 m horizontal cross section.*

5.3 Summary

Despite of the simplified geometry, many important phenomenon of grate fired furnaces were well modelled. The entrance region of the secondary air jets was well resolved, and local circulations were formed by the jets, as is often the case, for an example see Yin et al. [2008].

The overall flow pattern in the upper furnace was, that a large vertical recirculation zones was formed in the rear side of the furnace, causing the mean flow to be pushed towards the front side. Consequently, more of the combustion took place in the front part of the furnace, causing a deficit of oxygen in this region. Therefore, a band with high CO mass fractions was formed in the front part of the upper furnace, as is often the case in biomass furnaces.

In general, the conditions in the furnace were, in several aspects, comparable to a normal biomass furnace, except for the region right above the grate. Concerning both the overall and local flow patterns, the results were realistic. Temperatures were as expected, and the chemistry was satisfactory solved. The average mass fraction of CO in the outlet was however, not as high as expected.

6 Water injection case

In the case with water injection, water was injected together with air from the two upper rows of secondary air jets, SA_6 and SA_9. $0.3 \frac{kg\ \text{water}}{kg\ \text{air}}$ was injected, corresponding to a total injection of 0.35 kg water per second.

6.1 General results

The addition of water did not cause significant changes in the average temperature. At the outlet, the difference in average temperature was 6 K, which is below the expected 19 K but in the same order.

However, the difference in mass fraction of CO was more significant, with a difference of 112 ppm at the outlet. This corresponds to an increase in CO mass fraction at the outlet of about 50 % in the case of water compared to the standard case. This is also seen in Figure 6.1, which shows the average CO mass fraction of the two cases as a function of height above the grate.

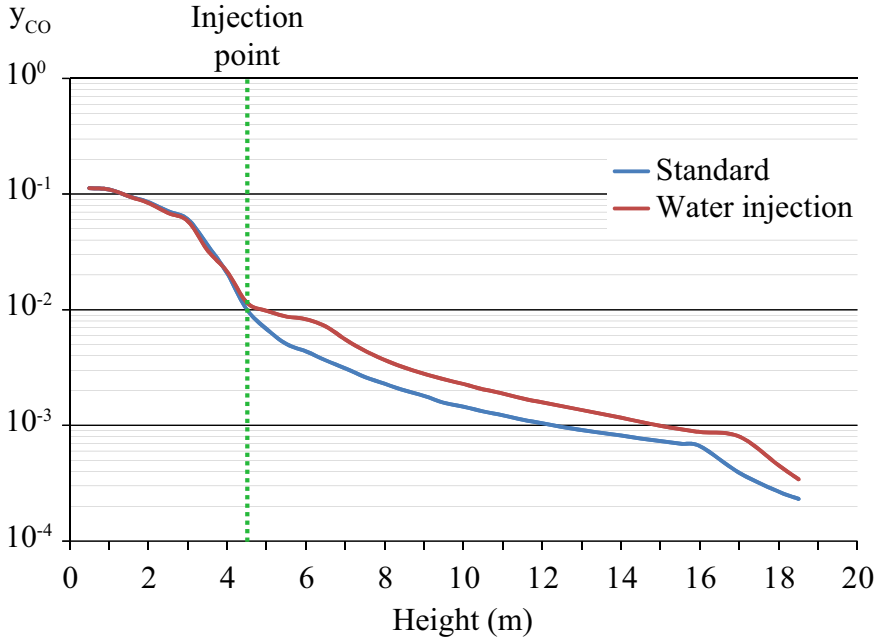

Figure 6.1: *Horizontal cross sectional average mass fraction of CO as a function of height above grate.*

In Figure 6.1 it is seen, that the difference in average CO mass fraction became significant at the height of the water injection point (4.5 m) as indicated on the figure. This indicates that the difference in CO mass fraction was caused by the injection of water from the upper secondary air jets, SA_6 and SA_9.

In Figure 6.2 temperature contours are seen for the standard case and the water injection case in the vertical cross section. In the case of water injection, the flame seems to be broader, and with slightly lower peak temperatures above the upper secondary air jets.

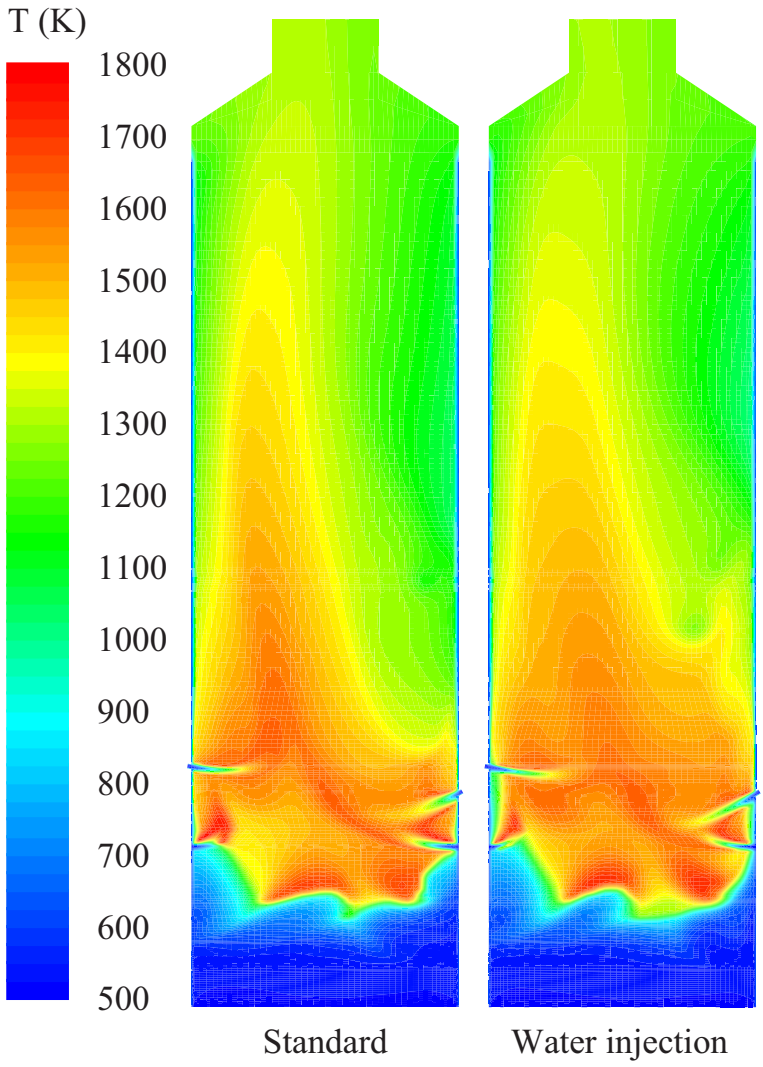

Figure 6.2: *Temperature in vertical cross section.*

6.2 Near jet region

Path lines for the air injected from the two rows of jets, SA_6 and SA_9, is seen in Figure 6.3 and Figure 6.4 for the two cases. From the Figures 6.3 and 6.4, a difference between the two cases in the jet penetration depth are seen. Due to the addition of water, the mass injected from the inlets, SA_6 and SA_9, was increased, causing an increased jet velocity compared to the standard case. From the figures, it is also seen that the oxygen in the secondary air are rapidly consumed.

The inlets were inclined 15^o downward. Therefore, if local temperature decreases existed, they should be located just below the inlets, in a height of about 4.3 to 4.5 m above the grate.

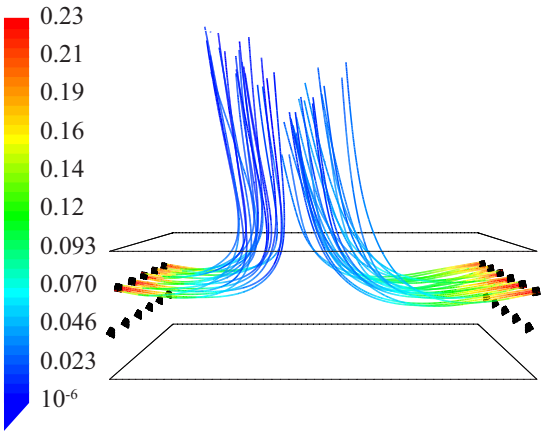

Figure 6.3: *Standard case: Path lines from secondary air jets SA_6 and SA_9 coloured by oxygen mass fraction.*

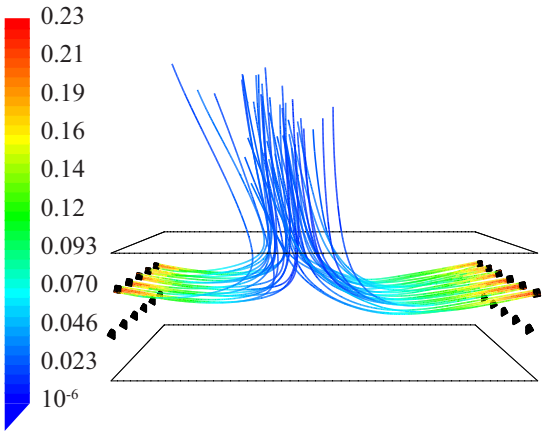

Figure 6.4: *Water injection case: Path lines from secondary air jets SA_6 and SA_9 coloured by oxygen mass fraction.*

Figure 6.5: *Location of three horizontal cross sections.*

Four horizontal cross section located just below the inlets are sketched in Figure 6.5. In Figure 6.6 the temperature in horizontal the four cross sections are seen for both the standard case and the case with water injection. Studying the figure, attention should be given to the local temperature decreases, which is causes by the SA_6 and SA_9 jets.

Comparing the cross sections located in the same heights it is seen, that stronger temperature decreases were generally present in the case of water injection. In the 4.45 m cross section, cold spots are seen in front of the inlets in both cases. In the cross sections 4.30 m and 4.35 m, a greater number of cold spots are seen in the case of water injection. The temperature in the cold spots was also lower in the water injection case, which is most pronounced in the 4.40 m cross section.

These local cold spots were most likely the origin of the increased mass fractions of CO in the water injection case. It was however hard to locate corresponding spots of poor CO reduction. In Figure 6.7 three of the planes from Figure 6.6 are seen, coloured by net creation rate of CO. CO reduction spots (*i.e.* negative values) are located in the region between oxygen rich air jets and hot combustion gas. Comparing the cross sections, no significant differences are seen.

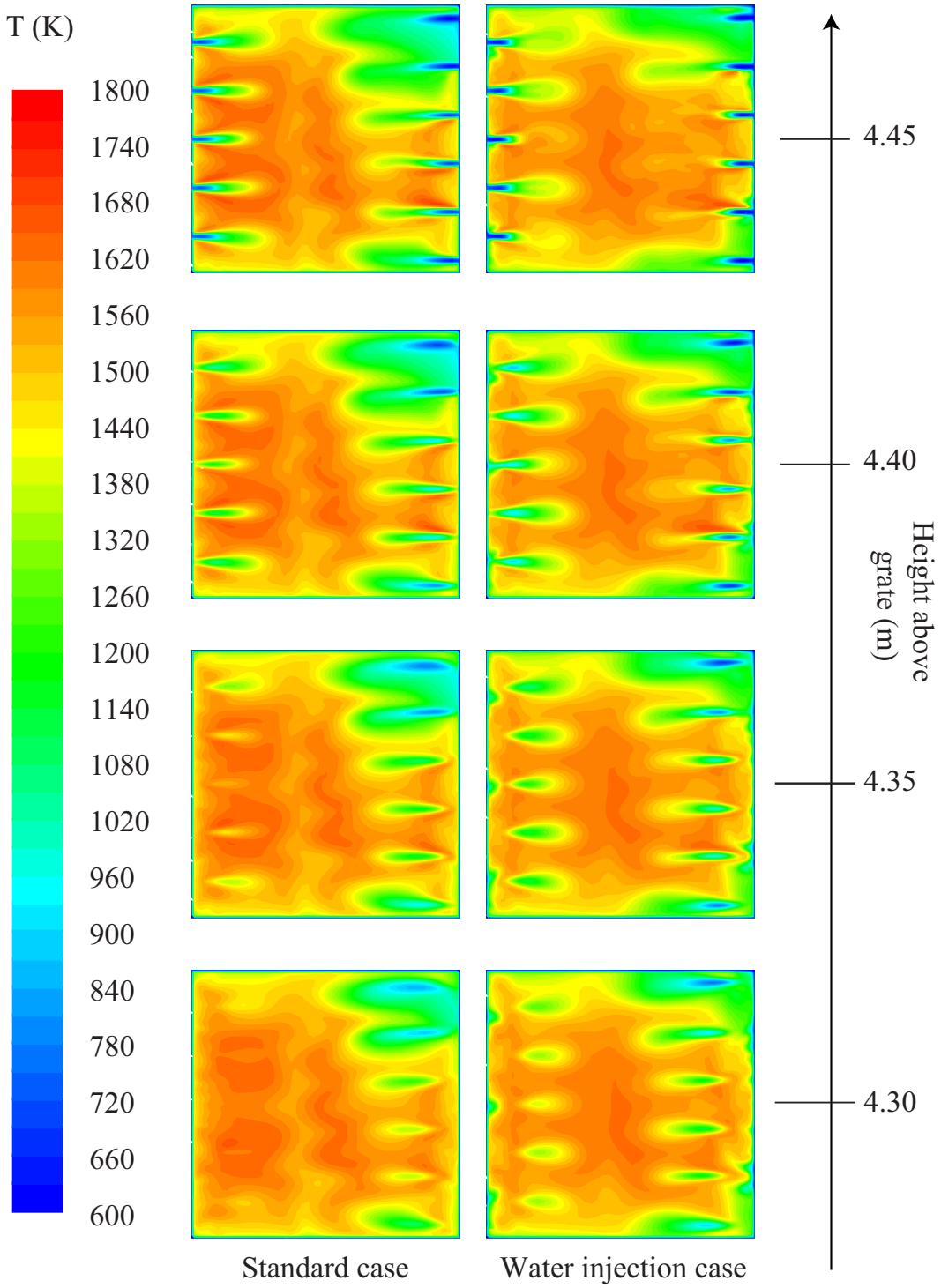

Figure 6.6: *Temperature in horizontal cross sections.*

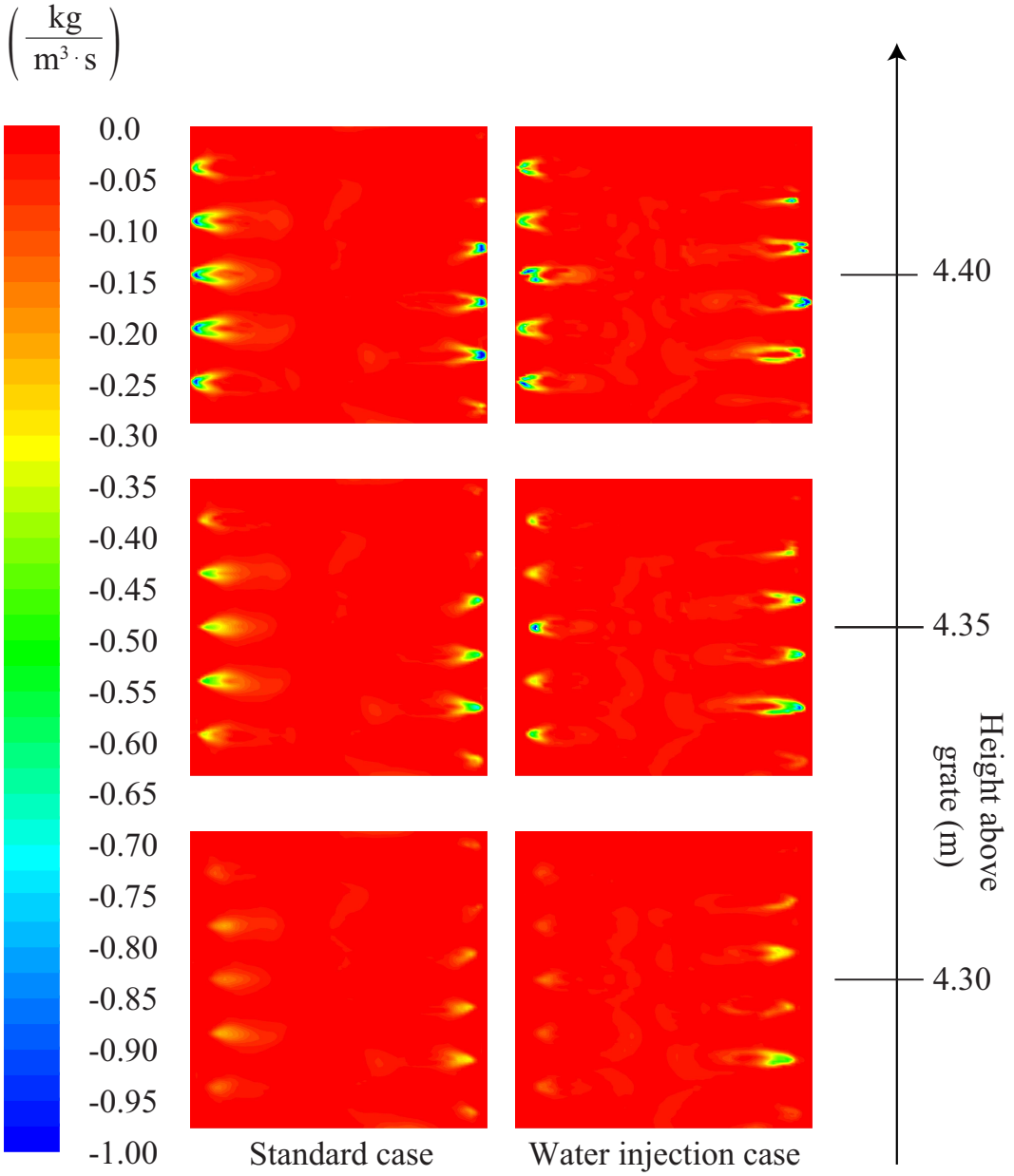

Figure 6.7: *Net creation rate of CO in horizontal cross sections.*

The average rate of reduction of CO differ most significantly from approximately 4.5 to 6 meters height as could be seen by studying Figure 6.1, (as the average net creation rate of CO are proportional to the curve gradient). Above the inlets, in a height of 5.5 m, the differences in CO creation rates were more significant as seen from comparing the cross sections in Figure 6.8.

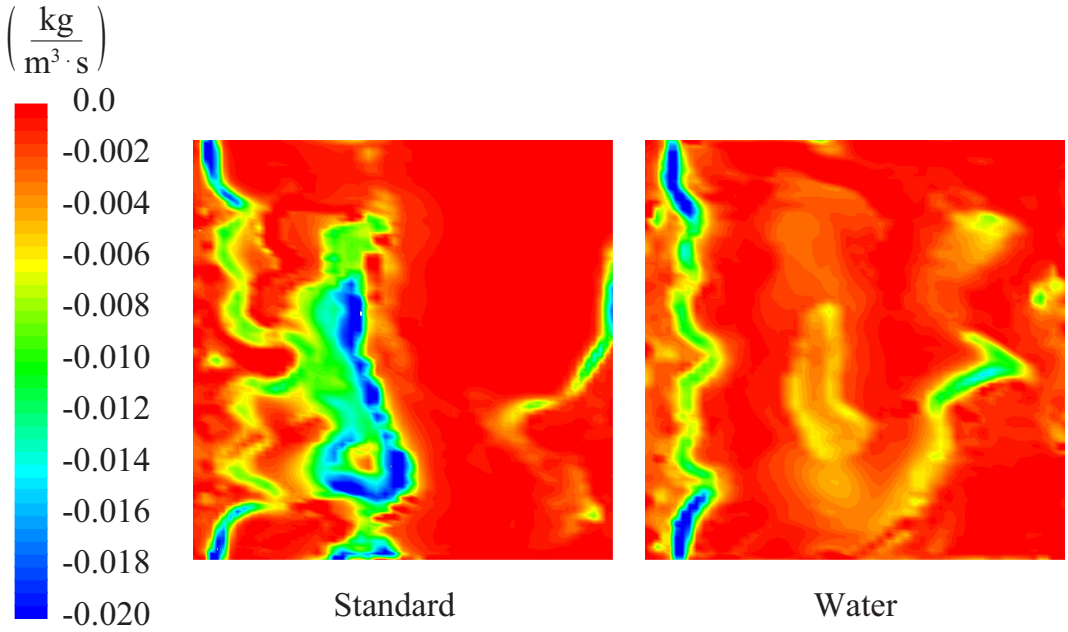

Figure 6.8: *Net creation rate of CO in a 5.5 m horizontal cross sections.*

The level of turbulence are also important for the reduction rate of CO. When solving chemistry with the EDC, both the turbulent kinetic energy and its dissipation rate influence the calculation of the species source term, as described in Section 2.3.1. Increasing k decrease the species source term, while increasing ϵ increase the source term. Studying the equations one would find, that ϵ effect the source term is strongest. The eddy dissipation rate for the 5.5 m horizontal cross section is seen in Figure 6.9. The eddy dissipation rate is clearly increased in the case of water injection. Therefore, the differences in the turbulence were most likely not the cause of the decreased CO reduction rate.

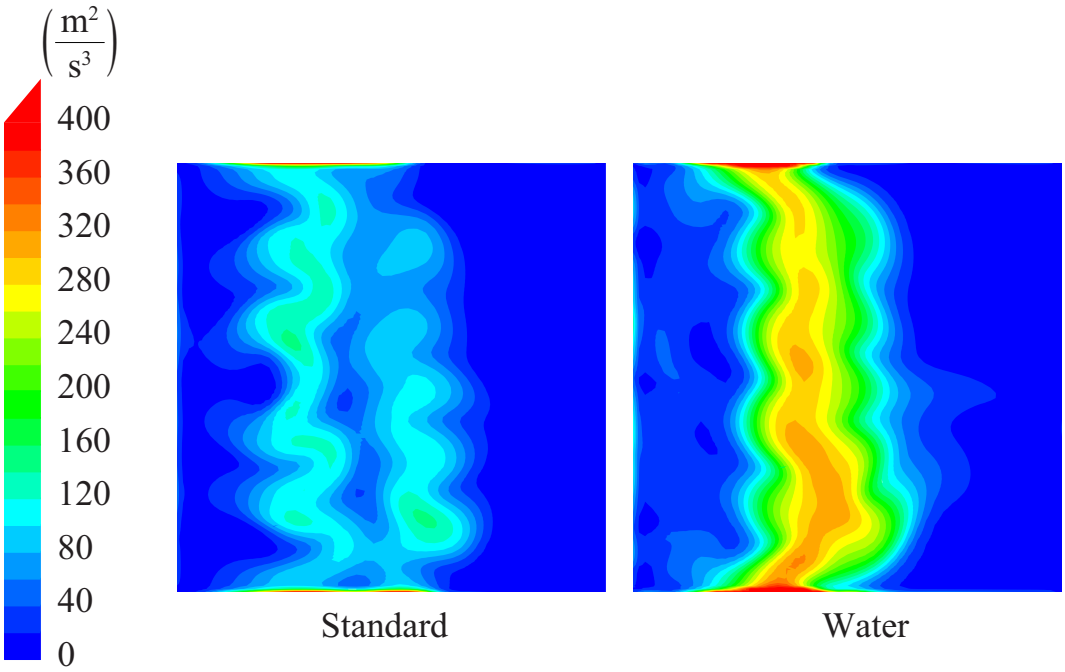

Figure 6.9: *Eddy dissipation rate in a 5.5 m horizontal cross section.*

6.3 Summary

The injection of steam together with the secondary air in the upper rows of secondary air jets was modelled. The addition of steam did not cause a significant decrease in the cross sectional average temperature. Still, the reduction of CO was inhibited exactly from the water injection point. The average CO mass fraction at the outlet was increased by 50% compared to the standard case.

Local "'cold spots"', where the temperature was largely decreased, was observed near the injection point. This caused possibly the inhibited the CO reduction, although no corresponding spots with significantly reduced rate of CO burnout were observed.

7 Insulated walls cases

In the two cases where parts of the furnace wall were insulated, increased temperature were, of course, expected in this region of the furnace. The insulated sections were both warmer and had a lower emissivity than the standard walls, which reduces the radiative and convective heat transfer.

7.1 General results

In Figure 7.1 the average temperature is seen for the standard case, case Ins40 and case Ins60.

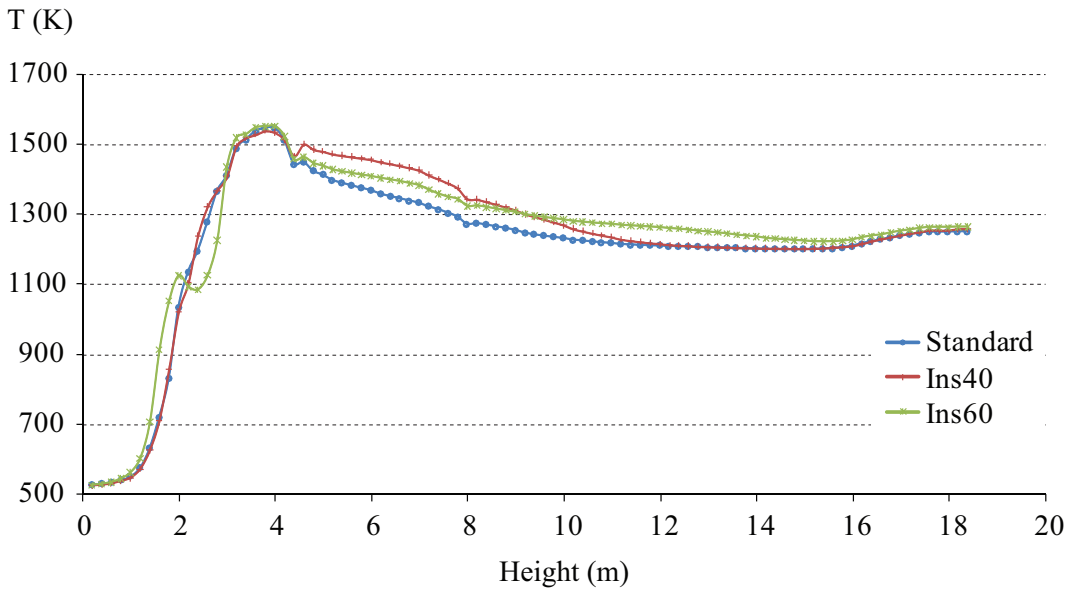

Figure 7.1: *Average temperature (K) as a function of furnace height (m).*

The effect of the insulation is seen in the average temperature. Notice that the average temperatures in case Ins60 are different at a height of about 2 meters. The temperature differences in the region of insulation are more easily seen in Figure 7.2.

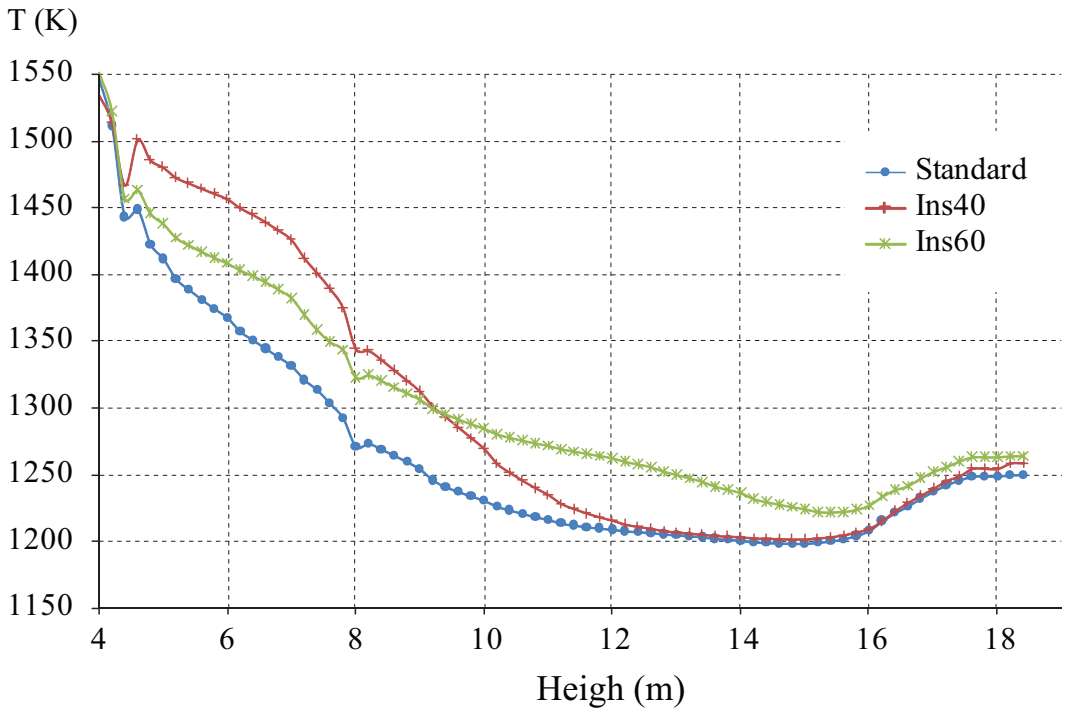

Figure 7.2: *Average temperature (K) as a function of furnace height (m).*

As seen from the figure, increased average temperature in the upper furnace were obtained in both cases.

- In case Ins40, the walls were insulated from 5 to 7 meters height, which resulted in a temperature increase in the order of 70 K in the region from 5 to 10 meters height.
- In case Ins60, the insulation area was from 6 to 9 meters height. In this case the temperature increase was in the order of 50 K in the region from 6 to 14 meters height.

The average temperature increase was highest in case Ins40 because the insulation was placed near the high temperature region in the furnace. On the other hand, the temperature increased only for about 5 meters. In case Ins60, the insulation was placed higher in the furnace. The insulation area was larger and therefore the temperature was increased for a larger region of the furnace. This reflects the expectations to the results. The temperature differences between the cases could also be recognized in Figure 7.3 if studying the figure with attention. What is more clear, is that the flame position in the lower furnace in case Ins60 is different from the other cases as marked by the arrow.

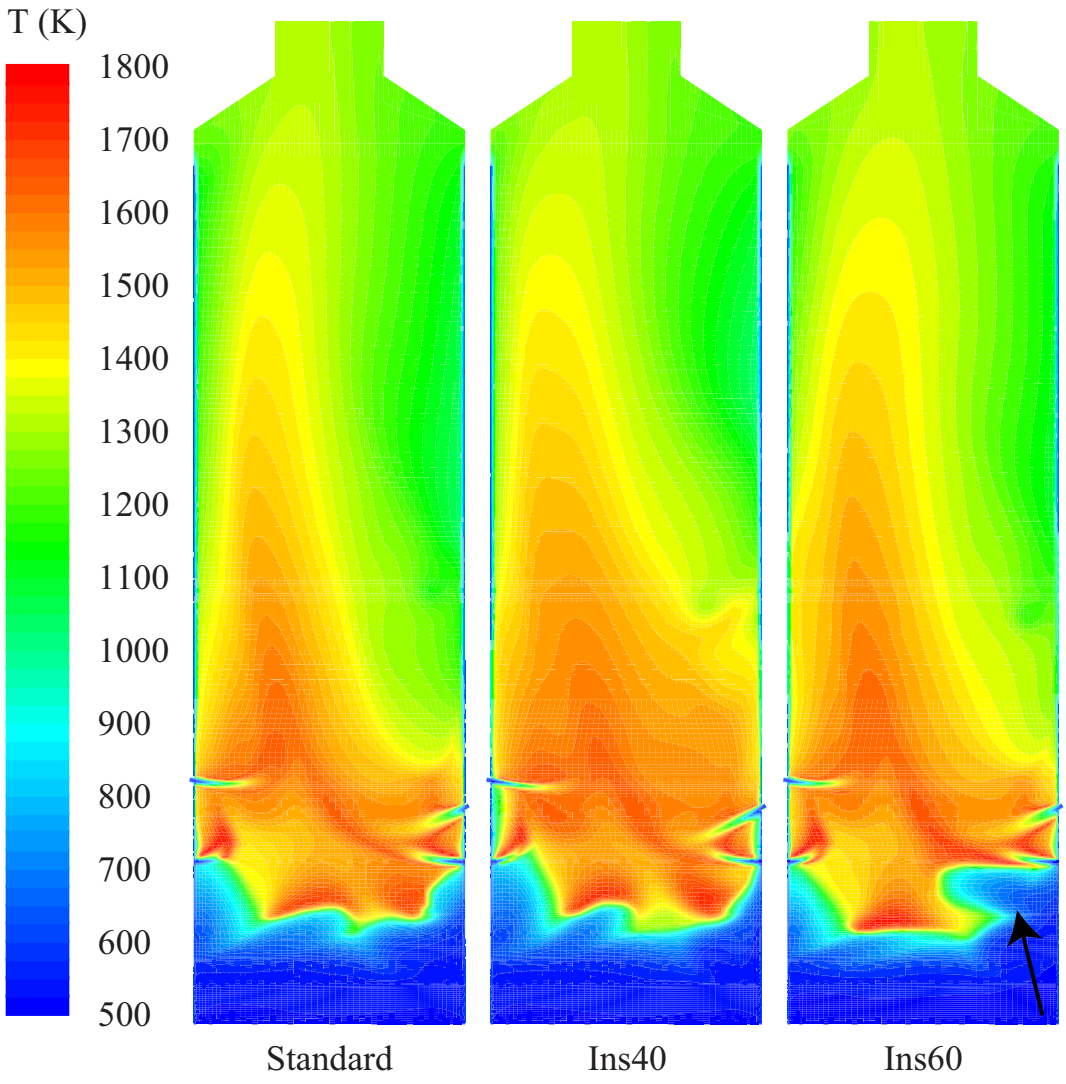

Figure 7.3: *Temperature in vertical cross sections.*

The increased temperature was expected to improve the CO burnout. The cross sectional average mass fraction of CO is seen in Figure 7.4 for the standard case and the cases with insulation. For case Ins40, the average mass fraction of CO was slightly higher, compared to the standard case, but decreases rapidly in the upper two meters of the furnace and is slightly lower at the outlet.

Concerning case Ins60, the reduction of CO was improved from a height of 6 meters, which was the starting point of the insulation. However, the average temperature was increased, compared to the standard case, from a height of 5 meters. This could indicate, that not only the average temperature, but also the near wall temperature are was important.

At the outlet, the average mass fraction of CO in the gas exiting the furnace were as given in Table 7.1.

Case	Mass fraction (ppm)	Improvement compared to standard case (%)
Standard	231	-
Ins40	213	8
Ins60	155	33

Table 7.1: *Mass-weighted average mass fraction of CO in outlet.*

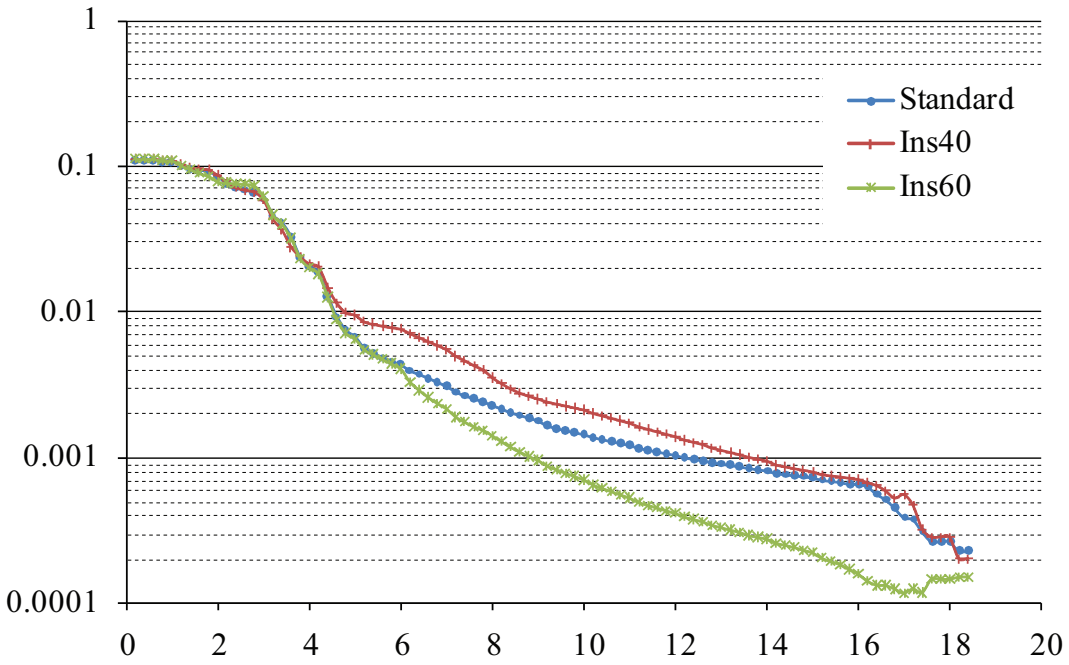

Figure 7.4: *Average CO mass fraction as a function of height. Logarithmic scaled.*

7.2 Thermal boundary layer

One thing to note is, that the CO level in the standard case was relatively low, but also that the difference between the standard case and the insulated cases was small. However, AET have experienced a more significant difference in practice [AET, 2009]. The reason for this could be that the phenomenon that causes the high CO levels in practice was not well captured by the model. One explanation could be that the high CO levels in practice is not in the mean flow but is created in the thermal boundary layer near the cold walls. In this case the grid resolution near the walls was too crude

to capture the chemical effect of the cold walls. In Figure 7.5 the temperature contour in a corner of a horizontal cross section in 12 m height is seen. As seen from the figure, the resolution of the temperature gradient near the walls was acceptable, and the resolution was sufficient for the walls effect on the mean flow. However, the EDC model models the chemistry based on a fine scale temperature T^* which is based on the cell values and does not take into account the gradients. A contour of the fine scale temperature is seen in Figure 7.6 for the same plane as Figure 7.5.

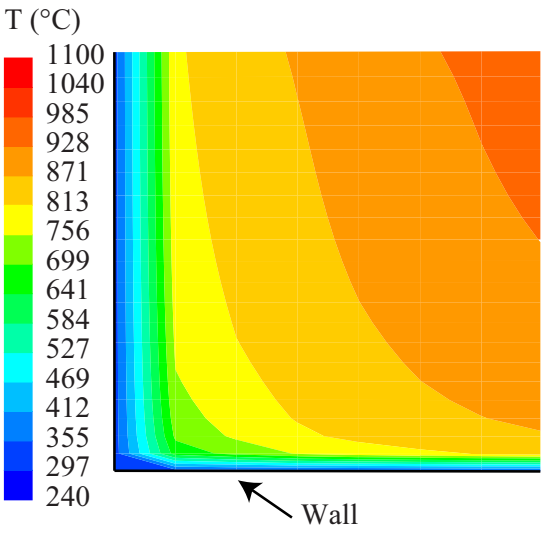

Figure 7.5: *Temperature (^{o}C) contour of a corner of a horizontal cross section in 12 m height.*

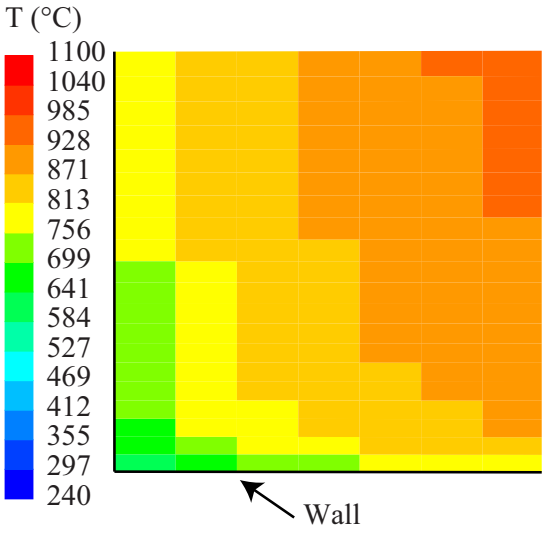

Figure 7.6: *Fine scale temperature (^{o}C) contour of a corner of a horizontal cross section in 12 m height.*

This suggests that the high CO levels when combusting wet fuel are due to convective interaction with the cold walls rather than due to a low temperature in the mean flow. This phenomenon was not modelled well by the model used. This means that to capture the phenomenon causing high CO levels in CFD simulations, a high resolution mesh near the walls boundaries is important. Moreover, if the phenomenon of convection with walls cause the high CO emissions, the chemistry needs to be modelled by a method like the EDC model, where temperature influences the kinetics.

7.3 Summary

The effect of insulating the walls was clearly seen in the cross sectional average temperature in the furnace. A reduced mass fraction of CO at the outlet was observed in both cases. In case Ins40, the reduction was not significant. In case Ins60, the CO

mass fraction at the outlet was decreased by 33% compared to the standard case. In this case, it was clear, that the reduction in outlet CO fraction was caused by the insulation. Perhaps the CO reduction was not only due to an increased average temperature, but also due to local phenomenon near the walls.

In practice, the CO reductions obtained by insulating furnace walls are more significant than found in these cases. The near wall convective cooling of the gas was not well captured by the model used. This was probably the reason for, that the outlet fraction of CO in the standard case was not as high as is often observed. For the same reason, the CO reduction obtained by insulating the walls was not as significant as experienced in practice [AET, 2009].

8 Conclusion

In this study, CO burnout in biomass furnaces was investigated through several numerically based studies. The kinetics of the combustion were studied with an extensive parameter variation and four CFD simulations with detailed chemical kinetics were carried out.

In the study of the combustion kinetics it was found that temperature plays an important role in the burnout of carbon monoxide. For improved CO reduction, the temperatures in the upper furnace should be maintained above 1300 K for an increased part of the total residence time. At temperature temperatures below about 1200 K the CO reduction process was significantly inhibited.

Extensive variation of species composition showed that considering the kinetics only, addition of water had a positive influence on CO reduction. The effect was, however, not as significant as the influence of temperature.

The CFD simulations of a simplified furnace exhibited overall conditions comparable to normal biomass furnaces. Overall flow and temperature patterns were well captured by the model, and results were realistic. The resolution of the effects of air jets was excellent regarding both chemistry and flow patterns.

Average values at the furnace outlet are summarized in Table 8.1 for all four simulation cases.

Case	**Mass fraction (ppm)**	**Outlet temperature (K)**
Standard	231	1250
Water injection	343	1244
40 m^2 insulated	213	1289
60 m^2 insulated	155	1264

Table 8.1: *Average values at furnace outlet.*

In the case where water was injected the outlet mass fraction of CO was increased by 50 %. This originated from local spots of low temperatures caused by the presence of water. Although the amount of OH radicals was significantly increased by the water injection, cold spots inhibited the CO burnout.

The two cases where areas of the furnace wall was insulated, CO emissions were reduced. The reductions were most significant in the case where 60 m^2 (19%) of the wall was insulated. Due to the insulation, the cross sectional average temperature was increased. The improved CO burnout was a consequence of the increased mean temperature. In practice differences that are more significant are observed by insulating the walls.

The practical phenomenon, which was not well resolved by the model used, was convection in the thermal boundary layer. Convective heat transfer between the gas and the cold wall could create cold regions with poor CO burnout. To resolve this phenomenon an improved resolution of the wall boundary layers would have been necessary. To resolve the phenomenon, finite rate chemistry have to be implemented, for example by using the EDC model. This should be considered in numerical models of biomass furnaces, where estimation of the CO emissions is desired.

In general, the effects of different temperatures, the creation of radicals etc. was very satisfactory modelled using a detailed kinetic mechanism with the EDC, features that cannot be resolved with and Eddy Break Up model or similar. Using the Eddy Dissipation Concept, extensive information on the chemistry was obtained. However, the simulations were computationally expensive. In numerical studies of full biomass furnaces, it would be convenient to identify amenable reduced mechanisms with about 20 reactions. Implementing a reduced mechanism with EDC produce better results than the widely used choice of EBU or similar models with regard to CO emissions.

Bibliography

AET (2009). Personal conversation with AET .

Cantera (2008). Open source software for reacting flows. version 1.7, www.cantera.org.

Cengel, Y. A. (2006). *Heat and mass transfer a practical approach*. McGraw-Hill.

CFD Online (2009). Online center for Computational Fluid Dynamics. www.cfd-online.com.

Dagaut, P., Lecomte, F., Mieritz, J., & Glarborg, P. (2003). Experimental and Kinetic Modeling Study of the Effect of NO and SO2 on the Oxidation of CO-H2 Mixtures. *International Journal of Chemical Kinetics*, *35*(11), 564–575.

Dong, W. & Blasiak, W. (2001). CFD modeling of ecotube system in coal and waste grate combustion. *Energy Conversion and Management*, *42*(15-17), 1887–1896.

Dupont, C., Chen, L., Cances, J., Commandre, J.-M., Cuoci, A., Pierucci, S., & Ranzi, E. (2009). Biomass pyrolysis: Kinetic modelling and experimental validation under high temperature and flash heating rate conditions. *Journal of Analytical and Applied Pyrolysis*, *85*(1-2), 260–267.

EU (2000). Europa-parlamentets og rådets direktiv af 2000/76/EF. Technical report. Concerning combustion of waste.

FLUENT (2006). *Fluent 6.3 User's Guide*.

Fogler, H. S. (2006). *Elements of Chemical Reaction Engineering*. Prentice Hall.

Frenklach, M., Bowman, T., Smith, G., & Gardiner, B. (2000). GRI 1.2. Available at: www.me.berkeley.edu.

Frenklach, M., h. Wang, Bowman, C. T., Hanson, R. K., Smith, G. P., Golden, D. M., Gardiner, W. C., & Lissianski, V. (1994). An optimized kinetics model for natural gas combustion. Work-In-Progress Poster Number 26.

Glassman, I. (1996). *Combustion*. San Diego, California: Academic Press Inc.

Goddard, C. D., Yang, Y. B., Goodfellow, J., Sharifi, V. N., Swithenbank, J., Chartier, J., Mouquet, D., Kirkman, R., Barlow, D., & Moseley, S. (August 2005). Optimisation study of a large waste-to-energy plant using computational modelling and experimental measurements. *Journal of the Energy Institute*, *78*, 106–116(11).

Kær, S. K. (2004). Numerical modelling of a straw-fired grate boiler. *Fuel*, *83*(9), 1183–1190.

Kær, S. K. (2005). Straw combustion on slow-moving gratesŮa comparison of model predictions with experimental data. *Biomass and Bioenergy*, *28*(3), 307–320.

Kreyszig, E. (2006). *Advanced Engineering Mathematics*. John Wiley and Sons.

Lans, R. P. v. d. (1998). Straw Combustion in a Grate Furnace. Technical Report CHEC rep. 9823.

Launder, B. E. & Spalding, D. B. (1974). The Numerical Computation of Turbulent Flows. *Computer Methods in Applied Mechanics and Engineering*, *3*, 269–289.

Magnussen, B. F. (1981). On the Structure of Turbulence and a Generalized Eddy Dissipztion Concept for Chemical Reaction in Turbulent Flow. *19th American Institute of Aeronautics and Astronautics Aerospace Science Meeting*.

Norman, T., Andersen, P., Grévain, D., & Dahlqvist, M. (2007). B&W Vølund guest lecture on CFD modelling of boilers. At Aalborg University, nov. 2007.

Python (2008). Python Programming Language. version 2.54, www.python.org.

Rogaume, T., Auzanneau, M., Jabouille, F., Goudeau, J. C., & Torero, J. L. (2002). The effects of different airflows on the formation of pollutants during waste incineration. *Fuel*, *81*(17), 2277–2288.

Ryu, C., Yang, Y. B., Nasserzadeh, V., & Swithenbank, J. (2004). Thermal reactor modeling of a large municipal solid waste incinerator. *Combustion Science and Technology*, *176*(11), 1891–1907.

Scharler, R. & Obernberger, I. (2000). Numerical Modelling of Biomass Grate Furnaces. *Proceedings of the 5th European Conference on Industrial Furnaces and Boilers*.

Schlichting, H. D. (1979). *Boundary-Layer Theory*. McGraw-Hill Book Company.

Shih, T.-H., Liou, W. W., Shabbir, A., Yang, Z., & Zhu, J. (1995). A new k-e eddy viscosity model for high reynolds number turbulent flows. *Computers and Fluids*, *24*(3), 227–238.

Spalding, D. B. (1970). Mixing and chemical reaction in steady confined turbulent flames. *13th Symposium International on Combustion*.

Strand, M. (2007). Particulate and CO Emissions from a Moving-Grate Boiler Fired with Sulfur-Doped Woody Fuel. *Energy and Fuels*, *21*(6), 3653–3659.

Tillman, D. A. (1987). *Biomass Combustion*, chapter 9. Biomass. John Wiley and Sons Ltd.

Turns, S. R. (2000). *An Introduction to Combustion - Concepts and Applications*. McGraw-Hill Companies Inc.

Versteeg, H. K. & Malalasekera, W. (2007). *An Introduction to Computational Fluid Dynamics*. Edinburgh Gate, England: Pearson Education Limited.

Westbrook, C. K. & Dryer, F. L. (1984). Chemical kinetic modeling of hydrocarbon combustion. *Progress in Energy and Combustion Science*, *10*(1), 1–57.

Yang, Y. B., Newman, R., Sharifi, V., Swithenbank, J., & Ariss, J. (2007). Mathematical modelling of straw combustion in a 38 mwe power plant furnace and effect of operating conditions. *Fuel*, *86*(1-2), 129–142.

Yin, C., Rosendahl, L., Kær, S. K., Clausen, S., Hvid, S. L., & Hille, T. (2008). Mathematical Modeling and Experimental Study of Biomass Combustion in a Thermal 108 MW Grate-Fired Boiler. *Energy and Fuels*, *22*(2), 1380–1390.

Yin, C., Rosendahl, L. A., & Kær, S. K. (2008). Grate-firing of biomass for heat and power production. *Progress in Energy and Combustion Science*, *34*(6), 725–754.

Zanzi, R., Sjöström, K., & Björnholm, E. (1996). Rapid high-temperature pyrolysis of biomass in a free-fall reactor. *Fuel*, *75*(5), 545–550.

Zevenhoven, R. & Kilpinen, P. (2004). Control of pollutants in flue gasses. Technical report, Sponsored by "The Nordic Energy Research Programme" and "Helsinki University of Technology".

Zhou, H., Jensen, A. D., Glarborg, P., Jensen, P. A., & Kavaliauskas, A. (2005). Numerical modeling of straw combustion in a fixed bed. *Fuel*, *84*(4), 389–403.

CFD setup

A

A.1 Meshing details

Through this appendix further meshing details is given on grid used in the CFD simulations. All parts of the grid is structured and meshed with hexahedronal cells. In Figure A.1 the grid at and around the tertiary air inlets is seen. These are meshed by only 9 faces to keep down the number of cells and avoid big changes in cell sizes.

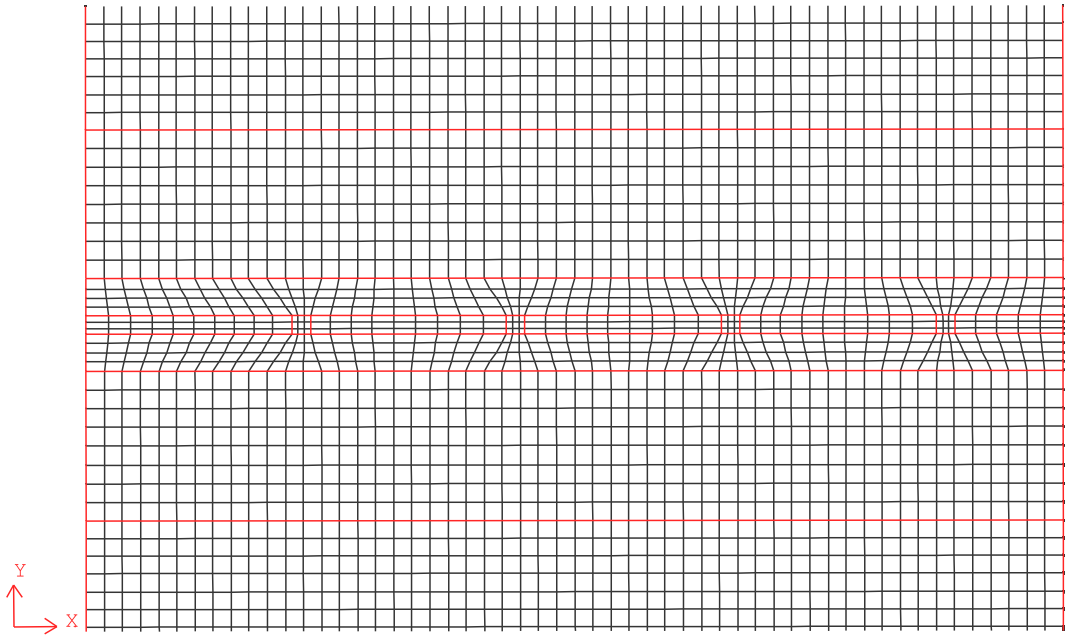

Figure A.1: *Mesh on left wall with tertiary air inlets.*

The grid on the rear side of the lower furnace is seen in Figure A.2, showing the grid around the secondary air inlets an the backside of the furnace. Most inlets is meshed by 16 faces to give an acceptable resolution. A further improvement of the inlets had been to model the last one meter of the inlet pipes before entering, to let the velocity profile develop. However, for simplicity the pipes are also rectangular, while they are normally circular. Modelling of the last one meter pipe before entering, would only be beneficial if the pipe shape was not simplified.

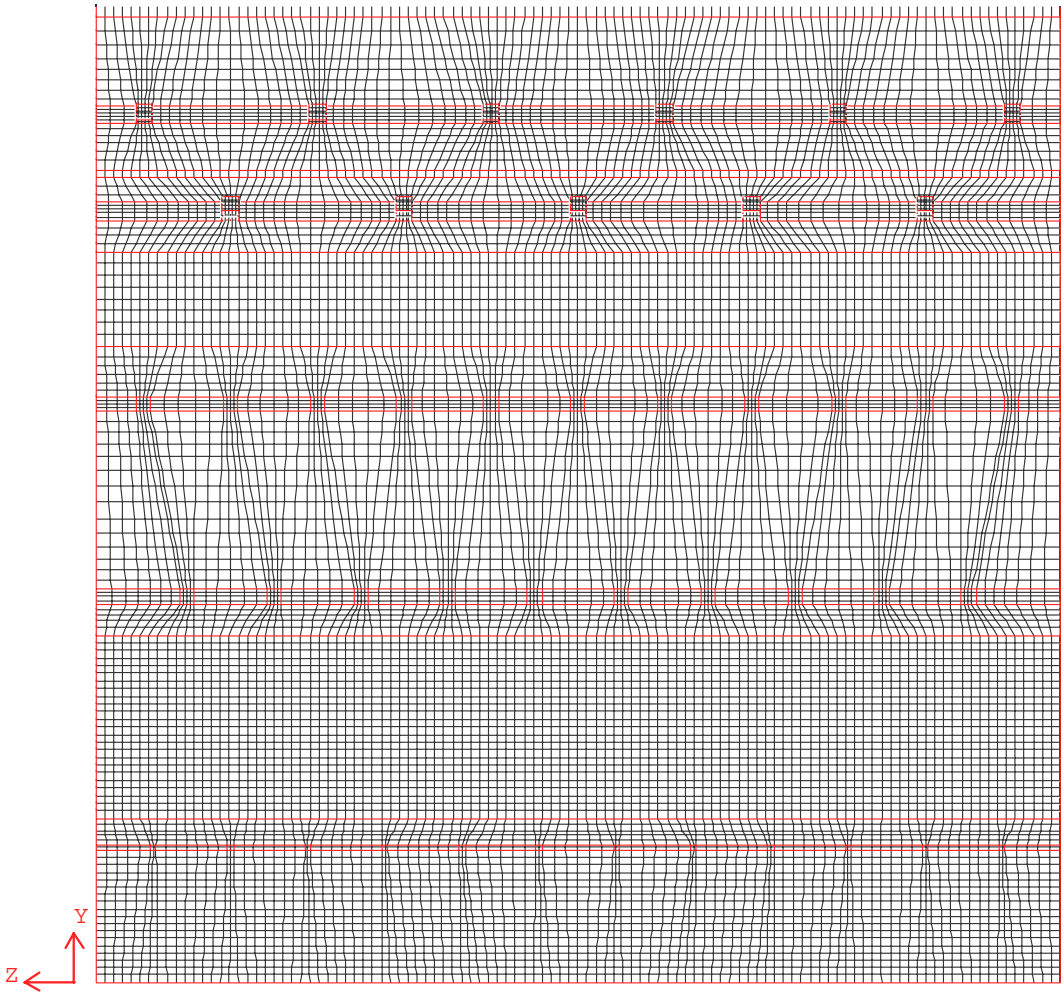

Figure A.2: *Meshed on rear wall with secondary air inlets.*

A.2 FLUENT settings

In the following the standard case setup in the CFD simulations in FLUENT is summarized. The general and most important settings is discussed in Section 2.4.2. Here, all relevant settings are summarized in a number of tables, summarizing turbulence settings Table A.2, radiation settings Table A.3, species transport settings Table A.4 and boundary settings Section A.2.1 and solution procedure is described in Section A.3

Option	**Choice**
Solver	Pressure based
Dormulation	Implicit
Time	Steady

Table A.1: *Solver settings.*

Option	Choice
Turbulence model	Realizable $k-\epsilon$
Near wall treatment	Standard wall function
Other options	Default

Table A.2: *Turbulence settings.*

Option	Choice
Radiation model	Discrete Ordinates (DO)
DO/energy coupling	none
Solar radiation	none
Gas emmision model	Gray radiation

Table A.3: *Radiation settings.*

Option	Choice
Species model	Species transport and reaction
Turbulence-Chemistry interaction	Eddy dissipation Concept (EDC)
Volume fraction constant	2.1377 (default)
Time scale constant	0.4082 (0.05 in initial solutions)
Reactions	Volumetric
Chemistry	Heterogenous
Kinetic mechanism	GRI-1.2

Table A.4: *Species transport and chemistry settings.*

A.2.1 Boundary and operating conditions

Gravity was enabled, with a gravitaional acceleration of $9.81\ \left(\frac{\mathrm{m}}{\mathrm{s}^2}\right)$.

Option	Choice
Inlet type	Mass flow inlet
Mass flow rate	14.73 kg/s
Turbulence (intensity/lengthscale)	5% / 50 mm
Temperature	523 K
Radiative emmisivity	0.0
Species composition	Basis mixture Table 2.5

Table A.5: *Grate boundary setttings.*

Option	Choice
Inlet type	Mass flow inlet
Mass flow rates	Given in Table 2.8
Turbulence intensity (hydraulic diameter)	10%
Temperature	543 K
Radiative emmisivity	0.0
Species composition (by mass)	O_2: 23.14%, N_2: 76.76%, Ar: 0.1%

Table A.6: *SA+TA inlets boundary setttings.*

Option	Choice
Outlet type	Outflow
Radiative emmisivity	0.0

Table A.7: *Outlet boundary setttings.*

Wall section	Temperature (K)	Emmisivity	Roughness height (mm)
Side walls	603	0.6	5
Walls in topsection (16-18.5 m)	603	0.0	5
Insulated walls	903	0.3	5

Table A.8: *Wall boundary settings. Roughness height based on Norman et al. [2007]*

A.3 CFD Solution procedure

Obtaining a solution of a combustion simulation with detailed chemistry requires some care. Firstly, the initially iterations need to be performed without chemical reactions, otherwise divergence will probably be the result. About 500 iterations is in this case enough for the mean flow to develop. Secondly, the settings regarding chemistry integration is important.

Integration of the chemistry is computationally expensive, but the use of the ISAT algorithm decreases the integration time by several orders of magnitude (i.e. 10 - 100 fold reduction in time) compared to direct integration of the ODE system. The ISAT algorithm maps the result of the direct integrations through the initial iterations in a ISAT table. Using mapping gradients and interpolation of table values, the result in later iterations is found as a query in the table, if the initial conditions agree to a specified tolerance. In this way, most direct integrations is avoided and replaced by queries [FLUENT, 2006]. Iteration time, even when using the ISAT algorithm, varied

from 2 to 45 minutes per iteration depending on the specified error tolerance and the allowable table size. The bigger the table, the better performance, so the computer memory was the limiting factor.

Through most iterations, chemistry iteration is only required for every 10th flow iteration. However, in the latter phases of the simulation, chemistry iteration is required for every flow iteration. The steps of the solution procedure used, are seen below.

- Simulation conditions was set, and all variables initialized with appropiate values. Underrelaxation factors was set as given in Table A.9.
- Cold flow iterations were carried out until the flow began to converge (500-1000 iterations)
- Volumetric reactions was enabled, with one chemistry iteration per every 10 flow iteration. The time scale constant was set to $C_\tau = 0.04$. About 300 iterations were carried out.
- The time scale constant was increased to $C_\tau = 0.3082$ which give a sufficient integration time in the present case. Several thousand iterations was carried out until no progress was observed.
- Chemistry iteration frequency was set to solve the chemistry for every flow iteration. Iterations were carried out until no further progress is observed (several thousand).
- Flow and turbulence field equations were disabled *i.e.* the flow and turbulence field were held constant. Chemistry was solved until convergence.

If more time had been available, the appropriate procedure for continuing had been [FLUENT, 2006]:

- After chemistry convergence, enable flow and turbulence equation, to let the flow finaly setle down.
- Decrease ISAT error tolerance from the default $3 \cdot 10^{-3}$ to $3 \cdot 10^{-4}$. Increase allowable ISAT table size if possible. Iterate to convergence is reached.
- Decrease ISAT error tolerance further if necessary and iterate to convergence.

These three steps was however NOT used, due to lack of time.

Simulation time with the used procedure was about 1.7-3 minutes per iteration on a 3 x 3 GHz Linux cluster, when a good ISAT table has been build. To build a good ISAT table, some hundred iterations with chemistry were needed. As the table was not build yet, this took a couple of days. For iterations without chemistry iteration time were about 0.6 minutes per iteration. The number of necessary iterations could probably be reduced with more efficient use. However no better guidelines was found searching the FLUENT manual [FLUENT, 2006] or the well known online CFD forum, CFD Online [2009].

Parameter	**Factor**
Pressure	0.8
Density	1.0
Body forces	1.0
Momentum	0.3
k	0.3
ϵ	0.3
μ_t	0.7
Species	0.5
Energy	0.7
Radiation	0.8

Table A.9: *Underrelaxation factors.*

Residuals histories

B

The iteration history of scaled residuals is seen in Figures B.1 to B.6. In Figure B.1, Figure B.2 and Figure B.1 residuals are seen for the iterations before flow equations were disabled. The big peak in residuals occuring in all three cases, are the point where the outlet type was changed from pressure outlet to outflow. This was done because backflow was encountered in about 30 faces (out of 2000) at the outlet boundary.

In Figure B.4, Figure B.5 and Figure B.6, residuals are seen for the iterations after the flow equations had been disabled.

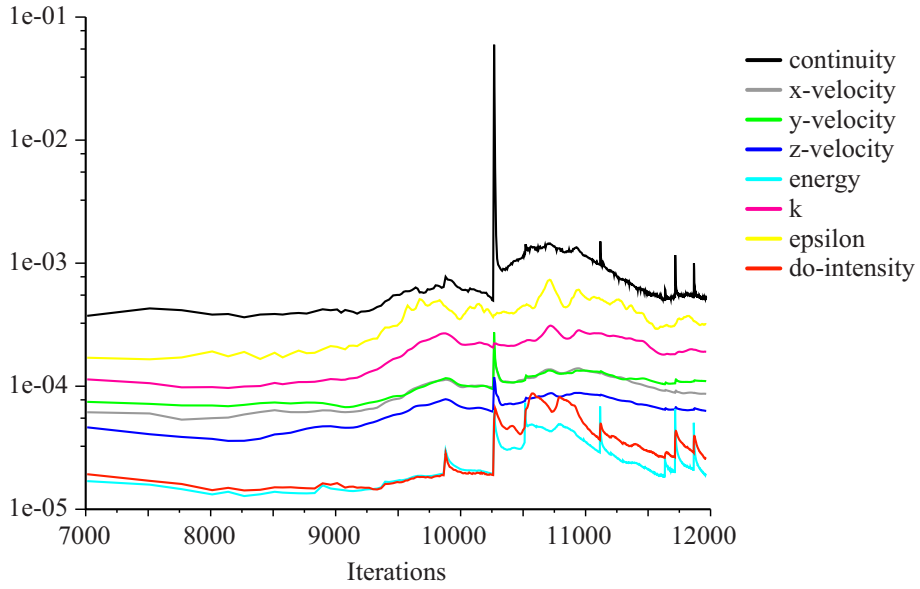

Figure B.1: *History of scaled residuals for flow variables, case with water injection.*

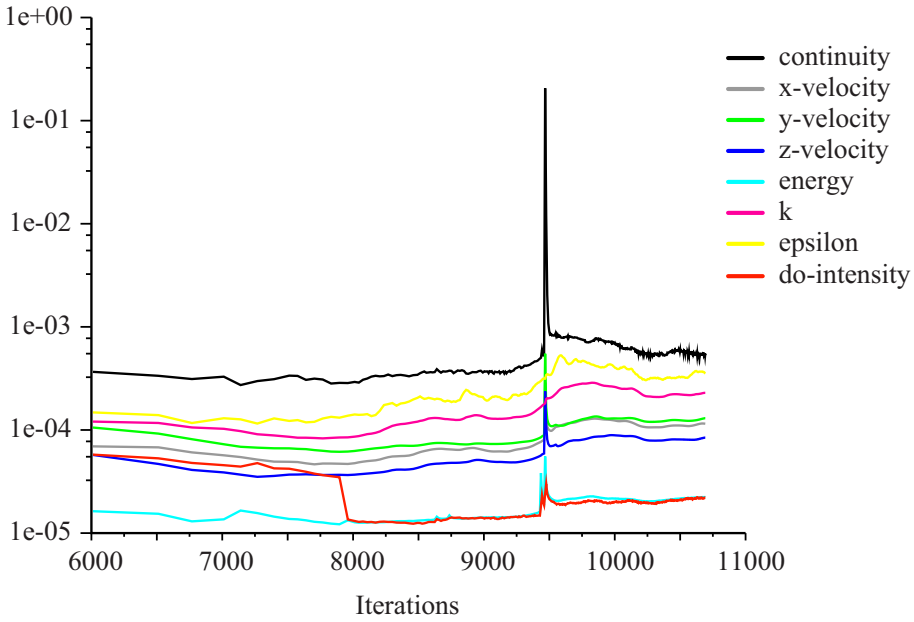

Figure B.2: *History of scaled residuals for flow variables, case Ins40.*

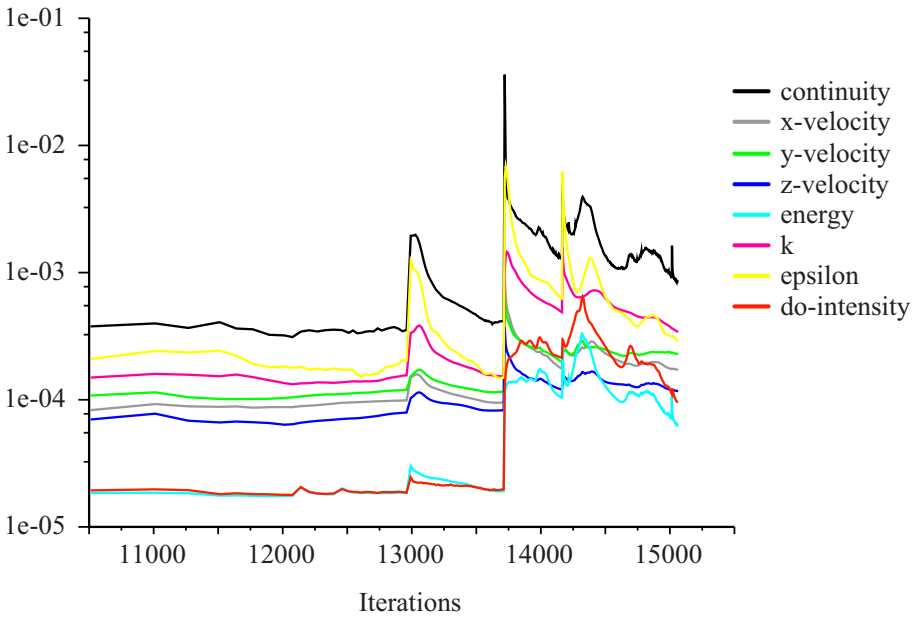

Figure B.3: *History of scaled residuals for flow variables, case Ins60.*

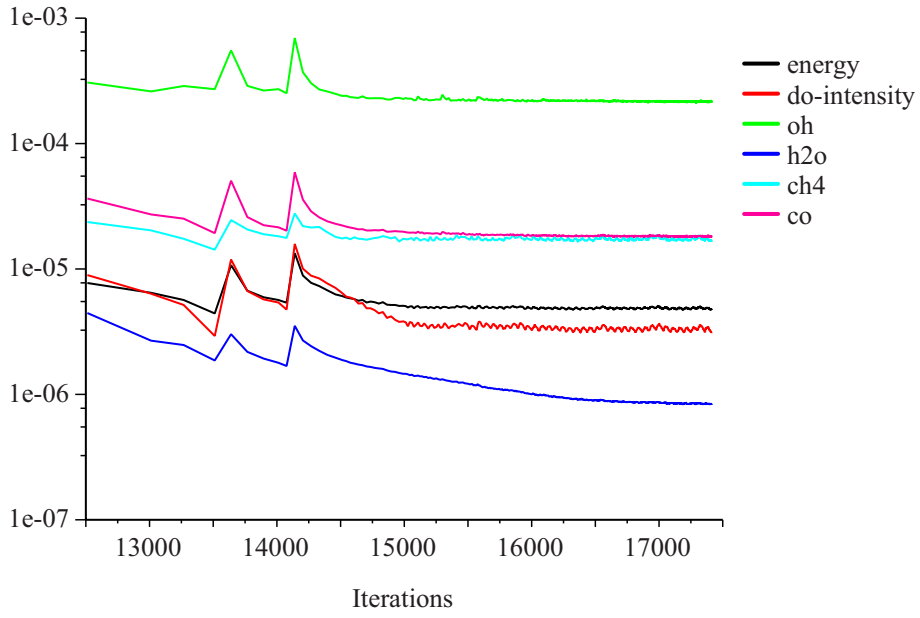

Figure B.4: *History of scaled residuals for flow variables, case with water injection. After flow equations were disabled.*

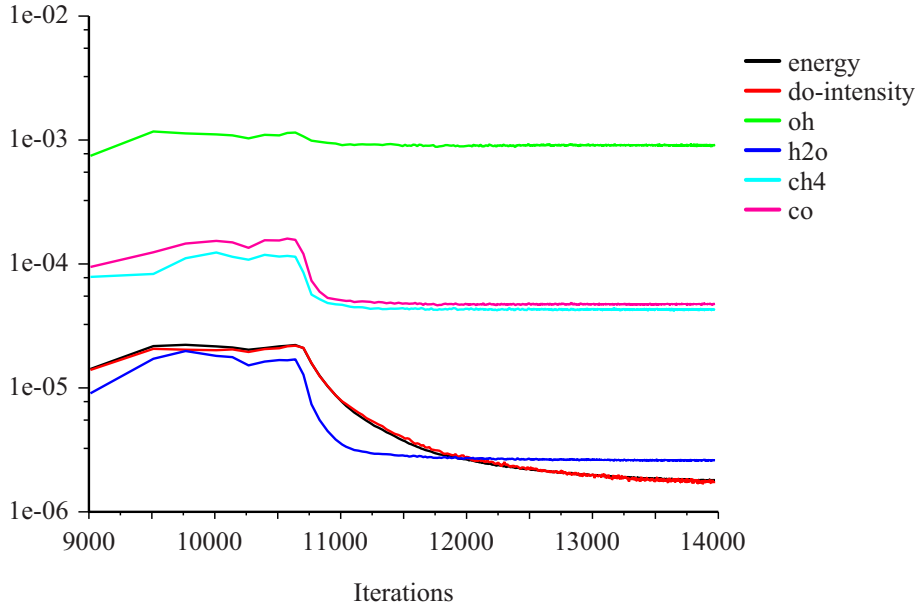

Figure B.5: *History of scaled residuals for flow variables, case Ins40. After flow equations were disabled.*

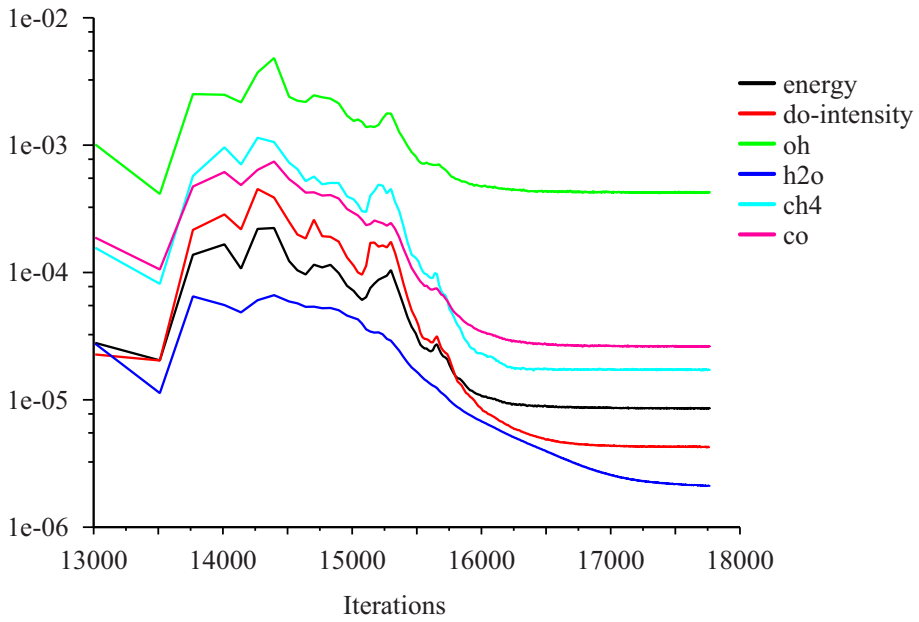

Figure B.6: *History of scaled residuals for flow variables, case Ins60. After flow equations were disabled.*

Theory

C

This appendix contain fundamental theory on the som topics relavant to the report. In Section C.1 fundamental theory on turbulence is described, regarding N-S equations, RANS approach and the realizable k-ϵ model.

C.1 Turbulence and Realizable k-e model

As described in Section 2.4.2 Navier-Stokes equations of motion, could be derived from Newtons second law, refering to Schlichting [1979] for details on the derivaiton. Navier-Stokes equations for incompressibel flow of a Newtonian fluid is seen in Equations C.1 to C.3 [Schlichting, 1979].

$$x\text{-momentum:} \quad \frac{\partial(\rho\mathbf{u})}{\partial t} + \text{div}(\rho u\mathbf{u}) = -\frac{\partial p}{\partial x} + \left(\frac{\partial^2 u}{\partial x^2} + \frac{\partial^2 u}{\partial y^2} + \frac{\partial^2 u}{\partial z^2}\right) \tag{C.1}$$

$$y\text{-momentum:} \quad \frac{\partial(\rho\mathbf{u})}{\partial t} + \text{div}(\rho u\mathbf{u}) = -\frac{\partial p}{\partial x} + \left(\frac{\partial^2 u}{\partial x^2} + \frac{\partial^2 u}{\partial y^2} + \frac{\partial^2 u}{\partial z^2}\right) \tag{C.2}$$

$$z\text{-momentum:} \quad \frac{\partial(\rho\mathbf{u})}{\partial t} + \text{div}(\rho u\mathbf{u}) = -\frac{\partial p}{\partial x} + \left(\frac{\partial^2 u}{\partial x^2} + \frac{\partial^2 u}{\partial y^2} + \frac{\partial^2 u}{\partial z^2}\right) \tag{C.3}$$

The Navier-Stokes equations form a set of three coupled Partial Differential Equations (PDE's). As is the nature of many PDE's, Naver-Stokes equations are only analytical solvable for distinct cases, e.g. Couette flow, see Schlichting [1979] for further details. Direct numerical solution of is very computational expensive, different approaches have been developed to make the equations tractable. A very common and widely used approach is the Reynold Average Navier-Stokes (RANS). The RANS approach assumes the instantaneous velocity to be described by a meanflow component **U**, and a fluctuating component $\mathbf{u}'$, as seen in vectornotation in equation (C.4).

$$\mathbf{u} = \mathbf{U} + \mathbf{u}' \tag{C.4}$$

The timeaveraging of the instantaneous velocity imply addiational stresses (Reynold stresses) appearing in the RANS momentum equation, which is seen for x-momentum in equation (C.5) (compressible flow).

$$\frac{\partial(\overline{\rho}\tilde{U})}{\partial t} + \text{div}(\overline{\rho}\tilde{U}\tilde{\mathbf{U}}) = \frac{\partial \overline{P}}{\partial x} + \text{div}(\mu\nabla\tilde{U}) + \left[-\frac{\partial(\overline{\rho u'^2})}{\partial x} - \frac{\partial(\overline{\rho u' v'})}{\partial y} - \frac{\partial(\overline{\rho u' w'})}{\partial z}\right] \tag{C.5}$$

Different models is available for modelling this extra stress term, among which the k-ϵ [Launder & Spalding, 1974] model is well known. The k-ϵ model defines the turbulent kinetic energy k, see equation (C.6) and its dissipation rate ϵ, see equation (C.7) to calculate the turbulent viscosity μ_t in equation (C.8). This is used in the Boussinesq relationship to determine the Reynold stress terms $-\rho\overline{u'^2}$, $-\rho\overline{u'v'}$ and $-\rho\overline{u'w'}$.

$$k = \frac{1}{2}(\overline{u'^2} + \overline{v'^2} + \overline{w'^2}) \tag{C.6}$$

$$\epsilon = 2\nu\overline{s'_{ij} \cdot s'_{ij}} \tag{C.7}$$

$$\mu_t = \rho C_\mu \frac{k^2}{\epsilon} \tag{C.8}$$

One of the major improvements in the realizable k-ϵ model is a new expression of C_μ connecting it to the mean flow instead of being constant as is the case in the standard k-ϵ model, thus making it applyable to a wider range of flows.

Correspondence

D

D.1 Uwe Schnell

The following contain the coorespondance between the autor of this report and Prof. Dr.-Ing Uwe Schnell
Stellvertreter des Institutsdirektors und
Leiter der Abteilung Feuerungs- und Dampferzeugersimulation
Institut für Verfahrenstechnik und Dampfkesselwesen
in Stuttgard.

Fra: Uwe Schnell [mailto:Uwe.Schnell@ivd.uni-stuttgart.de]
Sendt: 2. april 2009 15:59
Til: 'Thomas Meldgaard'
Emne: AW: Literature recommendations?

Dear Mr. Meldgaard,

unfortunately, I cannot recommend any literature source to you. I asked several of my colleagues dealing with wood/biomass combustion, but none of them could tell me anything about injection of agents for the generation of OH radicals, and by thus, enhancing CO oxidation.

Hope you will find any other sources.

Wish you good luck with your master thesis, and please give my regards to Tom Condra!

Best wishes, Uwe Schnell.

Von: Thomas Meldgaard [mailto:meldgaard.thomas@gmail.com]
Gesendet: Dienstag, 31. März 2009 10:37
An: Uwe Schnell
Cc: 'Thomas Condra'
Betreff: Literature recommendations?

Dear Uwe Schnell

I am a master student at Aalborg University writing to you with best regards from my supervisors, prof. Tom Condra and prof. Lasse Rosendahl.

I am working at my master thesis in the subject of CO reduction in biomass furnaces, and was recommended to contact you by Tom Condra. I know you might be busy, but I would be very grateful if you would spend some minutes on me.

I my master thesis I am investigating reduction of the CO level in biomass furnaces fired with very wet fuel, where CO is often a problem. I am not looking at mixing, but at controlling the furnace temperature to reduce CO, and perhaps to inject methane or other species to produce OH radicals. I am investigating the problem using Cantera and CFD simulations with detailed chemistry.

I was thinking, that perhaps, you could recommend some relevant literature regarding CO reduction by controlling the temperature or by injecting species? Both English and German literature are welcome. Thank you very much if you would take a look on it.

With best regards

Thomas Hartman Meldgaard
Master student
Thermal Energy and Process Engineering
Aalborg University
Meldgaard.thomas@gmail.com

D.2 Bjørn Hjertager

The following contain the correspondence the autor of this report and Prof. Dr.-Ing Bjørn Hjertager, who is the co-developer of the EDC model used to solve the chemistry in the CFD simulations in this study.

<bjorn.hjertager@uis.no>
12.05.2009 13:26 To <meldgaard.thomas@gmail.com>
cc "'Thomas Condra'" <tc@iet.aau.dk>
Subject Re: EDC hjaelp

Hej,

Det svært at komme med nogle gode /nye forslag til hva du kan gøre. Jeg ville foreslå at bruge "upwind diffrecing" på alle konsentrationsligningerne. Selve ISAT algoritmen kender jeg ikke noget sælig om. Du kan jo også spørge Fluent helpdesk (du har måske gjort det allerede).

mvh

Bjørn Helge

Professor Bjorn H. Hjertager, Dr.ing.
Head of Department
Dept. of Mathematics and Natural Sciences
University of Stavanger
N-4036 Stavanger
Norway

E-mail: bjorn.hjertager@uis.no
Tel.: +47 51 83 18 07 (direct)
Mob.: +47 467 90 916
Fax:: +47 51 83 17 50

"Thomas Hartman Meldgaard" <meldgaard.thomas@gmail.com>
12.05.2009 12:59 To <bjorn.hjertager@uis.no>
cc "'Thomas Condra'" <tc@iet.aau.dk>
Subject EDC hjaelp

Hej Bjørn

Jeg er kandidatstuderende på Aalborg universitet og skriver med bedste hilsner fra min vejleder, Thomas Condra.
Tom håber at det går godt oppe mellem de norske fjelde :)
Jeg håber du lige har et par minutter til at se på mit spørgsmål.

Jeg arbejder på CFD simulering af forbrænding i en biomassekeddel i FLUENT med detaljeret kemi som jeg implementerer vha. EDC modellen. Målet er at se på CO reduktion ved at variere fyrrums temperaturen.

Kemien er 177 volumetriske reaktioner (GRI 1.2 mekanismen) importeret fra Chemkin og det går langt hen ad vejen godt med at løse det. Desværre, når temperatur, flow osv. nogenlunde er konvergeret har kemien svært ved helt at konvergere, fx: Gennemsnitlig CO i udløbet fluktuerer tilsyneladende tilfældigt mellem 500 og 700 ppm.

For at få det til at konvergere har jeg prøvet en del forskelligt: Forskellige underrelaxationer justering af EDC "time constant", forskellig diskretisering (1st order, 2nd order, QUICK), og forskellig tolerance på ISAT tabellen som FLUENT bruger til at løse kemien. Indtil videre uden held. (og jeg er desværre snart lidt presset da jeg afleverer specialet om tre uger :)

Har du en hurtig ide til hvad jeg ellers kunne prøve, og som måske kunne hjælpe til konvergens?

Tom siger: "a quick answer is better than no answer".

Med venlig hilsen
Thomas Meldgaard